The Pennsylvania State University

The Graduate School

Department of Energy and Mineral Engineering

INTERACTION OF FRACTURE FLUID WITH FORMATION ROCK AND PROPPANT ON FRACTURE FLUID CLEANUP AND LONG TERM GAS RECOVERY IN MARCELLUS SHALE RESERVIORS

A Thesis in

Energy and Mineral Engineering

by

Wenting Yue

Submitted in Partial Fulfillment
of the Requirements
for the Degree of

Master of Science

December 2012

The thesis of Wenting Yue was reviewed and approved* by the following:

John Yilin Wang
Assistant Professor of Petroleum and Natural Gas Engineering
Thesis Advisor

Derek Elsworth
Professor of Energy and Geo-Environmental Engineering

Turgay Ertekin
Professor of Petroleum and Natural Gas Engineering;

R. Larry Grayson
Professor of Energy and Mineral Engineering;
Graduate Program Officer of Energy and Mineral Engineering;

*Signatures are on file in the Graduate School

ABSTRACT

The exploitation of unconventional gas reservoirs has become an integral part of the North American gas supply. The economic viability of many unconventional gas developments hinges on the effective stimulation of extremely low permeability reservoir rocks. With improving drilling and stimulation techniques, many unconventional plays have become realistic contributors to the energy budget. The Marcellus shale reservoir contains large amount of natural gas resources and its proximity to high demand markets makes it an attractive target for energy development.

Hydraulic fracturing is the stimulation method of choice in shale gas reservoirs. Even though hydraulic fracturing technique improves ultimate gas recovery, there are several factors that impact the production of natural gas from a hydraulically fractured shale gas well.

This study was undertaken to quantify the impact of selected post hydraulic fracture factors that affects shale gas wells. With the use of commercial reservoir simulator that models cumulative production and flow rate from a vertical well located in a 160 acre Marcellus shale gas reservoir, we are able to quantify how much impact this various factors will have on the ultimate gas recovered from the reservoir under consideration. A base model contains multi-phase flow and proppant crushing was simulated and used as the base result for which other factors was incorporated and compared.

The new knowledge from this research should enable engineers to better design fracture treatments and helps operators manage the well in the Marcellus shale formation. The observation and recommendations will also be useful for further studies in this area.

TABLE OF CONTENTS

LIST OF TABLES

LIST OF FIGURES

ACKNOWLEDGEMENTS

First and foremost I want to thank my advisor Dr. John Yilin Wang. I have been both studying from and working with Dr. Wang for almost 2 years, and it has been the most rewarding time in my life. He not only instructed me with professional knowledge in my research area, but also enlightened me on what it means to be research and how to finish a research with proficiency. He taught me devotion and conscientiousness with his words and deeds. I would like to thank my committee members Dr. Turgay Ertekin and Dr. Derek Elsworth.

I would like to give my thanks to my parents Baoguo Yue and Liping Ren. If it is not for their support and care, I wouldn't have the chance to study here and pursue my dream. Their encouragement is my greatest buttress during difficulties.

I thank Tunde Osholake and Ihsan Burak Kulga. Both their thesis and research have given me great inspiration and guidance. I thank all the group members in 3S lab for their help in my research. I thank every friend here. They filled my life with surprise and happiness. I want to give my special thanks to Yi Wang. His accompany and encouragement kindled my confidence.

At last, I want to thank Computer Modeling Group ltd. for providing me the access for the base software CMG. I also want to thank The Pennsylvania State University, thank Energy and Mineral engineering department. The experience and knowledge I had here will benefit my entire life.

Chapter 1

Introduction

Fossil fuel, such as coal and petroleum, plays an important part in people's lives. Although people started using coal to burn and cook in ancient times, the massive usage of coal and petroleum was started from the industrial age. The invention of steam engine pushed the efficiency of production into a new frontier, and brought the exploration and harness of fossil fuel into an unprecedented stage. The unsatisfied demand and crave for fossil fuel has pushed human being to explore both conventional and unconventional fuel in order to meet with the energy demands from our society.

Shale gas refers to natural gas that is trapped within shale formations. Shales are fine-grained sedimentary rocks that can be rich sources of petroleum and natural gas. Over the past decade, the combination of horizontal drilling and hydraulic fracturing has allowed access to large volumes of shale gas that were previously uneconomical to produce, as is shown in Figure 1-1. The production of natural gas from shale formations has rejuvenated the natural gas industry in the United States.

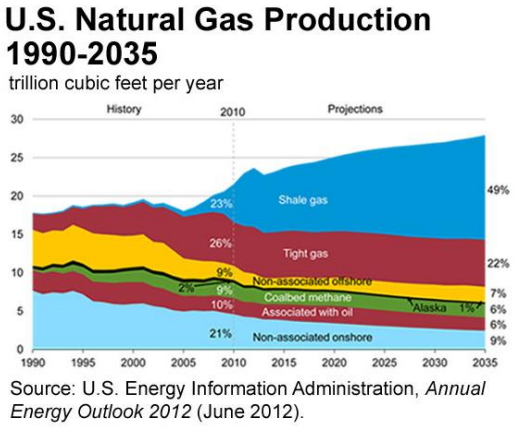

Figure 1-1 U.S. Natural Gas Production 1990-2035

Marcellus Shale was discovered just in this new realization. Figure 1-2 is a map representation of where Marcellus shale is located. As recently as 2002 the United States Geological Survey in its Assessment of Undiscovered Oil and Gas Resources of the Appalachian Basin Province, calculated that the Marcellus Shale contained an estimated undiscovered resource of about 1.9 trillion cubic feet of gas. In early 2008, Terry Englander, a geoscience professor at Pennsylvania State University, and Gary Lash, a geology professor at the State University of New York at Fredonia, surprised everyone with estimates that the Marcellus might contain more than 500 trillion cubic feet of natural gas.

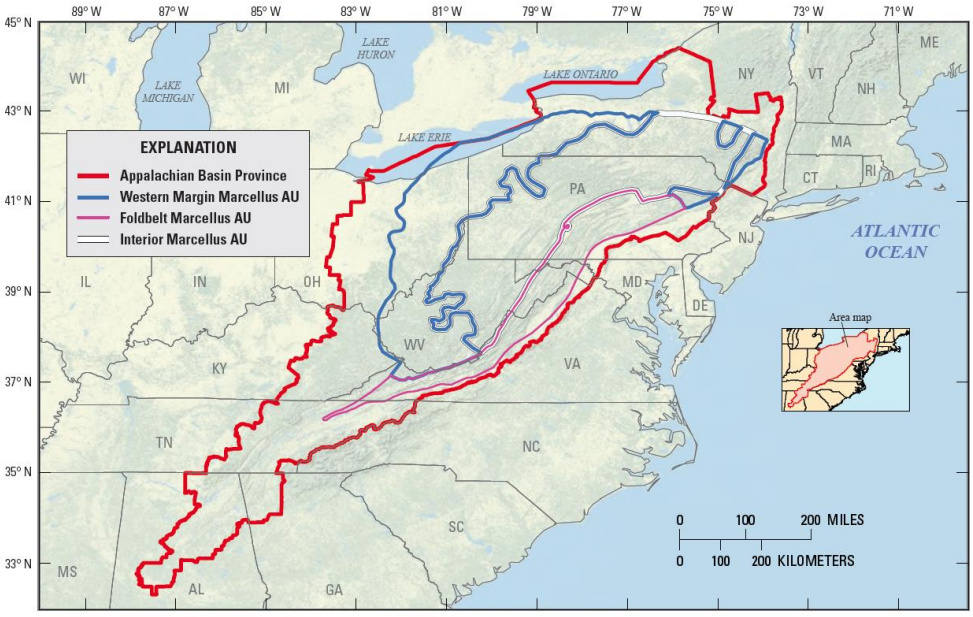

Figure 1-2 Map of the Appalachian Basin Province showing the three Marcellus Shale assessment units, ehich encompass the extent of the Middle Devonian from its zero isopach edge in the west to its erosional truncation within the Appalachian fold and thrust belt in the east.

Hydraulic fracture is the most effective way to stimulate gas formation. Over the past decade, the combination of horizontal drilling and hydraulic fracturing has allowed access to large volumes of shale gas that were previously uneconomical to produce. Shale gas wells the

must be hydraulically fractured before a well can produce economic amounts of gas. Figure 1-3 a good representation.

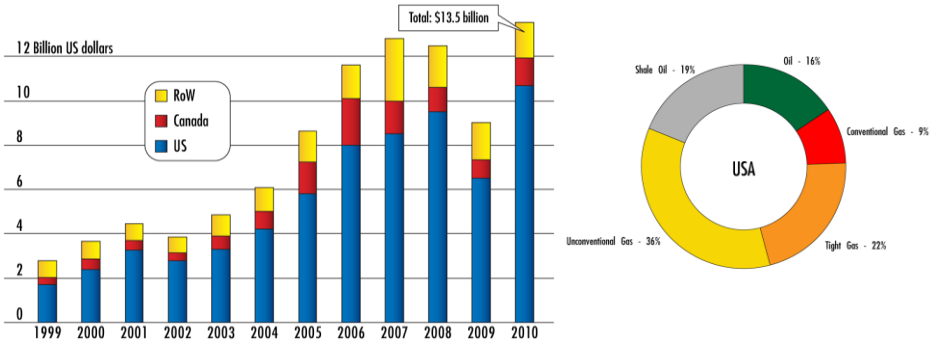

Figure 1-3 Size of the fracturing market (Economides 2010)

Although Marcellus Shale has a great production potential, currently we still know little about it. One of the most important facts is massive hydraulic fracture activity, without caution, may lead to severe damage on both the formation and fracture.

Regarding this problem, this project focuses on computer simulation method to help understand how much different kinds of fracture damage affect productivity. After observation and comparison, conclusions will be addressed regarding on a better understanding of what should be taken into consideration before hydraulic fracture

Chapter 2

Literature Review

Hydraulic fracture is the most effective stimulation method in shale gas reservoirs. The process of hydraulic fracture may cause formation damages at the same time, if not properly designed. All damaging factors may reduce the effectiveness that hydraulic fractures should have. Continued from Osholake's work (2011), there are three damaging factors considered in this thesis, interaction of flow back fluid and formation rock, proppant scale, and proppant diagenesis.

Interaction of flow back fluid and formation rock is used to describe the situation where clay in the formation swells after contacting foreign water. Hower mentioned that clay swell will cause severe damage on formation rock, the contact with foreign water will also cause clay's migration from original position. If flow channels are plugged, production will be affected (Hower 1974). Bahrami, Rezaee says as swell clays imbibe water into their crystalline structure, enlarge them in size, and hence plug the pore space (Bahrami, Rezaee et al. 2011). Dewan described different kinds of clay, their crystal structure, their disperse structure (Dewan 1983). Both Dewan and Hower pointed out that Montmorillonite is the most possible type of swell clay (Dewan 1983) (Hower 1974). The latest laboratory work conducted on the topic of interaction between flow back fluid and formation rock is documented in (Conway, Venditto et al. 2011). Conway and his colleages conducted a serious of experiments. They simulated a natural fracture in the lab, flow different kinds of fluids through the core samples, and measure conductivities of the natural fracture at the same time. They discovered that clay swell caused by the contact of foreign fluid may induce the closure of natural fractures. Conductivity data was recorded and has valuable usage in our research.

Scale precipitation always appears within the pore spaces of the formation matrix or proppant pack, or builds up in downhole tubing. Scale is found to be one of the reasons that causes successive decline of fracture conductivity. (Lehman, Parker et al. 1999) showed many photographic evidence of scale withdrew from down hole condition in his paper. (Mackay 2010) summarized produced water life-cycle into three distinct periods. The First period is production of formation water only. During this period, brine may have a carbonate scaling. The second period is production of formation water and injected seawater. There is potentially an increasing sulphate scaling tendency. The third period is production of formation water, injected seawater and re-injected produced water. In Garzon and Solares's work (Garzon, Solares et al. 2009), the OLI's ScaleChem (2001) prediction program was used to simulate the deposition environment in the sandface area and production string. According to his simulation scale did happen, and calcium carbonate and iron sulfide are the most likely mineral scales depositing in the sandface area. As for the latest research on proppant scale, Weaver (Weaver and Nguyen 2010) constructed a serious of experiments to test the effectiveness of WBAA agent in preventing proppant scale. In the experiment, the Teflon flow cells were packed with 20/40-mesh sand, simulating the proppant pack. The test used a flow combined at a 50:50 ratio from two different. These two brines, once mixed together, can form $CaCO_3$ scale. The pressure drop increase across the sand pack was witnessed, which not only further proves the fact that proppant scale may impair fracture conductivity, but also provide us with quantification of decreased conductivity.

Proppant diagenesis has been a hot topic since the day it was proposed. According to (Nguyen, Weaver et al. 2008), diagenesis is the alteration of sediments into rock at temperatures and pressures that can result in significant changes to the original mineralogy and texture. It causes a loss of fracture and a reduction of porosity resulting in reduced permeability and fracture conductivity. Nguyen and Weaver also provided photographic evidence of diagenesis, in which silica and aluminum crystal structures are found to be formed on the surface of proppant after

high pressure exposure in laboratory. As for latest research in this field, Raysoni and Weaver used static hydrothermal screening test method to test the validity of diagenesis. Raysoni and Weaver mentioned in their experiments (Raysoni and Weaver 2012; Raysoni and Weaver 2012) that, this method permitted a process to rapidly determine the relative proppant compatibility using actual formation core samples. Conclusions Raysoni and Weaver drew from static hydrothermal screening test method is that diagenesis chemistry does occur at realistic reservoir temperatures, and significant loss of permeability and proppant strength does occur "rapidly". They also obtained the quantification of decreased permeability of selected proppant pack. Unlike Wearver and his colleagues, Duenckel and Conway also did relevant research on diagenesis effect(Duenckel, Conway et al. 2011). Duenckel and Conway did both static hydrothermal screen test and ISO 13503-5 on proppant samples. The conclusions they draw from their experiments are diagenesis effect does occur in static testing but only in static testing. While in ISO 13503-5 test, diagenesis effect did not form under extended conductivity testing under flowing conditions with reservoir shale core at high temperatures and stress, and thus there is not yet evidence that zeolite precipitation poses significant concern in actual propped fractures. They also proposed that while no mechanical load was applied during the static test, standard saturated steam tables show that water in a closed container at 400 ℉ will generate about 250 psi of isostatic pressure, sufficient to activate the stress corrosion mechanism, which might be the reason of permeability decrease after proppant samples' aging.

Both of these papers are published in recent years, although some of the contents are contradict with each other, they tell us some significant points about diagenesis effect. In our opinions, the ISO-13503-5 long term conductivity test Duenckel and Conway did might not provide sufficient time for diagenesis effect to be revealed; the static hydrothermal screen test Raysoni and Weaver conducted did failed to report the crush percentage of tested proppants, and thus omit the possibility of crushed proppants impairing proppant pack permeability. Both of

these experiments should be refined to provide a more subjective result. We still take greater confidence in the existence of diagenesis effect under real conditions due to collections of mivrographs from a test in which efforts were made to identify this material formed during testing.

Chapter 3

Problem Statement

With improved drilling and completion technologies during the past decades, the development of unconventional shale oil and gas resources becomes viable and more and more important to the industry.

Hydraulic fracturing is the most effective stimulation method for tight gas reservoirs but there are still possible damages to hydraulic fracture that may decrease productivity. Possible damage factors: multi-phase flow of gas and water, proppant crushing, proppant embedment, proppant scaling, proppant diagenesis, interaction of fracture fluid and flowback fluid with existing natural facture and unpropped hydraulic factures, capillary, reservoir compaction, etc. Although there are laboratory evaluations of the damages above, we are yet to quantify each impact on gas recovery. As an extension of Osholake's work, the objective of this research is to understand and numerically simulate effect of three pertinent damage factors on fracture fluid cleanup and long-term gas recovery.

In this research, we first understood the mechanisms of three damages, interaction between formation rock and fluid, proppant scale and proppant diagenesis. We then built numerical models, conducted parametric studies, and quantified the impact of each damage factor on facture fluid flowback and long-term gas recovery. The new understanding would help engineers design better facture treatment in Marcellus Shale gas reservoirs.

Chapter 4

Damage Mechanisms

Hydraulic fracturing has been widely used in the industry. Hydraulic fracturing tends to increase the productivity of shale gas wells if applied successfully. One of the most important facts is massive hydraulic fracture activity without appropriate caution may lead to severe damage to both the formation and fracture.

In this thesis, three major damage effects were investigated: 1interaction of fluid and formation rock, 2 proppant scale, and 3proppant diagenesis.

4.1 Interaction between fluids and formation rock (N.F. and unpropped H.F.)

Many hydrocarbon producing formations contain clays that can influence primary results. Clays are present in a majority of hydrocarbon bearing formations and their presence can cause many problems in the production of oil and gas. All of clays are capable of migrating and causing permeability damage when a formation is contacted by foreign fluids. Clay composition and their location in the rock permeability can vary extensively. Normally, fluids foreign to a formation alter the ionic environment which is responsible for the clays being dislodged from their original positions. A change in the swelling or water retention of montmorillonite enhanced their probability of migrating. Thus, any time a clay is present, it can be assumed that permeability damage may occur if the proper precautions are not observed. The degree of damage will depend upon the concentration and types of clays present, their relative position on the rock and the severity of the ionic environmental change (Hower 1974).

The nature of shale and clay

Shale is a mixture of clay minerals and silt laid down in a very low-energy environment, principally by settlement from still water. Silt consists of fine particles, mostly silica, with small amounts of carbonates and other nonclay minerals. The solids of a typical shale may be consist of up to about 50% clay. Fig 1 shows the typical composition of shale (Dewan 1983).

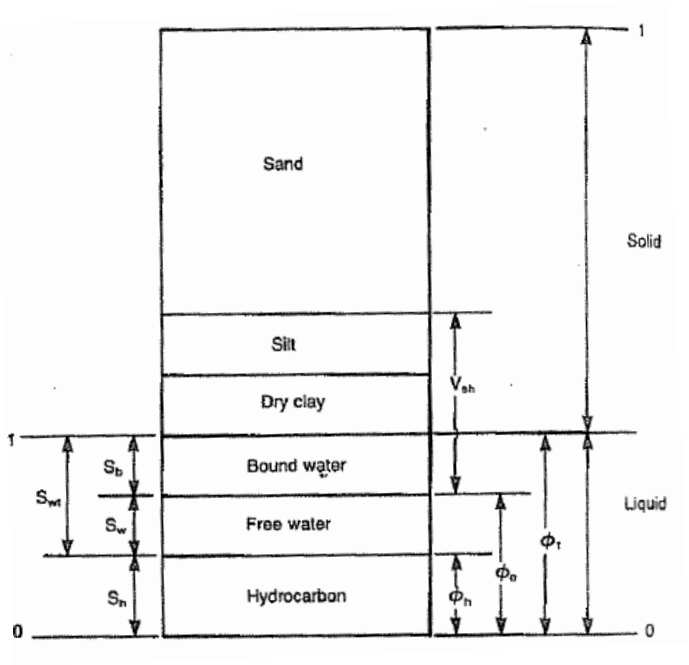

Figure 4-1 Partitioning of a shale in Dual-Water Model (Dewan 1983)

Clay is comprised of crystalline clay minerals, as is shown in Figure 4-1. Clay minerals are classified into four specific groups according to their crystal-structure, which are montmorillonite, illite, kaolinite and chlorite (Dewan 1983).

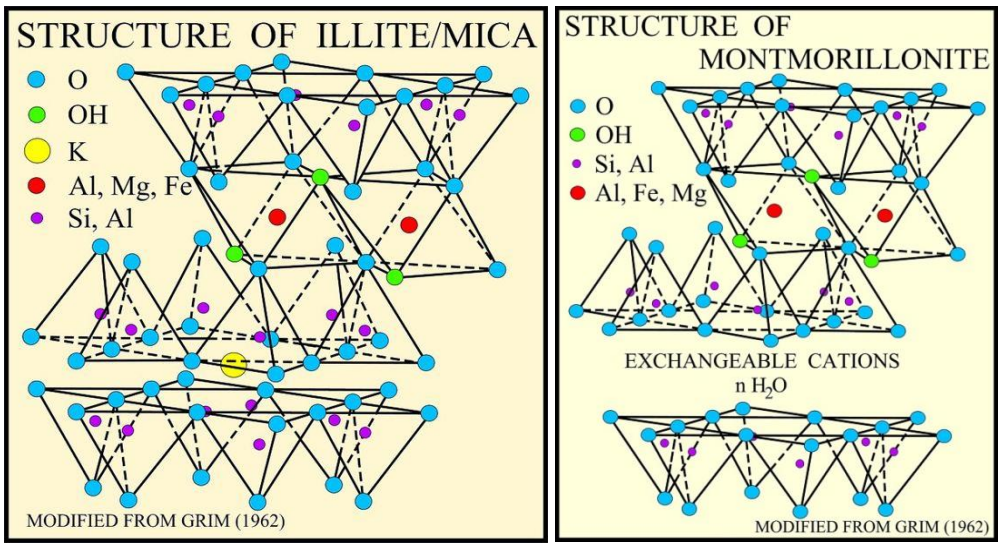

Figure 4-2 Structure of Illite/Mica and Montmorillonite

The distribution of clay could be: laminated, dispersed, and structural, as is shown in Figure 4-3.

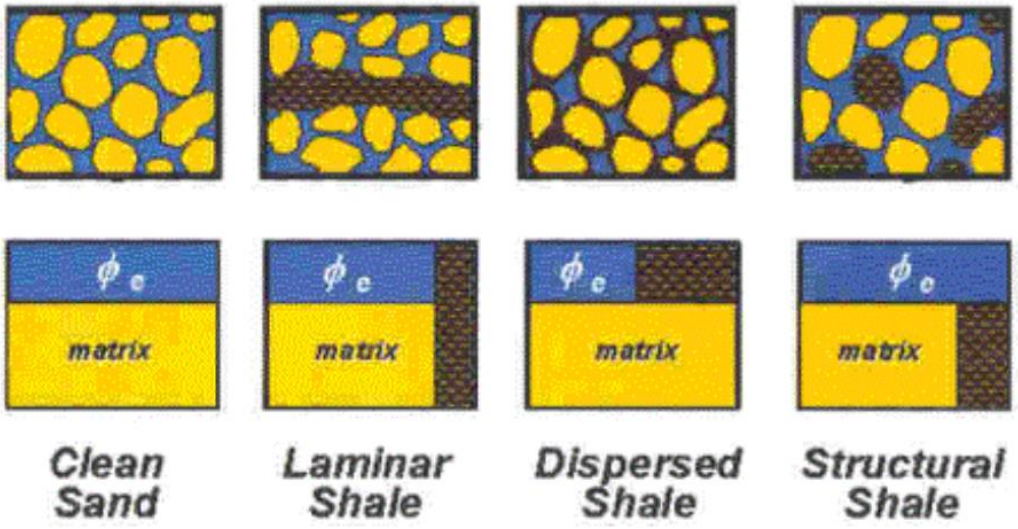

Figure 4-3 Clay distribution (www.spec2000.net/11-vshbasics.htm)

Damage mechanism

Damage effect resulted from interaction between fluid and shale formation can be resulted in two aspects: clay swelling and clay migration.

As is mentioned earlier, clay is normally of crystallized form. Invasion of aqueous phase into the matrix causes swelling of clay porous rocks. The damage mechanism is controlled by absorption of water by a water-exposed-surface hindered diffusion process. When clays are exposed to low salinity solutions it causes formation damage, as swelling clays imbibe water into their crystalline structure, enlarge them in size, and hence plug the pore space (Bahrami, Rezaee et al. 2011). This circumstance is shown in Fig 4. We can see from the figure that after absorption, montmorillinite swells to a larger extent. This is basically how clay swells after the contact of water.

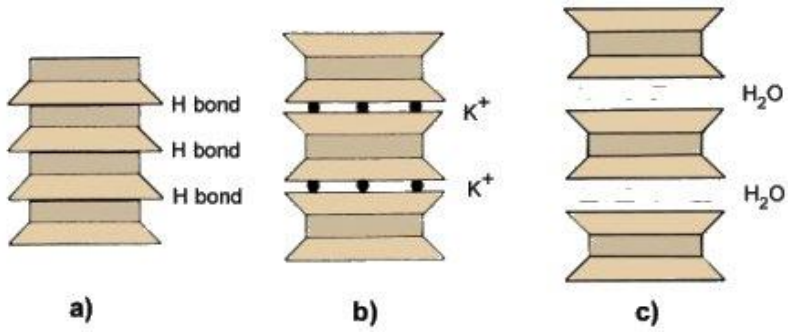

Figure 4-4 Montmorillinite interact with H_2O

The clays may be classified as swelling and nonswelling. Montmorillonite is the only clay that swells by absorbing ordered water layers between clay crystals. Mixed layer clay, which contains montmorillonite, will also swell, although the illite portion of this clay is relatively non-water swelling. Kaolinite and chlorite, as well as illite, may be classed as non-water swelling clays. They do not build viscosity in water as effectively as montmorillonite since their crystals tend to remain as packets instead of being dispersed as do the montmorillonite crystals. However, we must not ignore the fact that these so-called non-water swelling clays do adsorb some water. Thus, all clays do adsorb water with montmorillonite adsorbing the most (Hower 1974).

Clay migration will also cause permeability damage under fluid flow. According to reference, when fluid pass though effective permeability zone, some narrow pass ways could be

blocked by dispersed clays or other fines, and thus result in aggravated permeability damage. This overall effect is primarily found during the flow of water.

Sources of damaging fluids

Most common damaging fluids are filtrates from drilling fluid, cement, workover fluids, water flooding and stimulation fluids. Some of these fluids remain in the rock for long periods of time and penetrate the rock to different depths. Such water can also affect the hardness of many sand formations. The dissolving of only a small amount of minerals that were acting as cementing agents for the rock could release clays and feldspars from their original positions. High pH solutions that contain very little dissolved salts will act to disperse clays thus compounding the problem of clay migration (Hower 1974).

Possible solutions for clay migration

Clay problems should be considered by the well operator in the initial planning of the well (Hower 1974). Damage caused by fluid invasion can be minimized by choosing the proper base fluid for facture treatments. Muds and cement slurries can be treated with potassium chloride to minimize damage when fluid is lost to the formation (Hower 1974). The addition of 2% KCl to water-based fluid for temporarily controlling clay swelling is widely accepted as a standard practice for a very long time. Research on the technology of matrix acidizing treatments has revealed that the use of 2% KCl transforms into 1.5% saltwater as a result of ion exchange. The 1.5% saltwater solution is too weak to prevent clay swelling. Clay swelling can be prevented using a 1 molar (7%) KCl salt solution as is introduced by reference (Gijtenbeek, Neyfeld et al. 2006).

Wellbore heating is also a treatment that can remove aqueous phase traps around the wellbore. Electrical heaters can be used to elevate downhole temperature high enough such that water is vaporized into the gas phase, resulting in reduced water saturation around the wellbore (Bahrami, Rezaee et al. 2011).

Experimental quantification

Conway and his colleages (Conway, M. W., J. J. J. Venditto et al. 2011) conducted a serious of experiments regarding clay stabilization and flow stability in various north American gas shales. In this test, they adopted flow test on several shale samples. The schematic figure is shown in Figure 4-5**.** In the figure we can see that a core sample of Marcellus shale was firstly cut from middle, then confined with stress that is similar to σ_{min}, then different fluid were flown though the core sample in sequence, during the experiment, conductivity value was measured. The sample was firstly treated with 7% KCl after hexane and was marginally stable, and less so to synthetic produced water, and completely lost flow capacity with fresh water containing 2 Gallon/ 1000 gallon Choline Chloride.

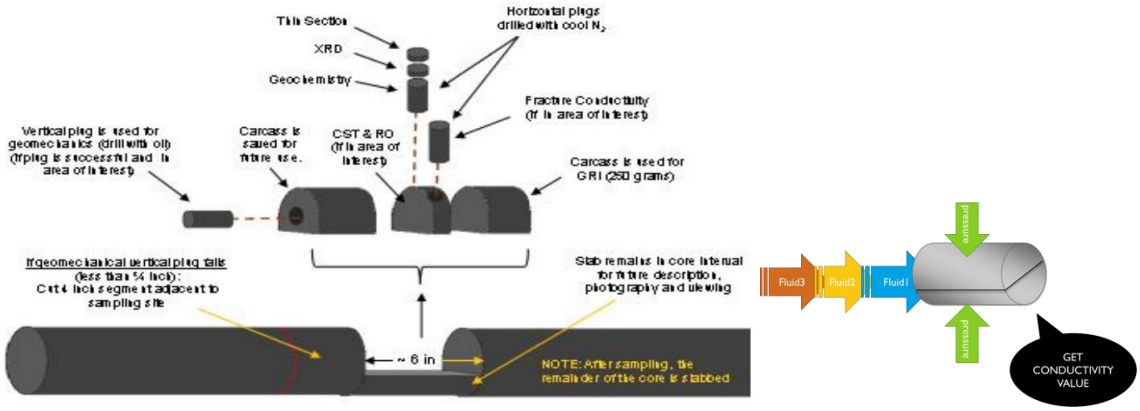

Figure 4-5 Sampling procedure to obtain representative samples for testing from heterogeneous reservoirs and schematic of Conway's experiment on clay stabilization (Conway, M. W., J. J. J. Venditto et al. 2011)

The data acquired in the test is shown in the following **Figure 4-6**.

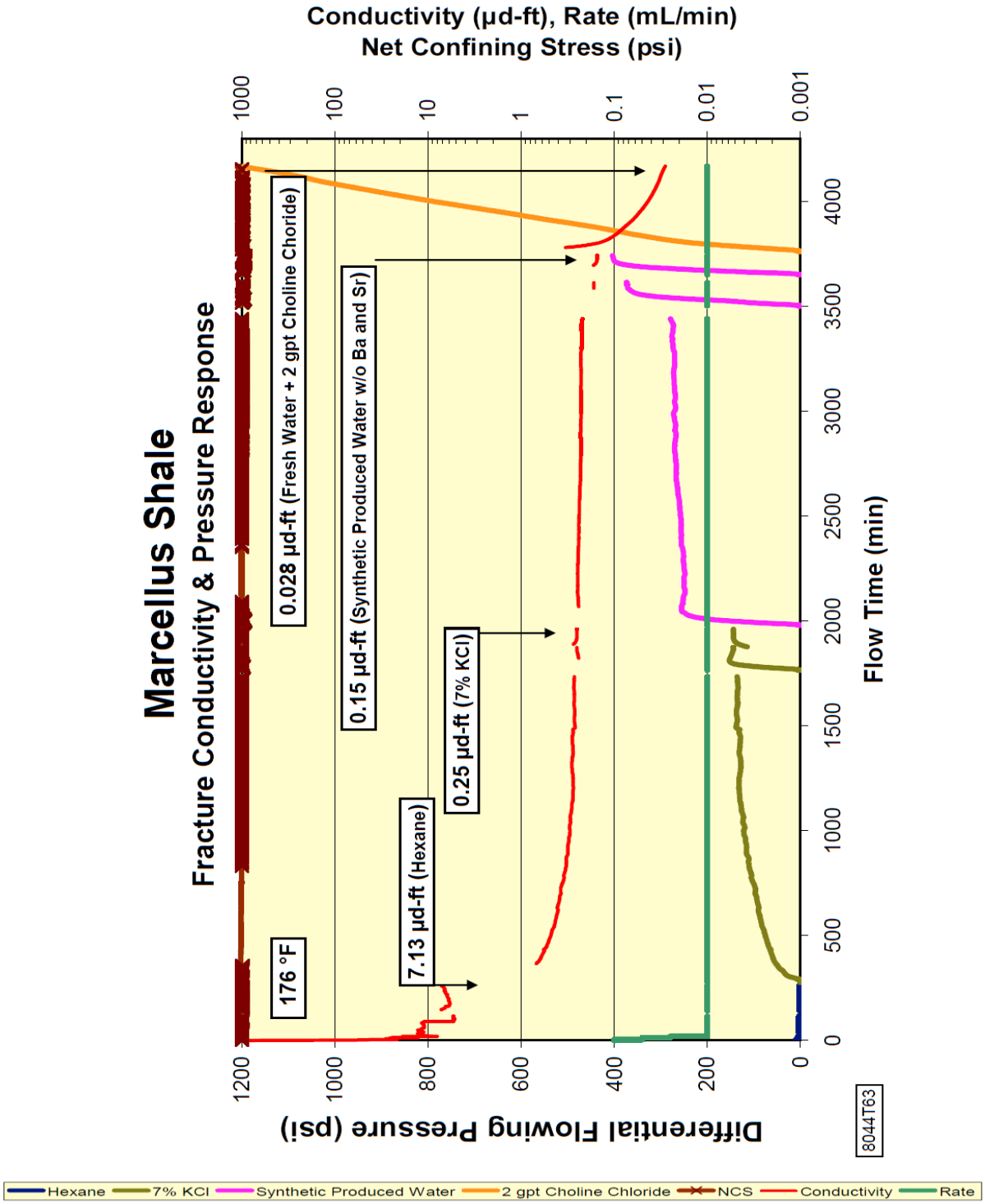

Figure 4-6 Flow characteristics of various salinity fluids through a created fracture in Marcellus Shale (Conway, Venditto et al. 2011)

7% KCl is regarded as fracture fluid, which, in our case, is the first kind of fluid that is in contact with formation. The synthetic produced water w/o Ba and Sr, in our case, can be regarded as the formation water. Fresh water can be regarded as aquifer water. As we can acquire from previous literature review from (Mackay 2010), fluid will be produced in a sequence of formation water, injected water, and aquifer water. When taking into consideration of the first contact of foreign fluid with formation rock during hydraulic fracture, the sequence from fluids that affect formation rock will be injected water, formation water, injected water, and aquifer water.

Extracting data from the previous figure, we can conclude in the following Table 4-1. In Gale's work (Gale, Reed et al. 2007), he did an investigation on natural fracture works on Barnett Shale. He found out that the width of the natural fractures range from 0.003mm to more than 1mm. Considering the procession of the core sample in Conways's experiment, 0.65mm should be a moderate value of the width of the unpropped natural fracture. After transforming conductivity into permeability, we can get the data we need in the simulator.

Table 4-1 Data extracted from Conway's experiment

Fluid	7% KCl	Synthetic produced water	Fresh water	Constant value
Conductivity (last point) / ud-ft	0.25	0.15	0.028	0.2
Permeability / md	0.1172	0.0703	0.0131	0.0938

4.2 Interaction between fluids and proppants

Hydraulic fracture stimulation is widely used to improve the economics of hydrocarbon production from a reservoir. In many of these fracture stimulations, the fractures are "propped open" by filling them with a high-permeability pack of granular material (proppant) that ideally provides a highly conductive pathway from the reservoir to the well (Garzon, Solares et al. 2009).

However, post-fracture-stimulation well testing indicated that conductivity values obtained from lab are often one to two orders magnitude too high. In many fields, the productivity of fractures declines rapidly. In addition, many stimulated wells show loss of fracture conductivity with time, leading to reduced productivity and lost revenue (Garzon, Solares et al. 2009).

Pressure transient analysis and fracture conductivity

A fracture generated during a hydraulic-fracturing treatment is a fluid conduit and has conductivity. This conductivity is responsible for the difference in the pre- and post-fracturing well productivity. Cikes (Cikes 2000) used pressure transient analysis of post-frac pressure build up data to demonstrate that fracture conductivity decreased dramatically in high-temperature wells that were propped with high-strength proppants. He suggested that there must be some unknown damage mechanism causing the dramatic conductivity decline even in the wells that were not on production (Garzon, Solares et al. 2009).

Proppant pack conductivity decline: what counts

The hydraulic conductivity of a proppant pack more than a monolayer thick is limited by the porosity of the pack. The most efficient packing of particles is a rhombohedral arrangement that can produce a pack porosity with about 26% void space (Lehman, Parker et al. 1999). Small changes in pack porosity result in significant changes in pack permeability and fracture conductivity. Fracture conductivity is designed by controlling concentration of proppant used to hold the fracture width open and is limited by the porosity of the pack (Garzon, Solares et al. 2009).

Rapid loss in fracture conductivity has been attributed to, according to many researchers, frac gel damage, embedment, proppant crushing, and fines invasion, proppant scale, proppant diagenesis, etc. All these damage mechanisms have been well studied in the laboratory, resulting in materials and methods employed to minimize their effect on conductivity. While these methods have improved productivity, stimulated wells rarely achieve the theoretical conductivity expected from a given proppant. In addition, fracture conductivity often declines continuously, suggesting that there are other factors that influence long-term fracture conductivity (Garzon, Solares et al. 2009).

4.2.1 Proppant scaling

Fines are generally thought to be sourced by the crushing of proppant that occurs during fracturing-treatment operations, fracture closure, and closure-stress cycles during well production. In addition, some quantities of fines and formation debris are created during the initial fracture. In some cases, fines are produced from the formation matrix itself. Reactions of chemical elements in connate formation fluid and fracture fluid, pressure drop of nearly fully saturated solutions are all possible sources of chemical precipitation.

Wells completed with gravel packs, high-rate water packs, or frac-packs often respond with high productivity initially for some period of time. However, after this high initial production, the production flow rates begin to drop off, indicating the flow paths have been choked off. The well operators often perform acid treatments on proppant packs or frac-packs to help rejuvenate the well production after verification that the production decline was caused by fines plugging or scale deposit. The well production is often restored, but this is usually temporary. Scale precipitation reappears within the pore spaces of the formation matric or proppant pack, or builds up in downhole tubing because the scaling conditions still exist. Scaling problems are often an issue in fields (Lehman, Parker et al. 1999).

Evidence of chemical scaling

Evidence of in-situ chemical precipitation has been obtained from many wellbores. Figure 4-7 shows a proppant grain that was recovered from a producing well where conductivity loss had caused a severe production decline. This conductivity loss was largely attributed to siderite precipitation in the proppant pack. Figure 4-8 shows an example of geochemical precipitation that occurred post-stimulation during production. In this coal bed methane example, a calcium-carbonate species attaches to proppant grains by using coal fines or other organic particulates as nucleation sites (Lehman, Parker et al. 1999).

Figure 4-7 Ceramic proppant grain recovered from a downhole bailer sample following a postfracture production decline. The pore-filling texture is evidence of in-situ siderite precipitation. In this case, the proppant grain is a nuleation site for the geochemical precipitate (Lehman, Parker et al. 1999).

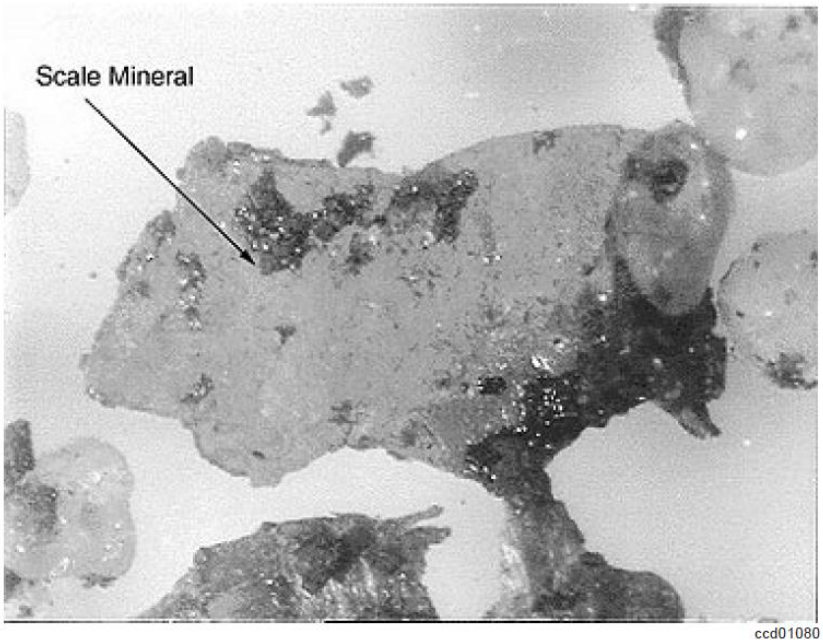

Figure 4-8 Geochemical precipitates affixed to coal fines recovered from a wellbore, marked by a premature, rapid decline in productivity. Precipitate textures revealed a combination of calcium carbonate, quartz proppant, and fines (Lehman, Parker et al. 1999).

According to many researchers, chemical precipitates have played a significant role in fracture conductivity reduction. Chemical precipitation occurs downhole during or after the hydraulic placement of proppant in a fracture. Aqueous fluid and formation equilibria or disequilibria govern the precipitation of primarily inorganic substances. The mineralogies observed and predicted can vary widely, but usually consist of carbonate species, sulfides, and various forms of iron oxides/hydroxides. Mechanisms controlling the precipitation and consequent loss of conductivity are explained through phase equilibria. These equilibriums involve a wide range of aqueous-fluid parameters including Eh, pH, partial pressure to various gases such as CO_2, and fugacity of sulfide (Lehman, Parker et al. 1999).

In another work done by Garzon and Solares (Garzon, Solares et al. 2009), the OLI's ScaleChem (2001) prediction program was used to simulate the deposition environment in the sandface area and production string. According to his simulation scale did happen, and calcium carbonate and iron sulfide are the most likely mineral scales depositing in the sandface area. He also simulated the influences of scale on well productivity when mineral scales accumulate in both sandface area, he observed significant drop of gas production when mineral scales are applied.

For mineral scales precipitating in the production strings, he analyzed 35 solid samples collected from the tubular of different gas producers. Figure 4-9 shows the distribution of mineral-scale compounds found in 35 collected solid samples, grouped by generic type.

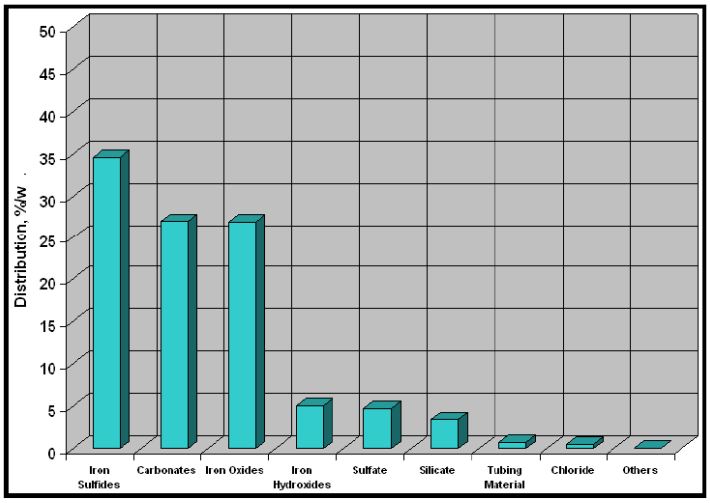

Figure 4-9 Distribution of mineral scale compounds found in 35 collected solid samples, grouped by generic type (Garzon, Solares et al. 2009)

Experimental quantification

To get an understanding of the quantification of this damage, we adopted the laboratory data from Weaver 2010's work(Weaver and Nguyen 2010). In their work, they constructed a serious of experiments to test the effectiveness of WBAA agent in preventing fines migration and proppant scale. Within their researches, the part of proppant scale is of our most concern.

In the experiment, the Teflon flow cells (1-in. ID and 4-in length) were packed with 20/40-mesh sand, simulating the proppant pack Pressure transducers were installed at the inlet and outlet of the flow-cell assembly as means to measure the pressure drop across the sand pack during fluid injection. The back pressure regulator was set at 800 psi. The sand pack was first saturated with four pore volumes (~100 mL) of 3% KCl brine. The cell assembly containing the sand pack was then heated up to 200 ^{o}F. This temperature was maintained during the entire flow period of the experiment.

The test used a flow rate of 1 mL/min of a solution that was combined at a 50:50 ratio from two different brines (shown in Table 4-2) immediately adjacent to the inlet of the flow cell.

These two brines, once mixed together, simulated a seawater source that can form $CaCO_3$ scale. The pressure drop across the sand pack was recorded during the injection of the brine mixture through the sand pack. A pressure increase versus time indicates a restriction of the flow path caused by scale buildup within the sand matrix. The blue line in Figure 4-10 illustrates this phenomenon. Figure 4-11 is the assembly of the experiment.

Table 4-2 Composition of brines for forming $CaCO_3$ scale

Brine 1		Brine 2	
Composition	g/L	Composition	g/L
NaCl	49.59	NaCl	49.59
$CaCl_2.2H_2O$	7.48	$NaHCO_3$	1.38
$MgCl_2.6H_2O$	4.43	_	_
KCl	2.0781	_	_
$BaCl_2.2H_2O$	1.0138	_	_
$SrCl_2.6H_2O$	0.8824	_	_

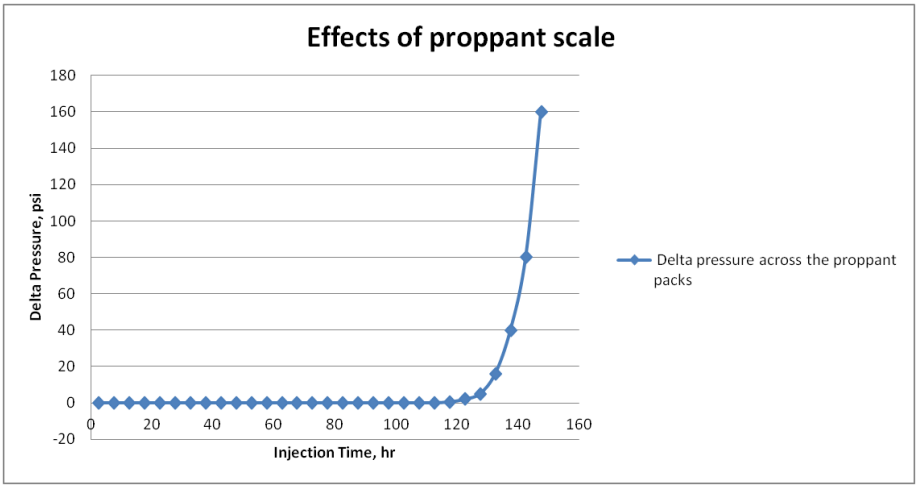

Figure 4-10 Delta pressure across the proppant packs

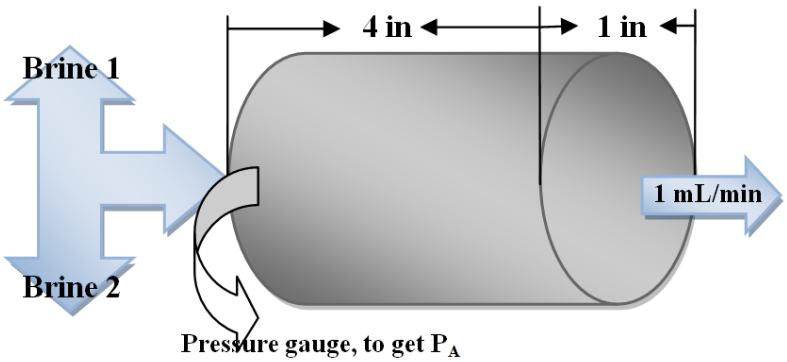

Figure 4-11 Configuration of experiments assembly

What worth noticing is that, delta pressure shown in Figure 4 is delta P_A, which represent the increased pressure at one location but different time. P_A^{n+1}- P_A^n.

According to Darcy's law:

$$Q = \frac{-KA(P_B - P_A)}{\mu L}$$

Transform into:

$$K = \frac{Q\mu L}{-A(P_B - P_A)}$$

According to the definition of Darcy, the unit of permeability, we did the unit convert for each of the components in the above equation, shown in Table 4-3.

Table 4-3 Unit convert table

	data in paper	unit	convert factor	data in simulator	unit
ID	1	in	2.54	2.54	cm
length	4	in	2.54	10.16	cm
Q	1	mL/min	0.0167	0.0167	cm3/s
A	0.785	in2		5.064506	cm2
T	200	F		93.333	C
backpressure(basic)	800	psi	14.696	54.4368	atm
Viscosity(water@200F@800psi)				1	mPa.s

The calculated permeability change is shown in the following table. The right most column is the incremental decrease of permeability value in the proppant pack in md. According to the table below, 5080 md is the expected permeability drop in the proppant pack. We can observe that water injection in our model is supposed to last for 6 days, but according to data in the following table**,** by the sixth day, permeability change become very close to 0.

Table 4-4 Calculated permeability change

Time, day	Time, hr	Delta pressure, psi	Back pressure, atm	Delta permeability, md	Delta permeability incremental, md
0.104167	2.5	0	0	NAN	
0.3125	7.5	0	0	NAN	
0.520833	12.5	0	0	NAN	
0.729167	17.5	0	0	NAN	
0.9375	22.5	0	0	NAN	
1.145833	27.5	0	0	NAN	
1.354167	32.5	0	0	NAN	
1.5625	37.5	0	0	NAN	
1.770833	42.5	0	0	NAN	
1.979167	47.5	0	0	NAN	
2.1875	52.5	0	0	NAN	
2.395833	57.5	0	0	NAN	
2.604167	62.5	0	0	NAN	
2.8125	67.5	0	0	NAN	
3.020833	72.5	0	0	NAN	
3.229167	77.5	0	0	NAN	
3.4375	82.5	0	0	NAN	
3.645833	87.5	0	0	NAN	
3.854167	92.5	0	0	NAN	
4.0625	97.5	0.0005	0.007348	4550.275478	4550.28
4.270833	102.5	0.005	0.07348	455.0275478	5005.30
4.479167	107.5	0.05	0.734798	45.50275478	5050.81
4.6875	112.5	0.1	1.469595	22.75137739	5073.56
4.895833	117.5	0.5	7.347975	4.550275478	5078.11
5.104167	122.5	2	29.3919	1.137568869	5079.25
5.3125	127.5	5	73.47975	0.455027548	5079.70
5.520833	132.5	16	235.1352	0.142196109	5079.84
5.729167	137.5	40	587.838	0.056878443	5079.90
5.9375	142.5	80	1175.676	0.028439222	5079.93
6.145833	147.5	160	2351.352	0.014219611	5079.94
…	…	…	…	…	…

Scaling influences

Thick deposits of various types of mineral scales are presently forming in the tubulars and formation of gas producers. These mineral scales precipitated when ideal thermodynamic conditions combine with dissolved minerals present in formation waters. Without remedial action over time, these deposits can grow thicker and end up plugging tubulars and the reservoir.

4.2.2 Proppant diagenesis

According to Nguyue and Weaver (Nguyen, Weaver et al. 2008), earth diagenesis occurs over geological time when permeable sandbeds are buried by subsequent deposits, resulting in exposure to high closure stress at high temperature. The sandbeds, through geochemical reactions, are converted to low-porosity, low-permeability rock.

Most hydrocarbon-bearing formation that require hydraulic fracturing to produce economically are mature, have already undergone diagenesis, and typically have high closure stress and temperature conditions. When the rock is cracked and packed with virgin proppant, conditions are right to promote geochemical reactions that cause diagenetic reactions to begin filling the porosity of the proppant pack. These reactions are, surprisingly, faster than normally expected.

The solubility of quartz is approximately 50 ppm at room temperature and increase proportionally with temperature. However, when two quartz grains are brought into contact, and a high mechanical stress is applied, the solubility at the contact points is greatly increased because of the strain placed on the molecular bonds. As the solubility at the contact points is greatly increased because of the strain placed on the molecular bonds. As the soluble silica diffuses through the water film to the pore space, the solution in the pore space becomes supersaturated

because it is no longer under high mechanical stress and subsequently precipitated, thereby reducing the pore volume as is shown in Figure 4-12.

Reduction of pore volume results in two effects: (1) the removal of material from between the grains flattens the surface between them and leads to compaction, which causes a loss of fracture width if the proppant is supporting a packed fracture and (2) a reduction of porosity resulting in reduced permeability and fracture conductivity. Both of these mechanisms depend on the presence of a wetting water film for the reactions to occur. These two effects are shown in Figure 4-13.

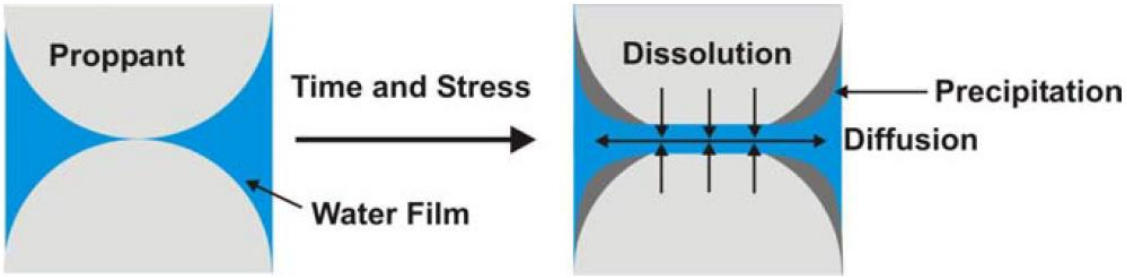

Figure 4-12 Illustration of the compation and solution mecanisms(Nguyen, Weaver et al. 2008).

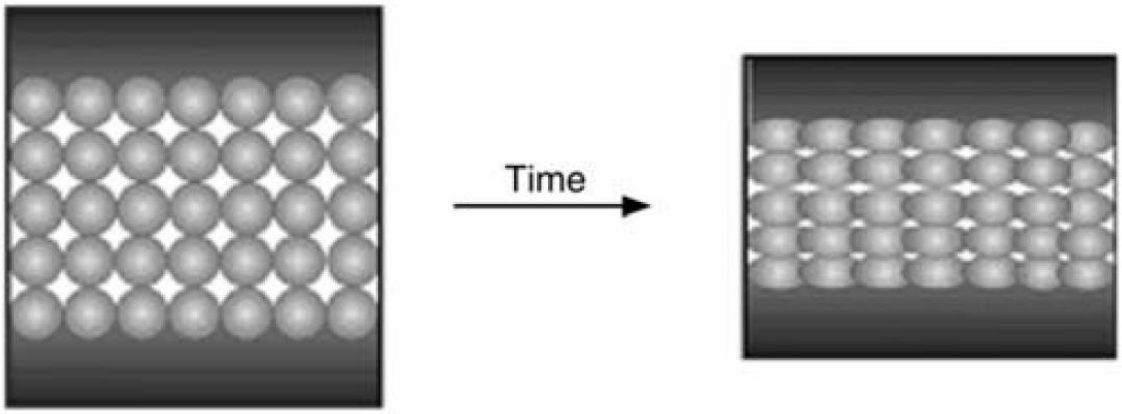

Figure 4-13 Schematic showing how a packed faracture with uniform-sized proppant might undergo diagenetic compaction resulting in loss of fracture width, pack porosity, and permeability (Nguyen, Weaver et al. 2008).

Figure 4-14 is a collection of micrographs from a test in which efforts were made to identify this material formed during testing. Zooming in by EDX on various areas of interest in

the sample provided considerable insight. The silica-to-aluminum ratio observed for the proppant was 0.9, as is typical for the ceramic proppant, while that for the Ohio Sandstone was 8.4. The porosity-filling precipitate was found to be 4.9, or an intermediate concentration of these metals. Visual inspection of the proppant packs after exposure reveals numerous areas of crystalline growth, as shown in the last two micrographs. The 2.8 ratio of Si/Al is characteristic of some clay minerals.

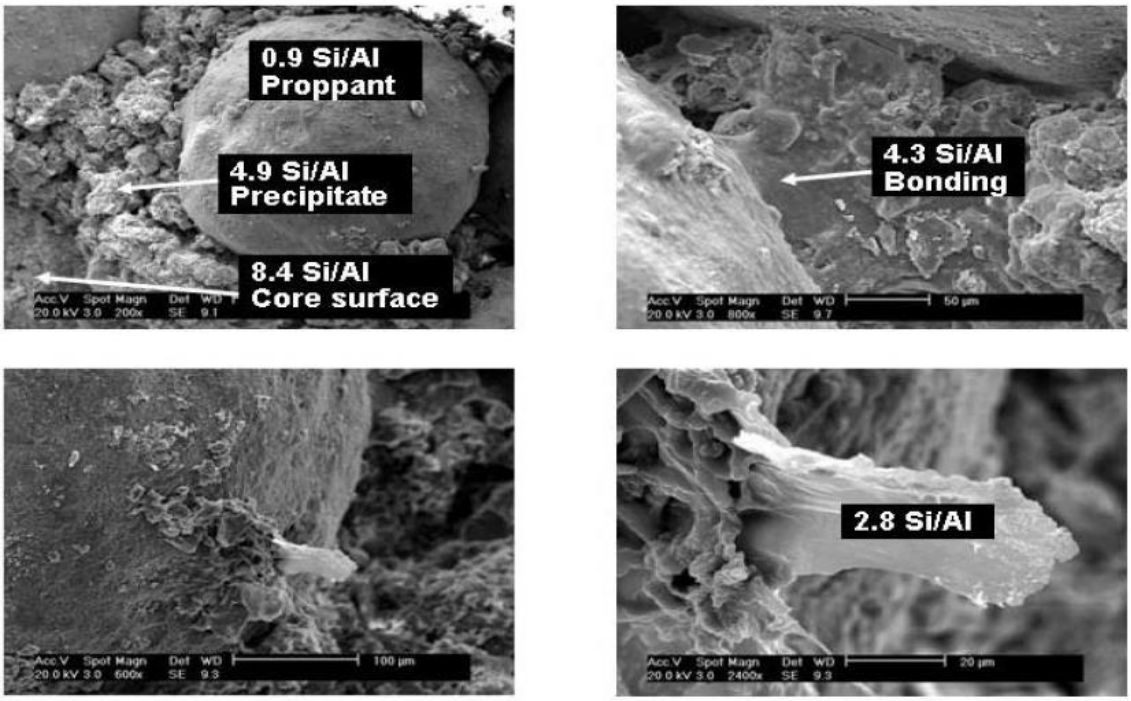

Figure 4-14 Micrographs shoing the apparent embedment of a 20/40-mesh ceramic proppant into Ohio Sandstone that occurred during conductivity testing at 6,000 psi closure stress and 225 ℉ (Nguyen, Weaver et al. 2008).

It is apparent from these observations that some sort of geochemical reaction is taking place when high mechanical stress is applied to the proppant by Ohio Sandstone in aqueous media, and that these reactions seem to be attenuated by temperature.

Diagenesis testing methods

Since diagenesis effect is firstly proposed by Weaver in 2005, this effect is still a comparatively new topic. Testing method regarding this damage effect is at a stage of fast improving. In the experimental data we adopted in this thesis, there are two kinds of relevant testing methods, static hydrothermal screening test method and ISO 13503-5 procedures for measuring the long term conductivity of proppants. The reason of addressing this section is that it is useful to explain the disagreement among different scientists in explaining diagenesis.

Static hydrothermal screening test method. Raysoni and Weaver mentioned in their experiments (Raysoni and Weaver 2012; Raysoni and Weaver 2012) that, this method permitted a process to determine the relative proppant compatibility using actual formation core samples, scraps, or drill cuttings. This test method used the static-cell proppant-evaluation method, except at realistic temperatures (300 and 450 ℉) and does not include the use of any closure stress. It was recognized that the lack of closure stress would provide an artificially low value on the impact of the geochemical attack on the proppant pack. It employed a simple test chamber filled with the selected proppant mixed with a sandstone formation sample that had been crushed and sized to be slightly larger than the proppant grains. The core space was typically filled with deionized water at a pH of 7. Once filled and initial permeability was determined, the chamber was sealed and placed in an oven at the test temperature and cooked for an extended time. Test times varied from 15 to 180 days, and temperatures ranged from 225 to 550 ℉. At the end of the specific test time, the pore fluid was removed from the cell, the pH was measured, and elemental content was determined. After the final permeability of the pack was measured, samples of the proppant formation, and test-generated fines were analyzed by X-ray fluorescence, SEM, and EDX. A schematic is shown in Figure 4-15.

In one series, only proppant hydrothermal aging is included, indicating a decrease in retained permeability as well as retained strength. A second series was run in which the proppant

was mixed with granulated and sieved formation material, which also provides an overview of the decrease in retained crush strength and retained permeability with increasing test duration. Figure 4-16 and Table 4-5 show the retained permeability data from these experiments. We can see diagenesis could decrease permeability data by 80% after 200 days.

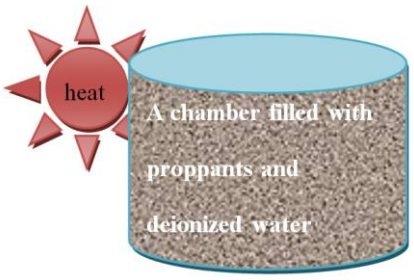

Figure 4-15 schematic of static hydrothermal screening test method

Things worth notice of this testing method are that, firstly there is no flow through the entire test, and secondly there is no external pressure through the entire test.

Conclusions Raysoni and Weaver drew from static hydrothermal screening test method is that diagenesis chemistry does occur at realistic reservoir temperatures, and significant loss of permeability and proppant strength does occur "rapidly".

In order to simulate the effect of proppant diagenesis on 20/40 Ceramics, relevant data was extracted from Jim Weaver's work in 2012. Table 4-5 shows the permeability data Weaver and his colleagues found during their test. The author also put these data into diagrams, and used exponential extrapolation to see the possible effect after 1 year, which is shown in Figure 4-16.

Table 4-5 Permeability data in long-term static-cell proppant evaluation (Weaver 2012)

Time/days		15	45	90	180
Retained permeability/%	Proppant and formation	76	55	49	25
	Proppant only	55	45.5	20	15

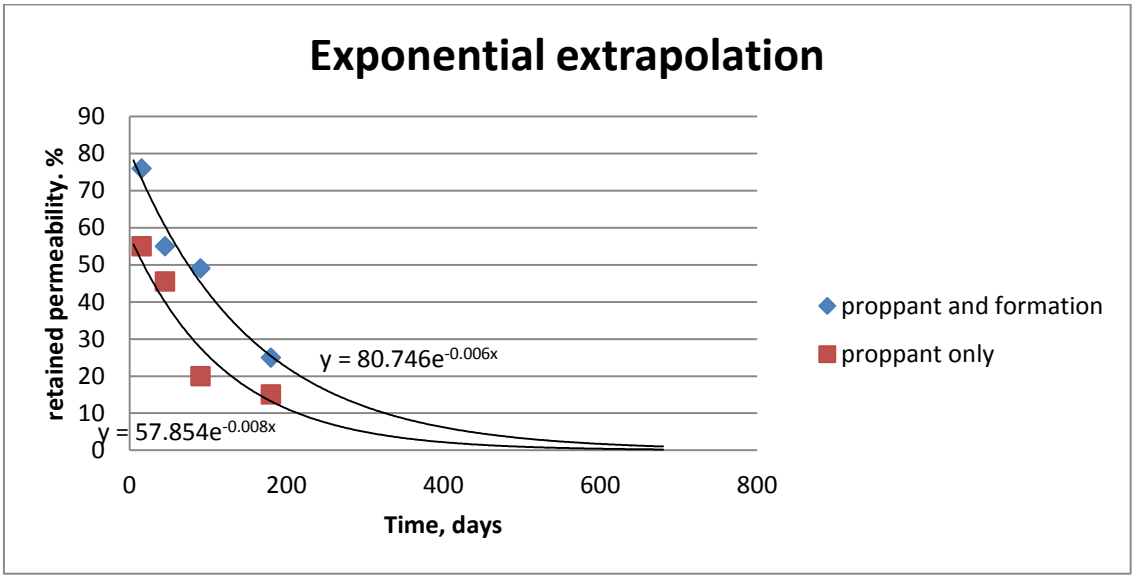

Figure 4-16 Impact of hydrothermal aging at 300 ℉ on a high-strength, aluminum-based proppant alone in deionized water and when mixed with granulated and sieved formation material. (Weaver, 2012)

Data above were used in our simulations. Simulation results are shown in chapter 6.

ISO 13503-5 procedures for measuring the long term conductivity of proppants.

Duenckel and Conway also did relevant research on diagenesis effect(Duenckel, Conway et al. 2011). For long-term conductivity test, they chose to use conventional method, which is ISO 13503-5. Detailed procedures and equipment requirements can be found in (Kaufman, Anderson et al. 2007). The overall long term conductivity procedure consists of applying a closure stress across a test unit for 50h ±2h to allow the proppant bed to reach a semi-steady state condition. As fluid is forced through the proppant bed, the proppant pack width, differential pressure, temperature, and flow rates are measured at each stress level. Proppant pack permeability and conductivity are calculated. A schematic figure is shown in Figure 4-17.

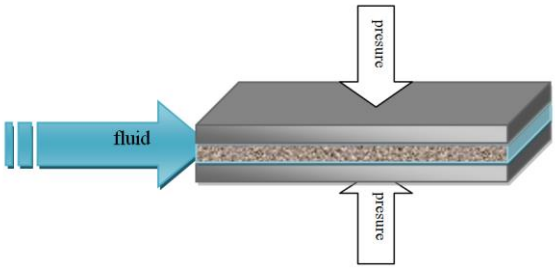

Figure 4-17 A schematic of ISO-13503-5

Test fluid is 2% by weight KCl, at least 99.0% pure, in deionized or distilled water solution filtered to at least 7 micron. It is critical to have a silica-saturated solution flowing through the proppant pack constantly. Ohio sandstone cores should have dimensions of 17.07 cm to 17.78 cm length, 3.71 cm to 3.81 cm wide, and a minimum of 0.9 cm thickness.

What worth noticing about this testing method is that, there is fluid flowing through the cores and proppant pack all the time, and there is external stress applied.

Duenckel and Conway did both static hydrothermal screen test and ISO 13503-5 on proppant samples. Although detailed data will be introduced in later chapters, the conclusion they draw from their experiments are diagenesis effect does occur in static testing but only in static testing. While in ISO 13503-5 test, diagenesis effect did not form under extended conductivity testing under flowing conditions with reservoir shale core at high temperatures and stress, and thus there is not yet evidence that zeolite precipitation poses significant concern in actual propped fractures. They also proposed that while no mechanical load was applied during the static test, standard saturated steam tables show that water in a closed container at 400 ℉ will generate about 250 psi of isostatic pressure, sufficient to activate the stress corrosion mechanism, which might be the reason of permeability decrease after proppant samples' aging.

Comparison between these two papers. Both of these papers are published in recent years, although some of the contents are contradict with each other, they tell us some significant points about diagenesis effect. In our opinions, the ISO-13503-5 long term conductivity test Duenckel and Conway did might not provide sufficient time for diagenesis effect to be revealed;

the static hydrothermal screen test Raysoni and Weaver conducted did failed to report the crush percentage of tested proppants, and thus omit the possibility of crushed proppants impairing proppant pack permeability. Both of these experiments should be refined to provide a more subjective result. We still take greater confidence in the existence of diagenesis effect under real conditions due to collections of mivrographs from a test in which efforts were made to identify this material formed during testing.

Chapter 5

Model Description

In this chapter, we will describe reservoir, facture and fluild properties, and the flow and storage mechanisms in our model. We will also describe how we modeled the interaction of fracture fluid with formation rock and proppant.

5.1 Reservoir, drainage area, and grid block

A two-dimensional, three-phase black oil reservoir simulator was used to model the selected three factors affecting performances of a hydraulically fractured well in the Marcellus shale gas reservoir. Figure 5-1 is a top view of the reservoir model used in this study. We have a square reservoir which has an area of 160 acres with a hydraulically fractured well located in the center. Due to symmetry of the well configuration, we only prepare to test about ¼ of the drainage area. Thickness of the pay zone is 300ft, and well is located at the upper left corner.

The grid block type is cartesian $16 \times 9 \times 1$ system. Each block has the same dimensions (88 ft for width) except for the first row and first column (0.2 ft for width) of the entire block system. Then we locally refined each grid block (2:16 2:16 1) into a 50 by 50 by 1 grid system in order to simulate the natural fracture network. Width of each refined grid range in the pattern of 0.2 ft, 0.8 ft, 3.4 ft ,3.4 ft, 0.8 ft, 0.2 ft, 0.8 ft, 3.4 ft, 3.4 ft, 0.8 ft, 0.2 ft … . Grids with 0.2 ft of width are treated as fractures. Fracture spacing is set as 8.8 ft. The wellbore is located in the 1 by 1 by 1 cell block, and is operated at constant bottom hole pressure. An expanded view of schematic of reservoir model is shown in Figure 5-2.

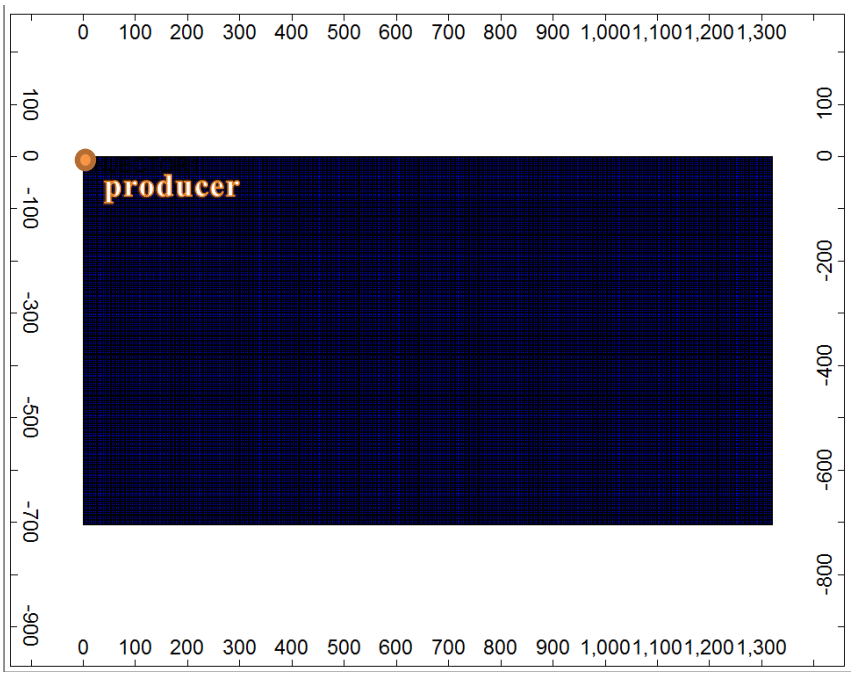

Figure 5-1 A schematic of the reservoir model

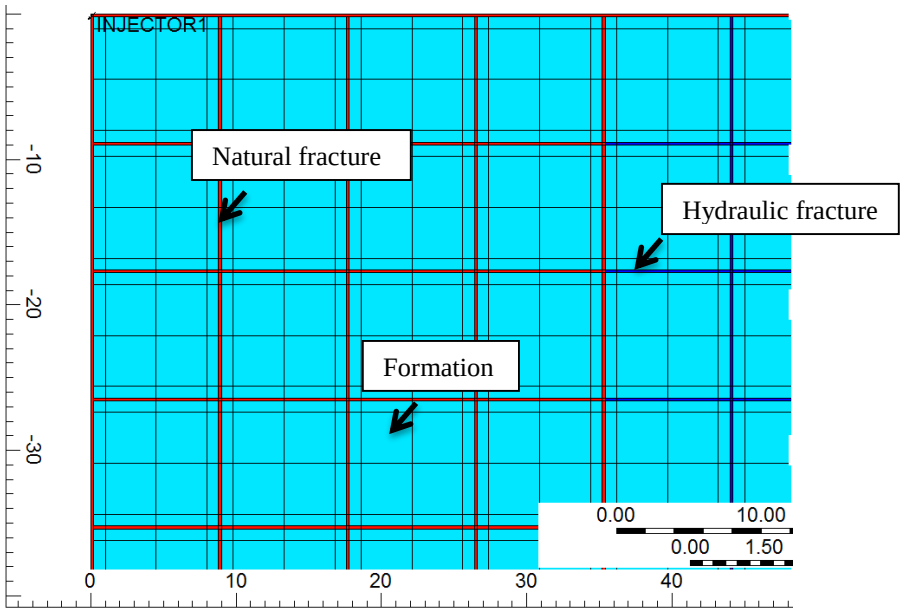

Figure 5-2 An expanded view of the model around well bore.

We can observe grid width pattern clearly in this figure. We can see 6 factures vertically, and 5 horizontally, which are spaced at 8.8 ft. Red lines represent hydraulic fracture, while blue

lines represent natural fractures. Green areas represent formation. Well is located in the upper-left corner.

5.2 Hydraulic fracture and proppant placement

As of now, proppant transportation within the created fracture network cannot be modeled accurately when fracture growth is complex. Proppant placement within the fracture network will be assumed as follows:

- The proppant is evenly and uniformly distributed throughout the complex fracture system
- The proppant is concentrated in a dominant primary fracture that is connected to un-propped complex fracture network

This approach was firstly adopted by (Cipolla et al. 2009) as in Figure 5-3.

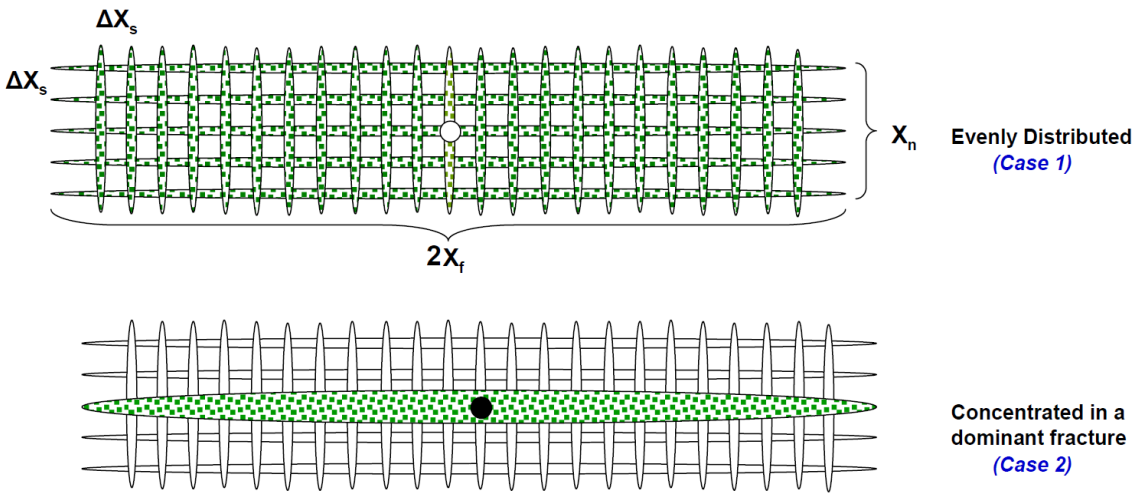

Figure 5-3 Proppant transport scenarios (Cipolla et al. 2009)

In the first scenario, a single hydraulic fracture of 500 ft is created in the first row of the entire grid system along x-direction. Permeability of this hydraulic fracture is set as 65,500 md. This number is obtained from Tunde's research (Osholake, T. A., J. Y. Wang, et al). We name this scenario as H.F.1.

In the second scenario, 5 hydraulic fractures are propped open in x-direction and 10 in y-direction, which gives a network of hydraulic fractures with 836 ft in total length and a stimulated reservoir volume (SRV) of 1,045,440 ft^3. Permeability of this hydraulic fracture network is set as

39,174 md, to maintain the same proppant volume with the first scenario. We name this scenario as H.F.2.

In the third scenario, 9 hydraulic fractures are propped open in x-direction and 10 in y-direction, which gives a network of hydraulic fractures with 1,152.8 ft in total length and a SRV of 2,090,880 ft^3. Permeability of this fracture network is calculated as 23,115 md, by the same method in the second scenario. A schematic of these three kinds of fracture settings are show in Figure 5-4. Permeability within natural fracture is set as 0.4793 md in ideal base model (case 1). (Detailed parameter set can be found in Appendix A). Permeability of matrix is set as 0.0001 md constantly. We name this scenario as H.F.3.

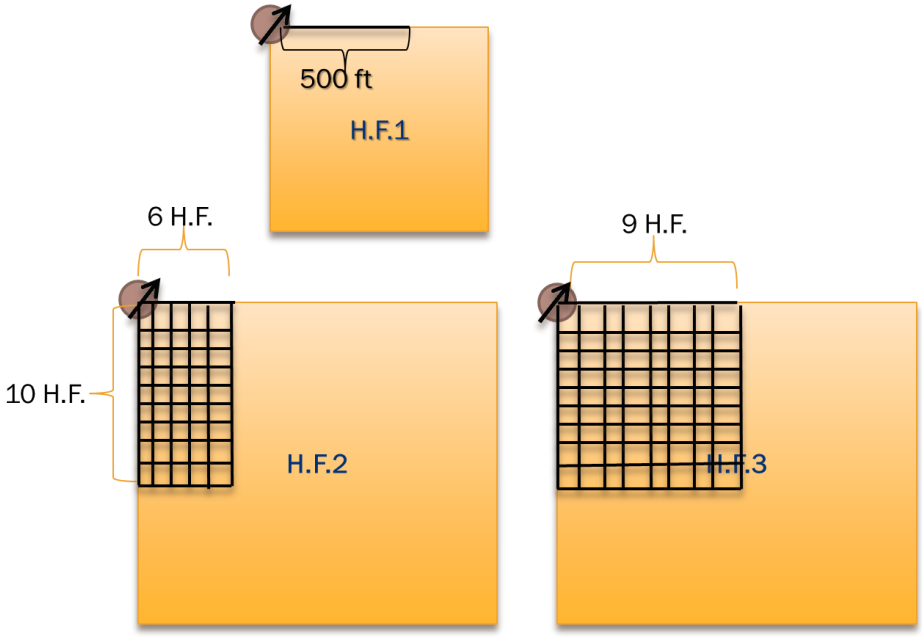

Figure 5-4 A schematic of hydraulic fracture settings employed in the research

Permeability calculation

Detailed permeability calculation of each H.F. scenario is found in the following part.

1. H.F.1

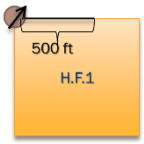

- Proppant volume V:

  V = length of H.F. × formation thickness × width of H.F.

  = 500 ft × 300 ft × 0.2 ft = 30,000 ft^3

  = 30,000 ft^3

- Permeability of H.F. $k_{H.F.1}$:

  $k_{H.F.1}$ = 65,500 md

2. H.F.2

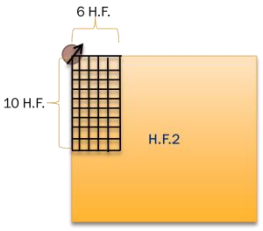

- Total length of propped H.F. L_2:

  L_2 = 8.8 ft × 5 × 10 + 8.8 ft × 9 × 5 = 836 ft

- Width of propped H.F. W_2:

  $W_2 = \frac{V}{L_2 \times 300\ ft} = \frac{30{,}000 ft^3}{836 \times 300\ ft}$ = 0.12 ft

- Permeability of H.F. $k_{H.F.2}$:

  $k_{H.F.2} = k_{H.F.1} \times \frac{W_2}{W_1}$ = 65,500 md × $\frac{0.12\ ft}{0.2\ ft}$ = 39,174 md

3. H.F.3

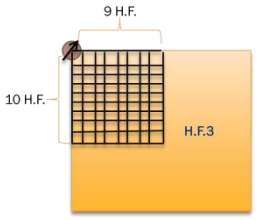

- Total length of propped H.F. L_3:

  $L_3 = 8.8\text{ ft} \times 9 \times 9 + 8.8\text{ ft} \times 8 \times 10 = 1416.8\text{ ft}$

- Width of propped H.F. W_2:

  $W_3 = \frac{V}{L_3 \times 300\ ft} = \frac{30{,}000 ft^3}{1416.8 \times 300\ ft} = 0.07\text{ ft}$

- Permeability of H.F. $k_{H.F.2}$:

  $k_{H.F.3} = k_{H.F.1} \times \frac{W_3}{W_1} = 65{,}500\text{ md} \times \frac{0.07\ ft}{0.2\ ft} = 23{,}115\text{ md}$

Porosity of matrix is set as 0.08. Hydraulic fracture porosity is set as 0.3, and natural fracture porosity is set as 0.1.

Our reservoir is initially saturated with gas (gas saturation is 0.8) and water (water saturation is 0.2). The oil phase is not in existence in our model. Initially, our reservoir is gas saturated and later hydraulically fractured with fracture fluid. During production, both water and gas will be produced.

5.3 Fluid properties

Fluid property values are shown in Figure 5-5, Figure 5-6, Figure 5-7, Figure 5-8, and Figure 5-9 (Osholake, Wang et al. 2011).

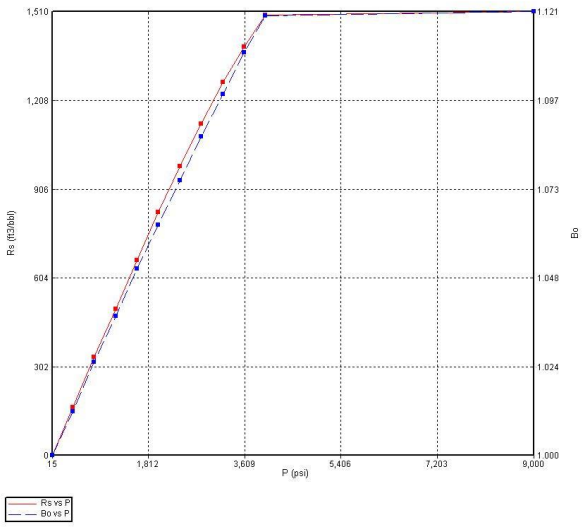

Figure 5-5 Rs and Bo changing with Pressure

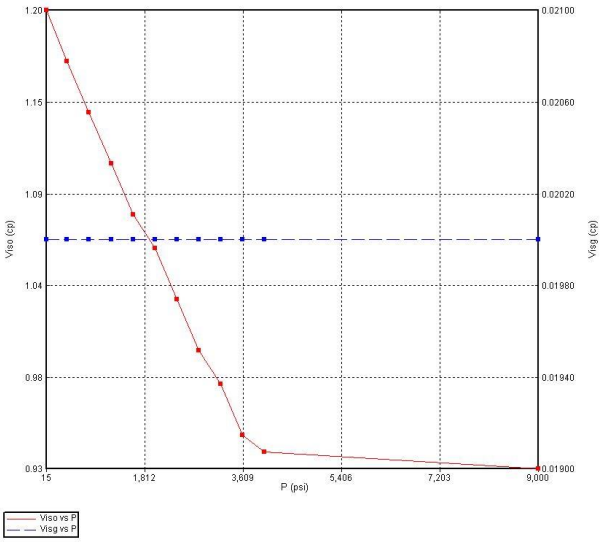

Figure 5-6 Oil and gas viscosity changing with pressure

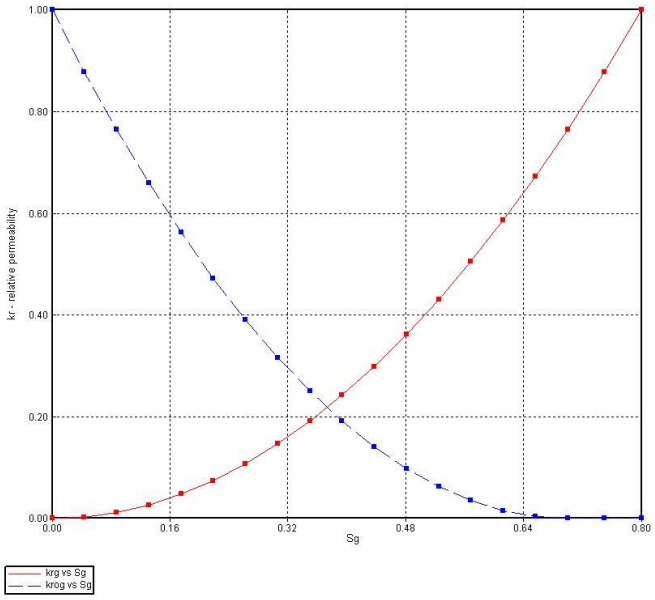

Figure 5-7 Relative permeability curve for gas phase

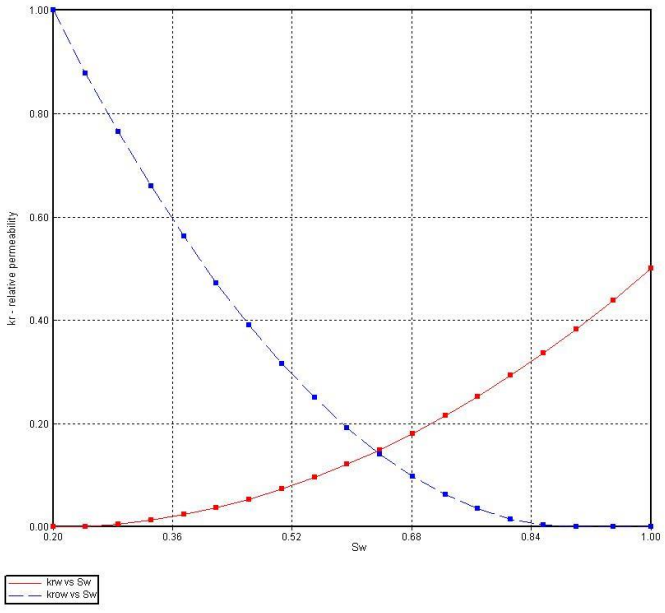

Figure 5-8 Relative permeability curves for water phase

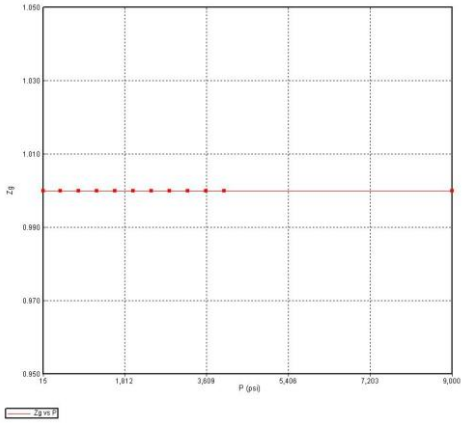

Figure 5-9 Zg is set constant at 1.00

5.4 Flow and storage mechanism

Our reservoir model is a dual porosity, dual permeability locally refined grid model. Permeability and porosity value is introduced earlier. We have two storage mechanisms in our model, gas is assumed to be stored in the matrix block and in the existing natural fracture system.

The flow mechanism employed in our model includes Darcy flow and transient non Darcy flow. The transient non Darcy flow is used to represent the behavior within the natural fracture and the hydraulic fracture and the Darcy flow is used to represent the flow behavior from the matrix block into the natural fractures.

Both upper (with depth of 5000') and lower (with depth of 8000') Marcellus shale are tested in this research. Reservoir pressure is set as 2325 psi for upper Marcellus, and 3720 psi for lower Marcellus. Under different formation depth, bottom hole pressure is set in 90%, 50%, and 10% of reservoir pressure. Detailed testing data can be found in Table 5-1.

Table 5-1 Depth, reservoir pressure and bottom hole pressure adopted in the research

Formation depth	8000’			5000’		
Reservoir pressure	3720 psi			2325 psi		
Bottom hole pressure	3348 psi	1860 psi	372 psi	2092 psi	1162 psi	232 psi

Chapter 6

Simulation and Analysis

In this research, three damaging factors that may affect ultimate gas recovery are investigated. The factors are: interaction between fluid with pre-existing natural fractures, proppant scale, and proppant diagenesis. Numerical reservoir models were constructed to quantify the impacts of each factor on cumulative production and gas flow rate for a period of 20 years.

6.1 Sensitivity analysis

Before numerical experiments, we conducted numerical sensitivity studies of gridding and drainage area to determine an optimized gridding and a suitable drainage area. As explained in this section, we have achieved faster simulation and accurate results.

6.1.1 Sensitivity analysis of gridding

In order to observe the sensitivity of block size on the simulated results, we designed five gridding systems, as shown in Table 6-1, for a reservoir with properties in Table 6-2 .

Table 6-1 Base information for sensitivity analysis on grid size

Run number	Grid number	Running time
Grid1	1200*1200	6.5 h
Grid2	900*900	4 h
Grid3	750*750	3 h
Grid4	600*600	1.5 h
Grid5	300*300	0.5 h

Table 6-2 Data set that are constant for sensitivity analysis

Reservoir pressure	3000 psi	Hydraulic fracture permeability	65500 md
depth	1050 ft	Natural fracture permeability	0.4395 md
FBHP	1000 psi	Fracture spacing	8.8 ft
Hydraulic Fracture	500 ft	Running time	30 years

The first gridding method (Grid1) has the finest and largest number of grids. Grid size in both x and y direction ranges in a pattern of 0.2 ft, 0.4 ft, 0.8 ft, 1.6 ft, 3 ft, 1.6 ft, 0.8 ft, 0.4 ft, 0.2 ft …which gives a total of 1200×1200 = 1,440,000 grids. The width of hydraulic and natural fractures will be the same at 0.2 ft. The gridding pattern is repeated until the reservoir boundary is reached. Also, each gridding pattern covers an existing natural fracture and its surrounding matrix block, which means 0.2 ft is natural fracture grid and 0.4 ft, 08 ft, 1.6 ft, 3 ft, 1.6 ft, 0.8 ft, 0.4 ft, are grids of matrix block. One could also tell that natural fracture spacing is 8.8 ft in both x and y directions. A schematic view of zoomed Grid 1can be found in Figure 6-1.

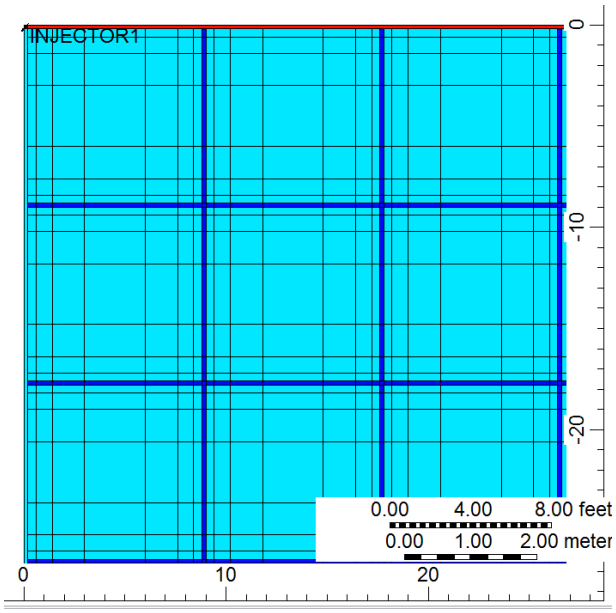

Figure 6-1 A schematic view of zoomed Grid1

For the second gridding method (Grid2), grid size in both x and y direction ranges in a pattern of 0.2 ft, 0.8 ft, 1.6 ft, 3.8 ft, 1.6 ft, 0.8 ft, 0.2 ft…which gives a total of 900×900= 810,000 grids . The width of hydraulic and natural fractures will be the same at 0.2 ft. The gridding pattern is repeated until the reservoir boundary is reached. Also, each gridding pattern covers an existing natural fracture and its surrounding matrix block, which means 0.2 ft is natural fracture grid and 0.8 ft, 1.6 ft, 3.8 ft, 1.6 ft, 0.8 ft are grids of matrix block. One could also tell that natural fracture spacing is 8.8 ft in both x and y directions. A schematic view of zoomed Grid2 can be found in Figure 6-2.

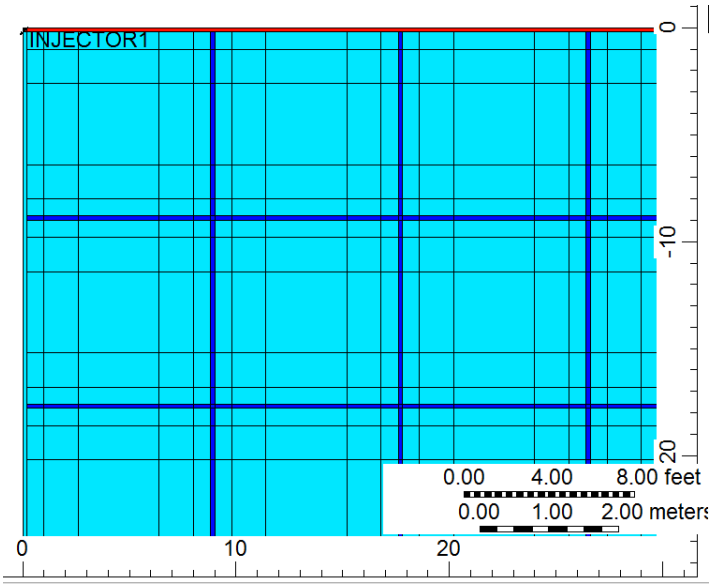

Figure 6-2 A schematic view of zoomed Grid2

For the third gridding method (Grid 3), width of grid in both x and y direction range in a pattern of 0.2 ft, 0.8 ft, 3.5 ft, 3.5 ft, 0.8 ft, 0.2 ft…which gives a total of 750×750=652,500 grids. The width of hydraulic and natural fractures will be the same at 0.2 ft. The gridding pattern is repeated until the reservoir boundary is reached. Also, each gridding pattern covers an existing natural fracture and its surrounding matrix block, which means 0.2 ft is natural fracture grid and 0.8 ft, 3.5 ft, 3.5 ft, 0.8 ft are grids of matrix block. One could also tell that natural fracture spacing is 8.8 ft in both x and y directions. A schematic view of zoomed Grid3 can be found in Figure 6-3.

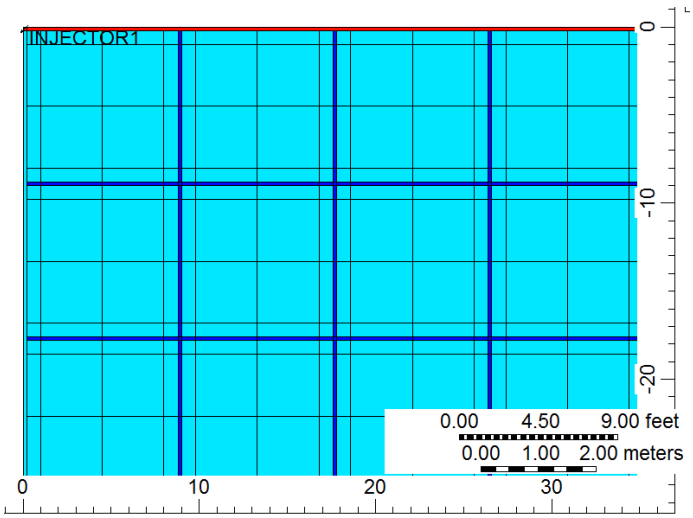

Figure 6-3 A schematic view of zoomed Grid3

For the fourth gridding method (Grid 4), width of grid in both x and y direction range in a pattern of 0.2ft, 1.6ft, 5.4ft, 1.6ft, 0.2ft…which gives a total of 600×600=360,000 grids. The width of hydraulic and natural fractures will be the same at 0.2 ft. The gridding pattern is repeated until the reservoir boundary is reached. Also, each gridding pattern covers an existing natural fracture and its surrounding matrix block, which means 0.2 ft is natural fracture grid and 1.6ft, 5.4ft, 1.6ft are grids of matrix block. One could also tell that natural fracture spacing is 8.8 ft in both x and y directions. A schematic view of zoomed Grid4 can be found in Figure 6-4.

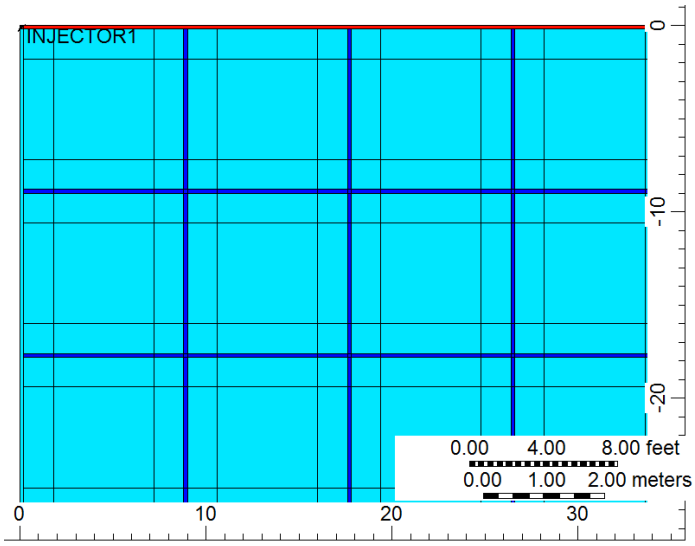

Figure 6-4 A schematic view of zoomed Grid4

For the fifth gridding method (Grid 5), width of grid in both x and y direction range in a pattern of 0.2ft, 8.6ft, 0.2ft…which gives a total of 300×300=90,000 grids. The width of hydraulic and natural fractures will be the same at 0.2 ft. The gridding pattern is repeated until the reservoir boundary is reached. Also, each gridding pattern covers an existing natural fracture and its surrounding matrix block, which means 0.2 ft is natural fracture grid and 8.6ft are grids of matrix block. One could also tell that natural fracture spacing is 8.8 ft in both x and y directions. A schematic view of zoomed Grid5 can be found in Figure 6-5.

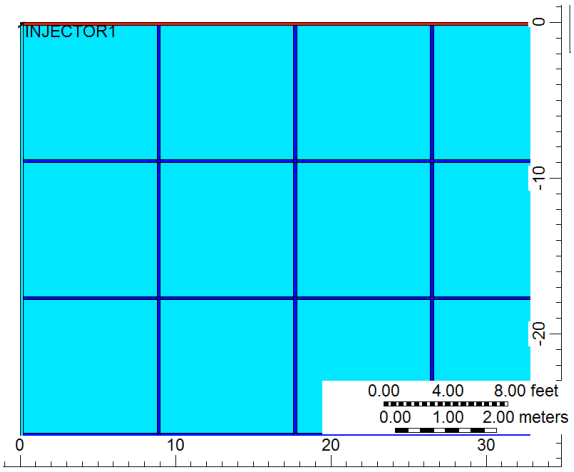

Figure 6-5 A schematic view of zoomed Grid5

Figure 6-6 and Figure 6-7 show cumulative gas production and gas flow rate for sensitivity analysis. As gird becomes finer, from Grid5 to Grid1, the simulated results approach to one solution. Since Grid3 have the least simulation time and its production result is close enough to the solution, we chose Grid3's grid system.

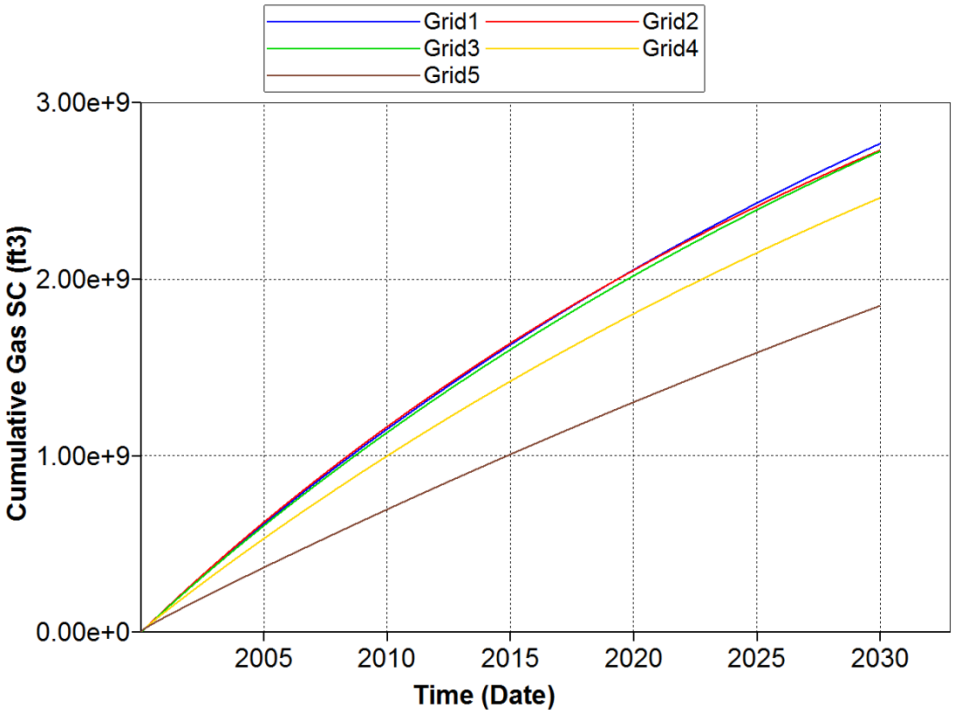

Figure 6-6 Cumulative gas recovery for sensitivity analysis on grid size

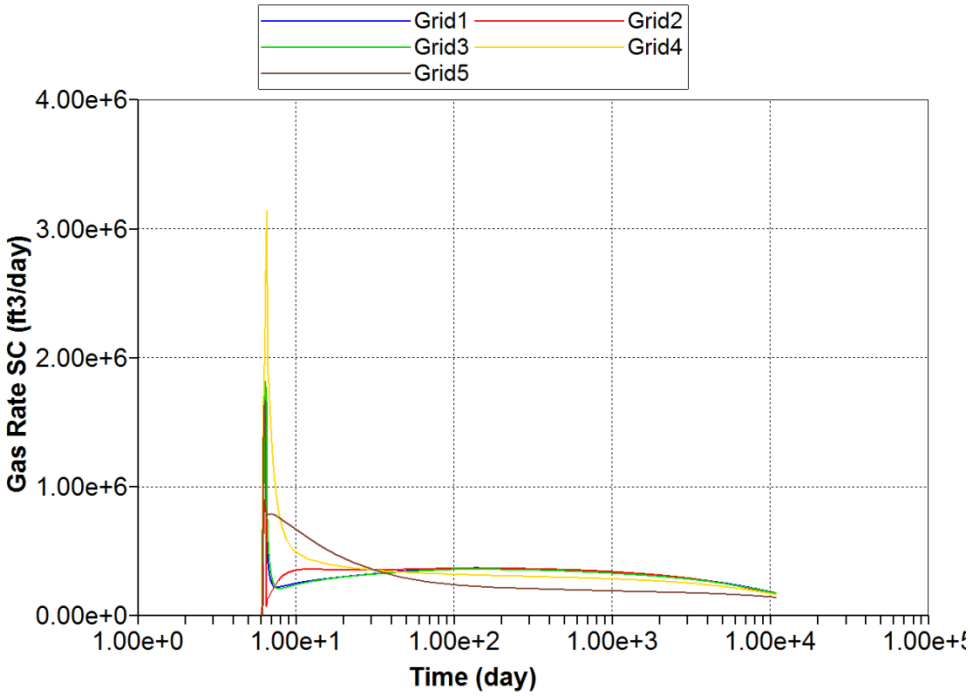

Figure 6-7 Gas rate for sensitivity analysis on grid size

6.1.2 Sensitivity analysis on drainage area

It takes about 36 minutes to run one simulation with gridding system No. 3, which is too long for practical application and this research. By examining the pressure and fluid distributions, we realized the many grid blocks are still in their initial status after even 20 years. So, we decided to reduce the drainage area to reduce computing time. As explained in Table 6-3. In Figure 6-8 to Figure 6-11, we investigated the sensitivity of drainage area, which is ¼ of the whole well spacing. Well bore is located at the top left corner for all 4 scenarios (Area1 to Area4). Reservoir properties are same as in Table 6-2**.**

Area1 has a drainage area of 20 acres, which is 600 ft by 1320 ft. A schematic view is shown in Figure 6-8.

Area2 has a drainage area of 16 acres, which is1056 ft by 660 ft. A schematic view is shown in Figure 6-9.

Area3 has a drainage area of 20 acres, which is 1320 ft by 660 ft. A schematic view is shown in Figure 6-10.

Area4 is exactly same with Grid3 in the previous section. It has a drainage area of 40 acres, which is 1320 ft by 1320 ft. A schematic view is shown in Figure 6-11. Details are summarized in Table 6-3.

Table 6-3 Base information for sensitivity analysis on drainage area

Run #	Drainage area, ft^2	Drainage area, acre	Run time, min
Area1	660×1320	20	20.8
Area2	1056×660	16	11.4
Area3	1320×660	20	20.8
Area4	1320×1320	40	36.2

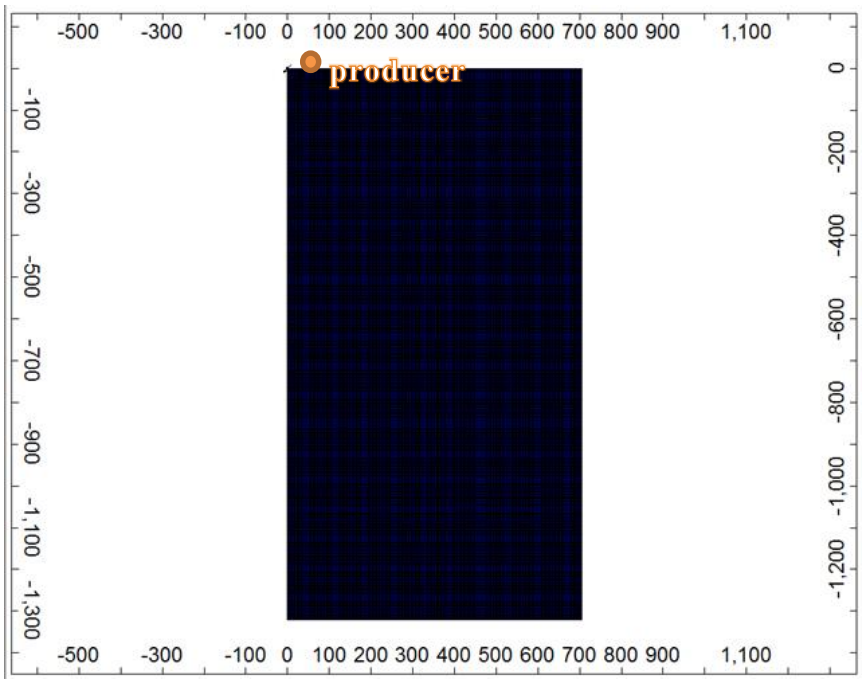

Figure 6-8 A schemetic of drainage area of Area1

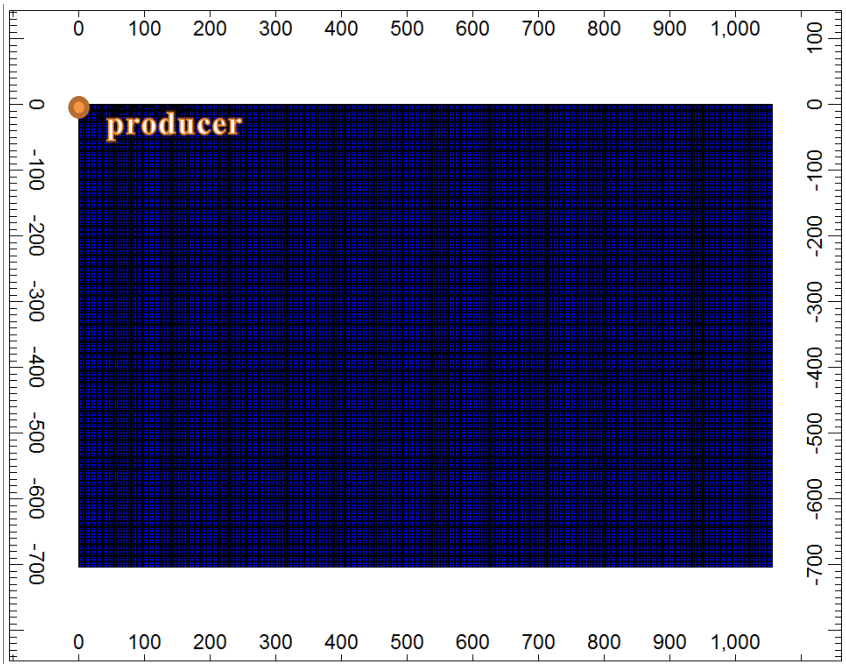

Figure 6-9 A schematic view of drainage area of Area2

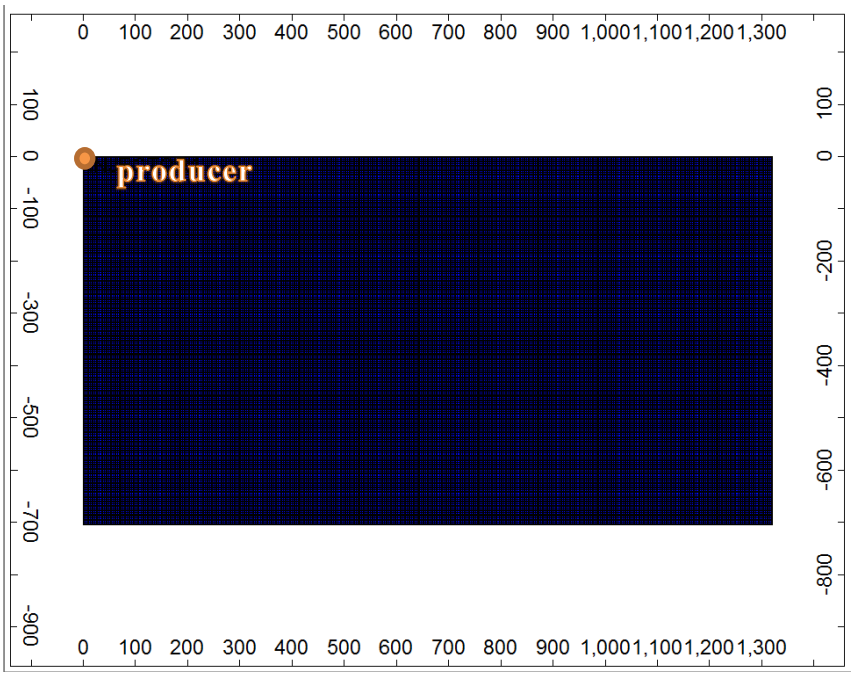

Figure 6-10 A schematic view of drainage area of Area3

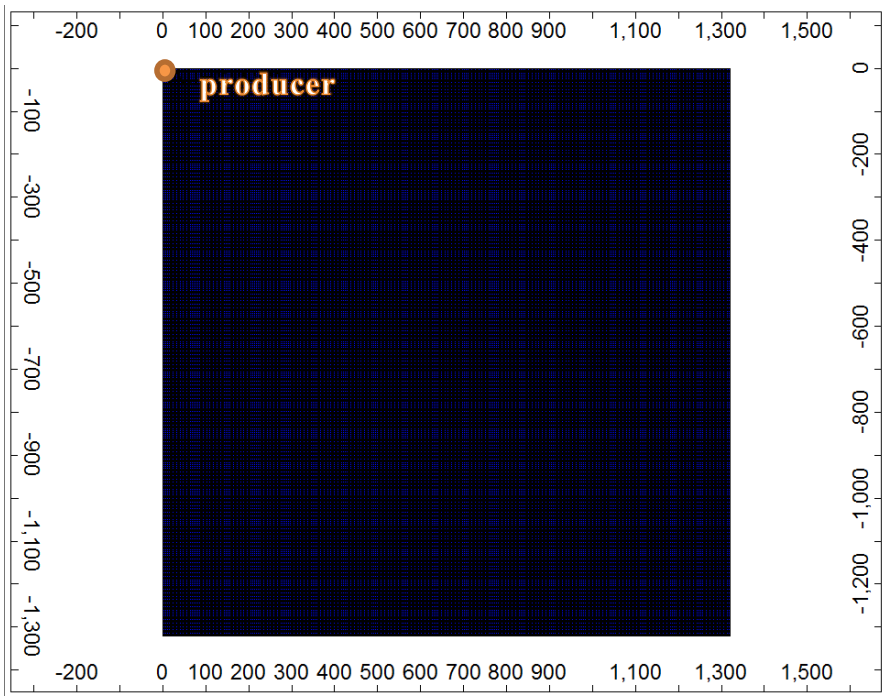

Figure 6-11 A schematic view of drainage area of Area4

Cumulative gas production curve of these four simulations can be found in Figure 6-12**.** Area4 gives an ultimate gas recovery of 4.969018+e8 ft^3, Area3 gives an ultimate gas recovery of 4.86075+e8 ft^3, Area2 gives an ultimate gas recovery of 4.76923+e8 ft^3, and Area1 gives an ultimate gas recovery of 4.61481+e8 ft^3. Gas production rate of these four simulations can be found in Figure 6-13.

From the figure we can see production of the upper half (Area3) is responsible for more than 97.8% of production of the entire square drainage area. Area2 produce a little bit less than Area3. Area1 produce even less.

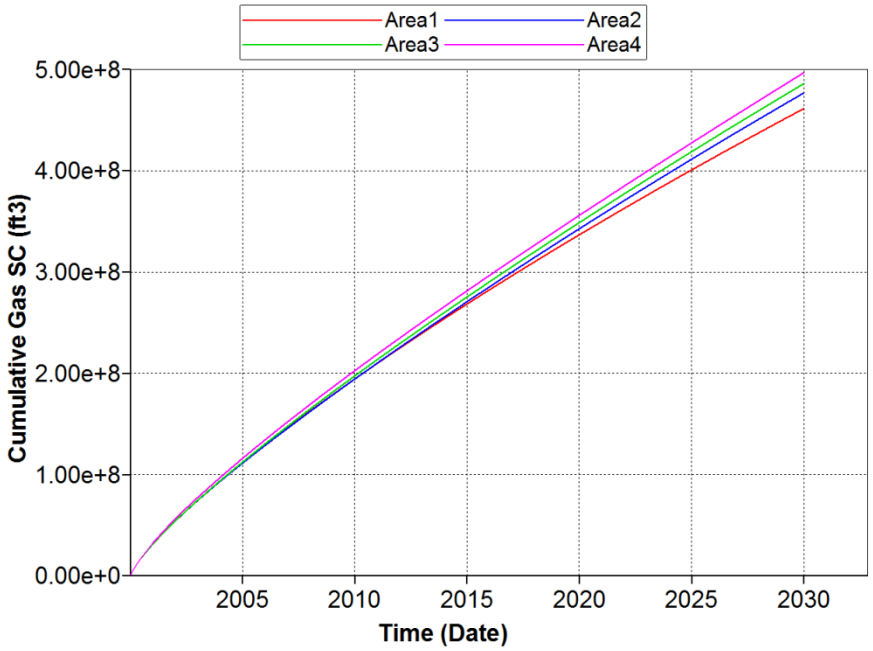

Figure 6-12 Cumulative gas production curve for sensitivity analysis on drainage area

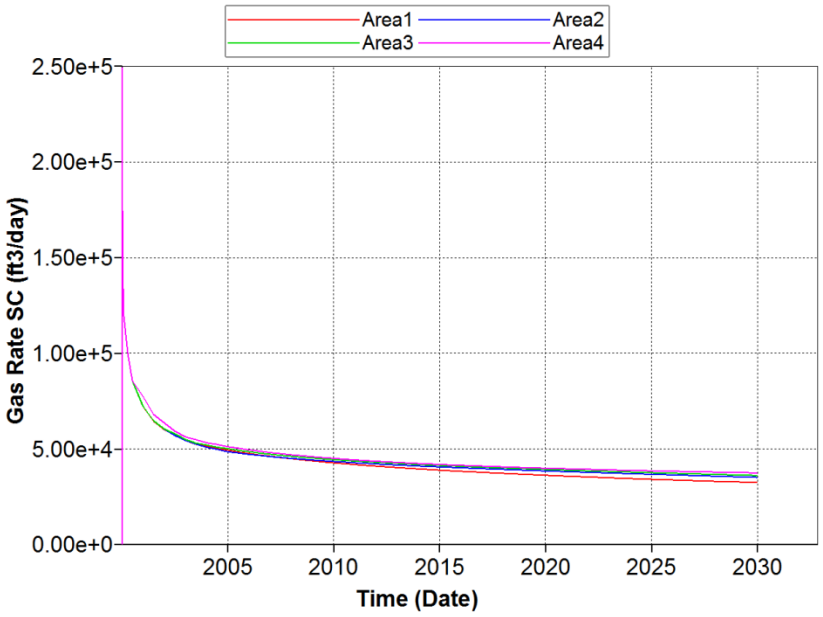

Figure 6-13 Gas production rate for sensitivity analysis on drainage area

Based on the comparisons, we chose drainage area of 20 acres (Area3 in Table 6-3) for our research as it gives accurate results and requires about 2 minutes to run one simulation rather than 36 minutes.

6.1.3 Construction of test models

Parametric studies include reservoir pressure, flowing bottom hole pressure, hydraulic fracture, permeability within pre-existing natural fractures and unpropped natural fractures, permeability within hydraulic fracture. A detailed list of simulations is listed in Appendix A. There are 43 models in the list.

6.2 The effect of interaction between fluid and formation rock (N.F. and unpropped H.F)

3 scenarios regarding this damage are studied. Detailed permeability parameters are isted in Table 6-4. Models we used to represent these scenarios are listed in Table 6-5. These parameters are summed from Table 4-1.

In the first scenario, we assumed no damage took place. Permeability of pre-existing natural fractures and unpropped hydraulic fractures is set at an ideal value, 0.4793 md. This number is adopted from (Osholake, T. A., J. Y. Wang, et al. 2011).

In the second scenario, we assumed fracture fluid is completely mixed with formation fluid. Therefore, the concentration of KCl and clay stabilizer of fracture fluid is decreased and that of formation is increased. The permeability of pre-existing natural fractures and unpropped hydraulic fractures will be damaged, and remains constant through production. The permeability value, 0.0938 md, is obtained from (Conway, M. W., J. J. J. Venditto et al. 2011). It is the average of the permeability of 7% KCl and sythetic produced water.

In real field, permeability of pre-existing natural fractures and unpropped hydraulic fracture is not constant through the life of a production well. Thus in the third scenario, we assumed fracture fluid is and formation fluid are produced one after another. Permeability of such fractures will be protected by chemical such as clay stabilizer and KCl as the production begin, and fracture fluid is produced. However concentration of KCl and clay stabilizer will decrease with formation fluid is produced, which will lead to damages of pre-existing natural fractures and unpropped hydraulic fractures. Since fracture fluid flows back for about 3 weeks according to experiences, natural fracture permeability is set as 0.1172 md during this period. Afterwards, natural fracture permeability is set as 0.0703 md. Both of these numbers are adopted from (Conway, M. W., J. J. J. Venditto et al. 2011)

Table 6-4 Permeability data applied in our research

Case #	1st date permeability, md	21st date permeability, md	Comments
1	0.4793	0.4793	No damage effect
2	0.0938	0.0938	$k_{n.f.}$ constant
3	0.1172	0.0703	$k_{n.f.}$ change with time

Table 6-5 Parameters used for damage effect of interaction between fluid and formation

Run#	File name	Pr (psi)	FBHP (psi)	H.F. scenario	SRV (ft^3)	N.F. k 1st day	N.F. k (md) 21st day	H.F. k (md)
HF1 ideal case*	data1	3720	3348	H.F.1	NA	0.4793	0.4793	65,500
HF1 kn.f.=0.0938md	data2	3720	3348	H.F.1	NA	0.0938	0.0938	65,500
HF1 kn.f.=0.1172md~0.0703md	data3	3720	3348	H.F.1	NA	0.1172	0.0703	65,500
HF2 ideal case*	data4	3720	3348	H.F.2	1,045,440	0.4793	0.4793	39,174
HF2 kn.f.=0.0938md	data5	3720	3348	H.F.2	1,045,440	0.0938	0.0938	39,174
HF2 kn.f.=0.1172md~0.0703md	data6	3720	3348	H.F.2	1,045,440	0.1172	0.0703	39,174
HF3 ideal case*	data7	3720	3348	H.F.3	2,090,880	0.4793	0.4793	23,115
HF3 kn.f.=0.0938md	data8	3720	3348	H.F.3	2,090,880	0.0938	0.0938	23,115
HF3 kn.f.=0.1172md~0.0703md	data9	3720	3348	H.F.3	2,090,880	0.1172	0.0703	23,115

* ideal case include effect of multiphase flow and proppant crushing .

6.2.1 Simulation results for H.F.1

As mentioned before, H.F.1 

has a primary planar hydraulic fracture.

Simulations results of gas recovery and gas rate are shown in the following figures.

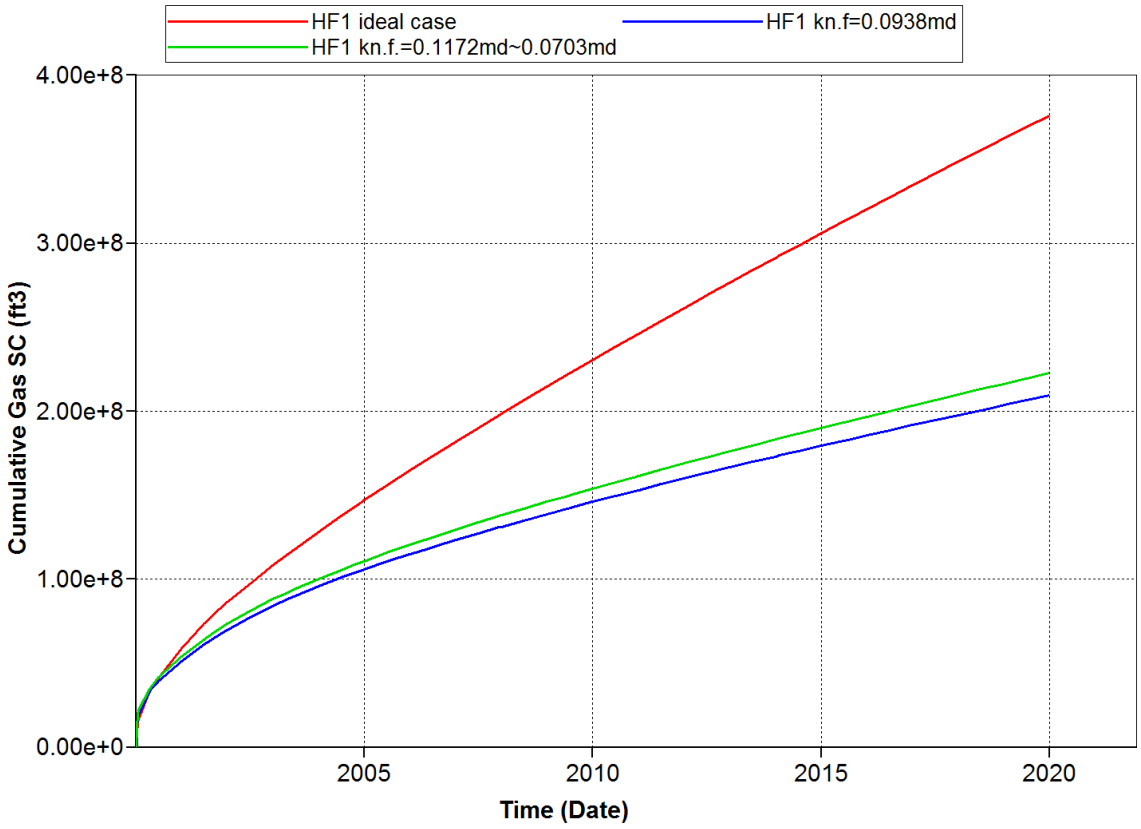

Figure 6-14 Interaction of Marcellus shale and fluid decease cumulative gas production for 20-40Ceramics proppant over 20 years with P_r = 3720 psi, FBHP = 3348 psi, for HF1.

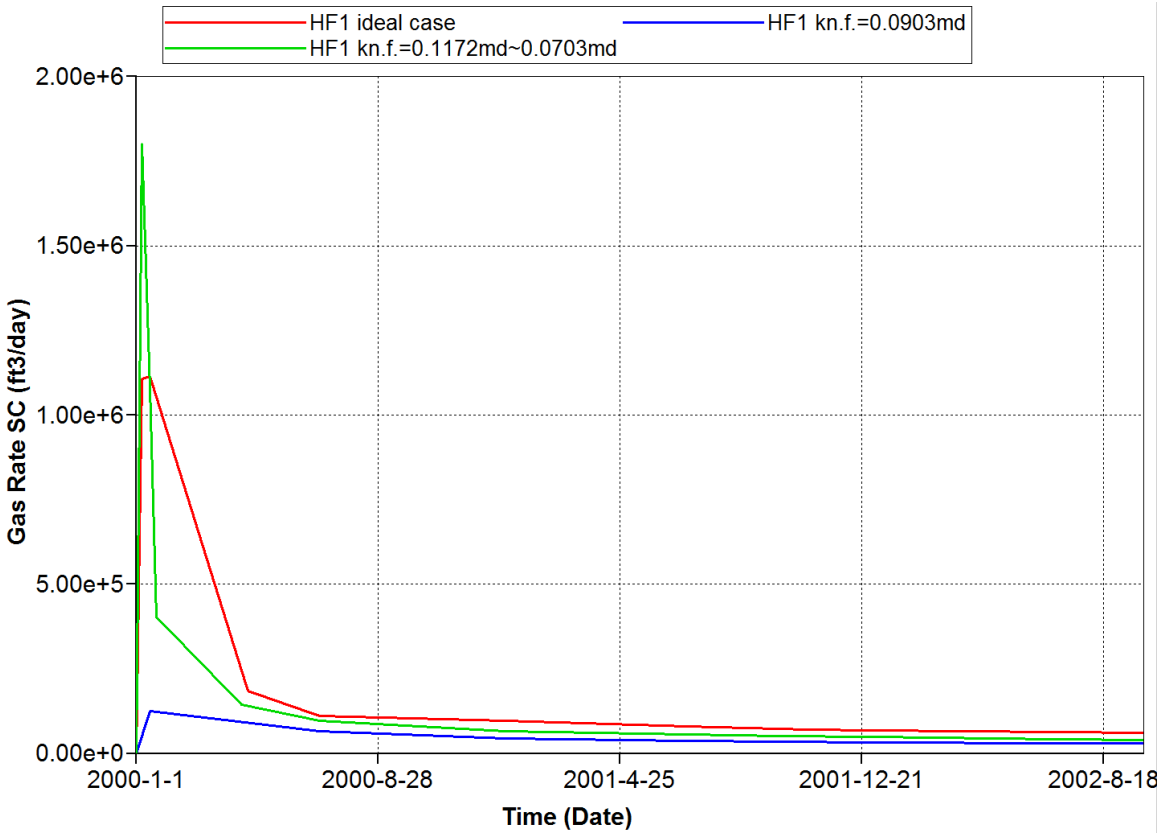

Figure 6-15 Interaction of Marcellus shale and fluid decease gas rate for 20-40Ceramics proppant over 20 years with P_r = 3720 psi, FBHP = 3348 psi, for HF1.

"HF1 ideal case" represents the case without damage, in which $k_{n.f.}$ equals to 0.4396 md. "HF1 $k_{n.f.}$=0.0938md" represents the case with damaged and constant natural fracture permeability, in which $k_{n.f.}$ equals to 0.0938 md. "HF1 $k_{n.f.}$=0.1172md~0.0703" represents the case with gradually decreasing natural fracture permeability, $k_{n.f.}$ for which starts from 0.1172 md and gradually decrease to 0.0703md with time.

As we can see from Figure 6-14**,** when the effect of interaction between formation rock and fluid was incorporated, a huge decrease in the overall gas recovery occurs. Gas production for a 20 year period is decreased from 3.76×10^8 ft^3 (HF1 ideal case) to 2.09×10^8 ft^3 (HF1 $k_{n.f.}$=0.0938md). The reduction is 44.4%, which implies that the damage caused by interaction of formation rock and fluid should be viewed as a serious damage factor. "HF1 $k_{n.f.}$ = 0.1172md ~

0.0703” gives a shows a reduction of 40.7% when compared with ideal case, which is a little bit larger decrease than “HF1 $k_{n.f.}$=0.0938md”.

We can observe similar trends from gas rate production. Since “HF1 $k_{n.f.}$=0.1172md~0.0703” has the highest initial permeability, the “peak value” for this model is the largest. However, since permeability gradually decreases, its gas rate also decreases and thus influenced the cumulative gas production. For (HF1 $k_{n.f.}$=0.0938md), it starts with a low natural facture permeability value, therefore, its initial “peak gas rate” is small.

Figure 6-16 to Figure 6-18 represent the evolvement of pressure distribution after a treatment for P_r = 3720 psi, FBHP = 3348 psi, $L_{h.f.}$ = 500 ft. $k_{n.f.}$ = 0.4396 md.

Figure 6-16 represents the pressure map after 7 days of treatment. We can see pressure is very high around hydraulic fracture area. We can also observe that well bore area shows intensified pressure distribution since the first 5 horizontal natural fractures that intersect with hydraulic fracture, and the formation blocks in between them shows higher pressure values. Also, pressure is invading through natural fracture networks.

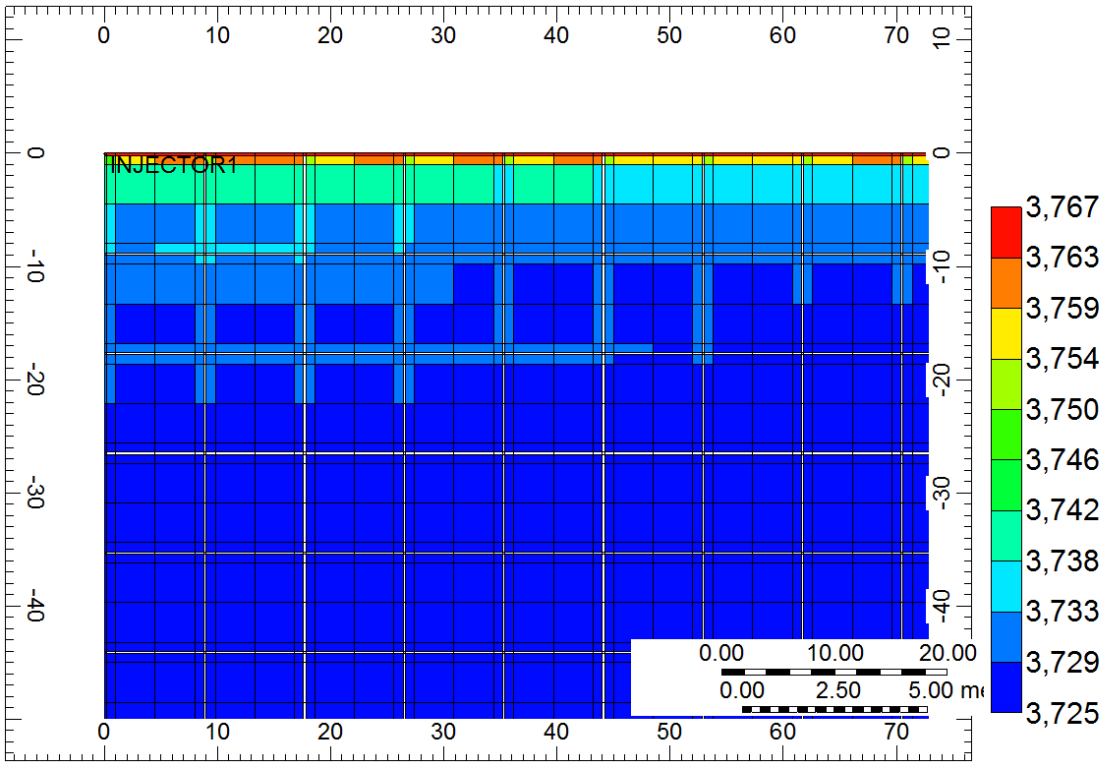

Figure 6-16 Pressure map (zoomed view around wellbore area) after a treatment for P_r = 3720 psi, FBHP = 3348 psi, $k_{n.f.}$ = 0.4396 md at day7 (HF1 ideal case).

Figure 6-17 represents the pressure map after 10 years of production. We can see obvious stimulated region, which occupies a little bit less than half of the entire drainage area. This area is prolonged in the direction of the planar hydraulic fracture. Near well bore area has lower reservoir pressure while the right lower corner still occupies reservoir pressure which is 3716 psi.

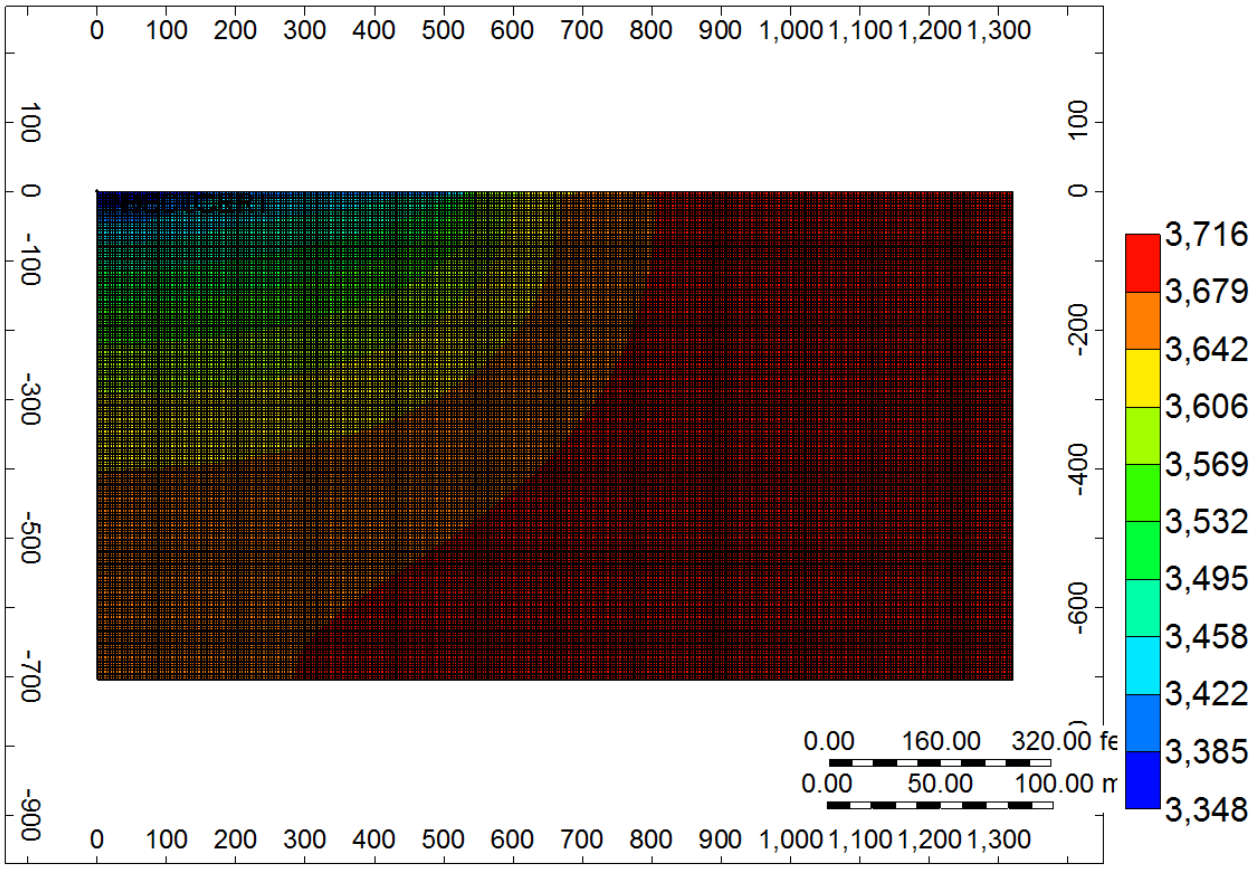

Figure 6-17 Pressure map after a treatment for P_r = 3720 psi, FBHP = 3348 psi, $k_{n.f.}$ = 0.4396 md after 10 years (HF1 ideal case).

Figure 6-18 represents the pressure distribution after 20 years. We can see the stimulated area is expanded to 2/3 of the entire drainage area. This area is still prolonged in the direction of planar hydraulic fracture. Near well bore area has lower reservoir pressure while the right lower corner still occupies high reservoir pressure which is 3688 psi. At the end of the production, there is still 1/3 of the entire drainage area excluded from being stimulated.

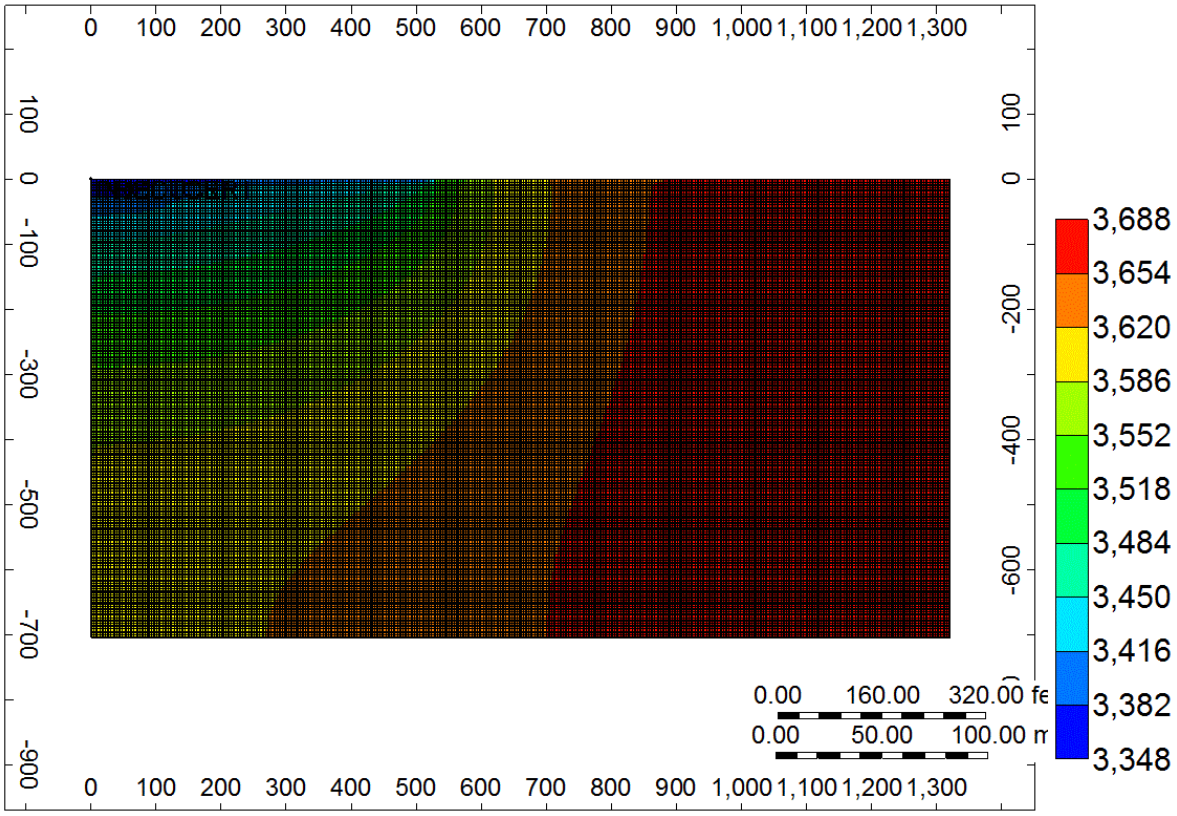

Figure 6-18 Pressure map after a treatment for P_r = 3720 psi, FBHP = 3348 psi, $k_{n.f.}$ = 0.4396 md after 20 years (HF1 ideal case).

The evolvement of water distribution after a treatment for P_r = 3720 psi, FBHP = 3348 psi, $L_{h.f.}$ = 500 ft. $k_{n.f.}$ = 0.4396 md is presented from Figure 6-19 to Figure 6-24. Figure 6-19 represents the near well bore view of the water saturation distribution after 7days of treatment. We can observe obvious water saturation change in the area around the hydraulic fracture. Most of the blocks in hydraulic fracture have 1.00 water saturation; only several blocks which is in adjacent with natural factures show signs of decrease water saturation. This is also an indication that water invades into formation block through natural fracture networks.

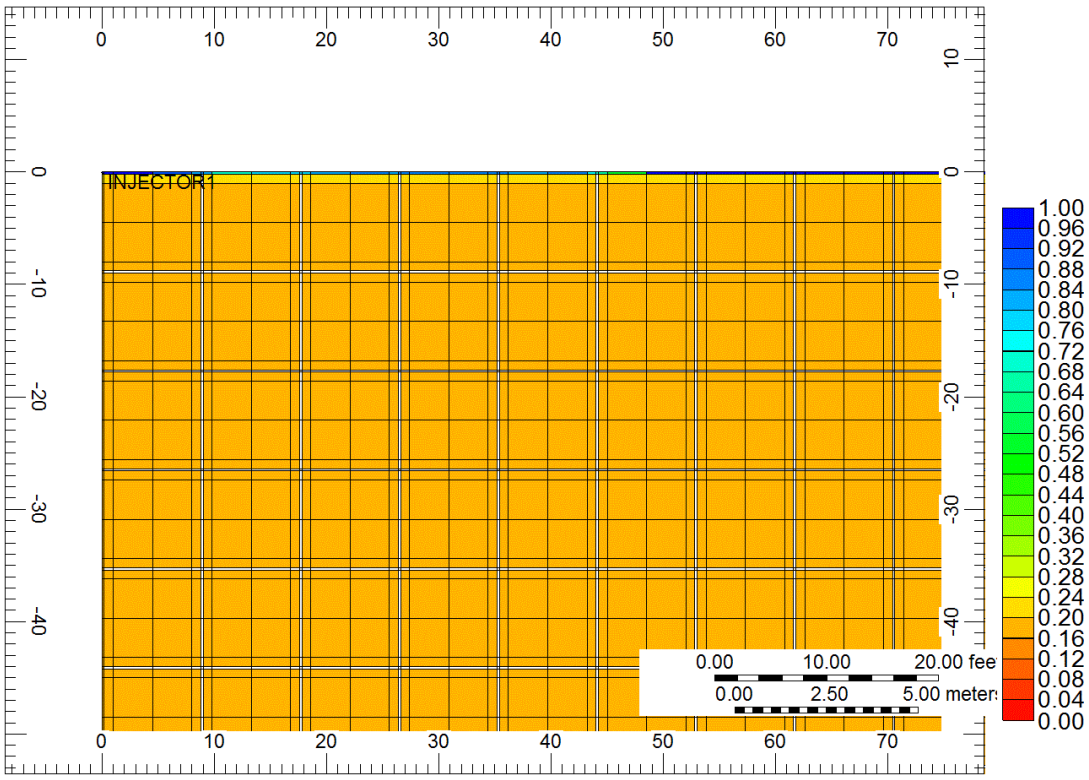

Figure 6-19 Water saturation distribution (zoomed view around wellbore) after a treatment for P_r = 3720 psi, FBHP = 3348 psi, $k_{n.f.}$ = 0.4396 md on day7 (HF1 ideal case).

Figure 6-20 represents water saturation after 2 weeks of production. We can see a higher water saturation value in the planar hydraulic fracture when compared with water saturation value in formation blocks. Water saturation value decreases from 1 to 0.6 after 2 weeks of production in hydraulic fracture. Besides hydraulic fracture, other formation blocks do not show obvious sign of water saturation value higher than 0.2, which represents that fracture fluid is nealy depleted after 2 weeks of production.

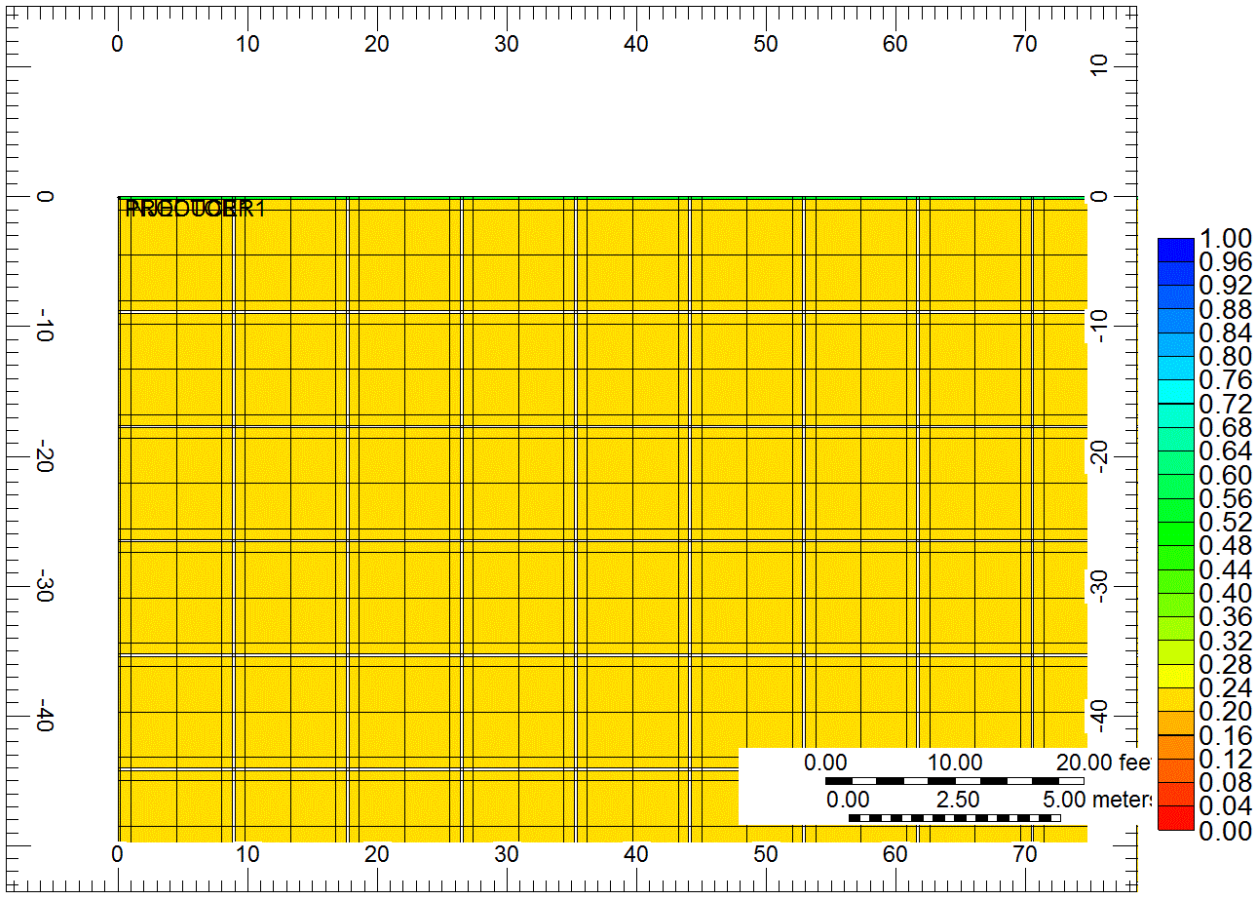

Figure 6-20 Water saturation distribution after a treatment for P_r = 3720 psi, FBHP = 3348 psi, $k_{n.f.}$ = 0.4396 md after 2 weeks (HF1 ideal case).

Figure 6-21 represents water saturation distribution after 6 months of production. We can see a higher water saturation value in the planar hydraulic fracture when compared with water saturation value in formation blocks. Water saturation value decreases from 1 to almost 0.4 after 6 months of production. Besides hydraulic fracture, other formation blocks are evenly distributed with water saturation value of 0.2, which represents fracture fluid is nearly depleted.

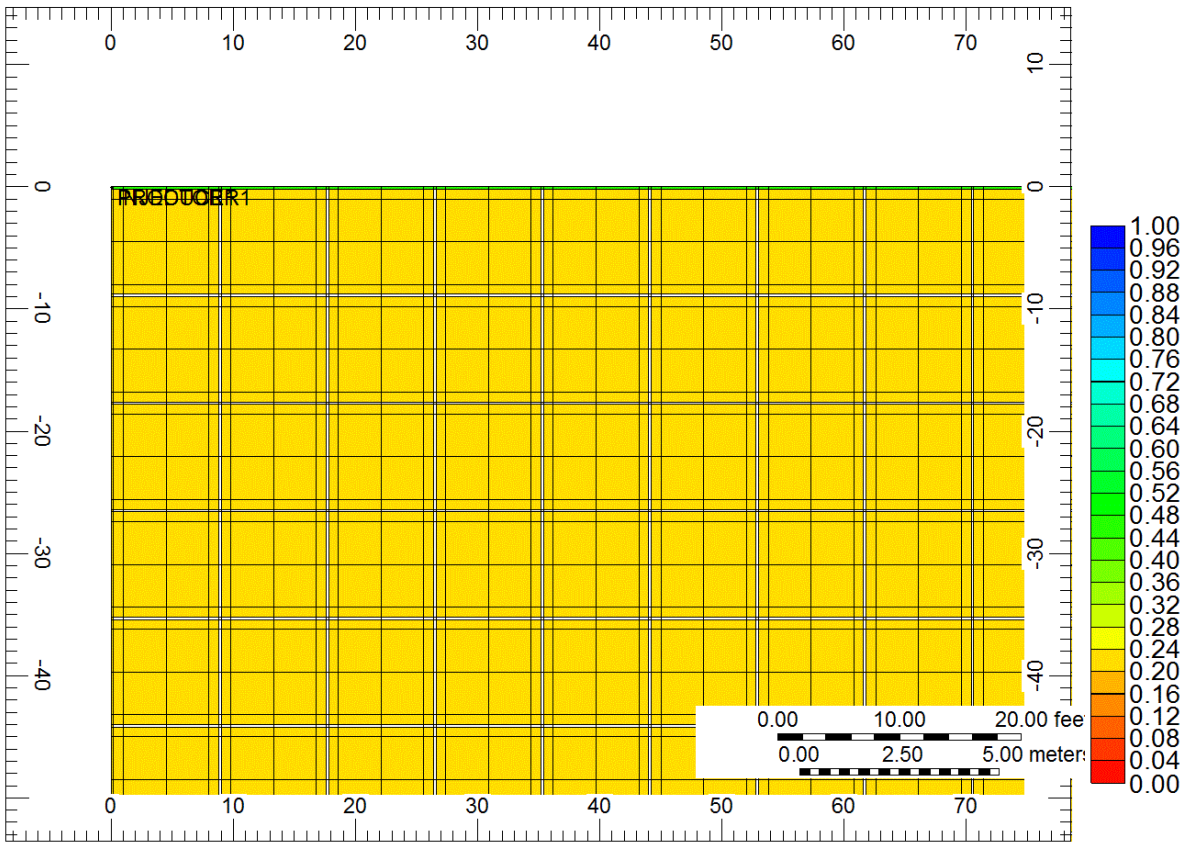

Figure 6-21 Water saturation distribution after a treatment for P_r = 3720 psi, FBHP = 3348 psi, $k_{n.f.}$ = 0.4396 md after 6 months (HF1 ideal case).

Figure 6-22 represents water saturation distribution after 3 years. Water saturation value in hydraulic fracture decreased to 0.32, and near wellbore hydraulic fracture blocks has higher water saturation than distant hydraulic fracture blocks.

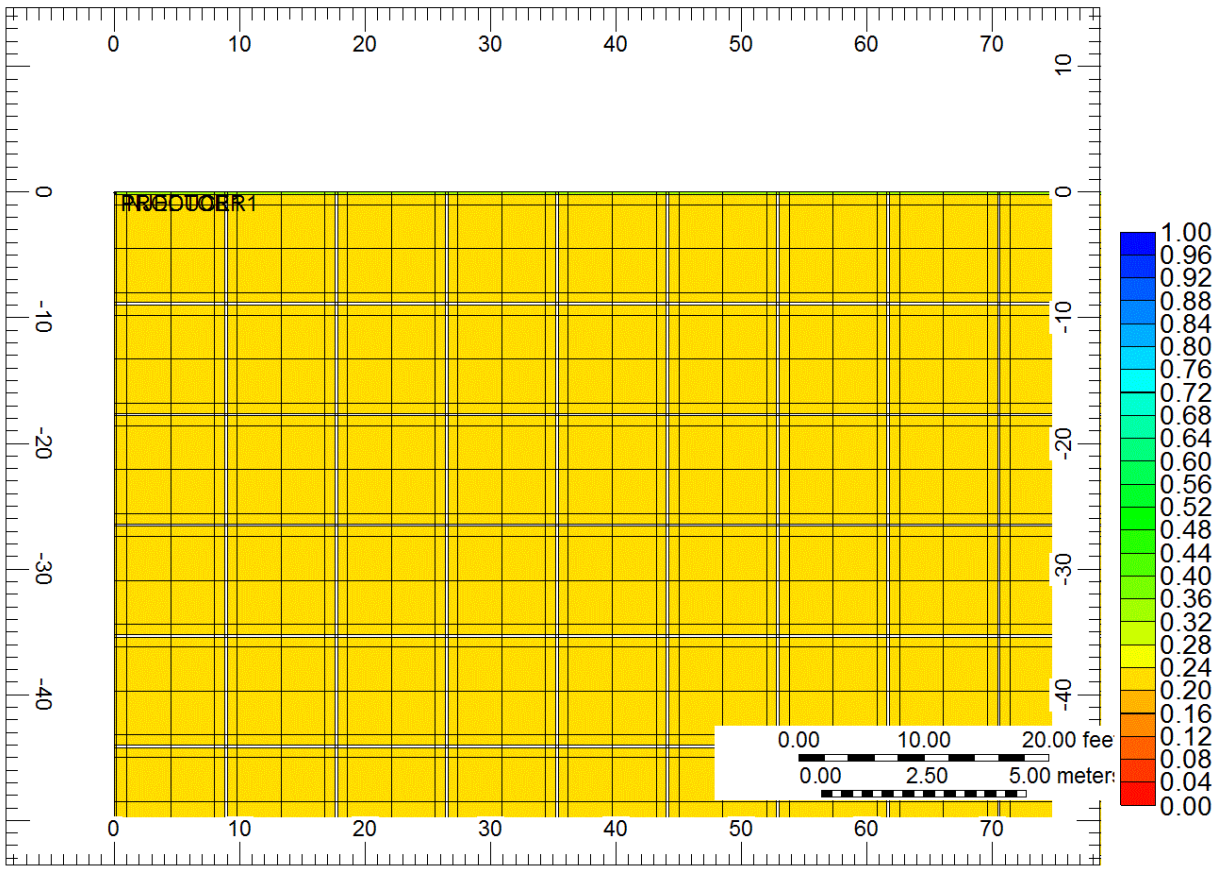

Figure 6-22 Water saturation distribution after a treatment for P_r = 3720 psi, FBHP = 3348 psi, $k_{n.f.}$ = 0.4396 md after 3 years (HF1 ideal case).

Figure 6-23 represents water saturation distribution after 10 years. We can see water saturation within hydraulic fracture is the same with that in the formation block. No matter hydraulic fractures or formations, reducible water is completely depleted from the reservoir.

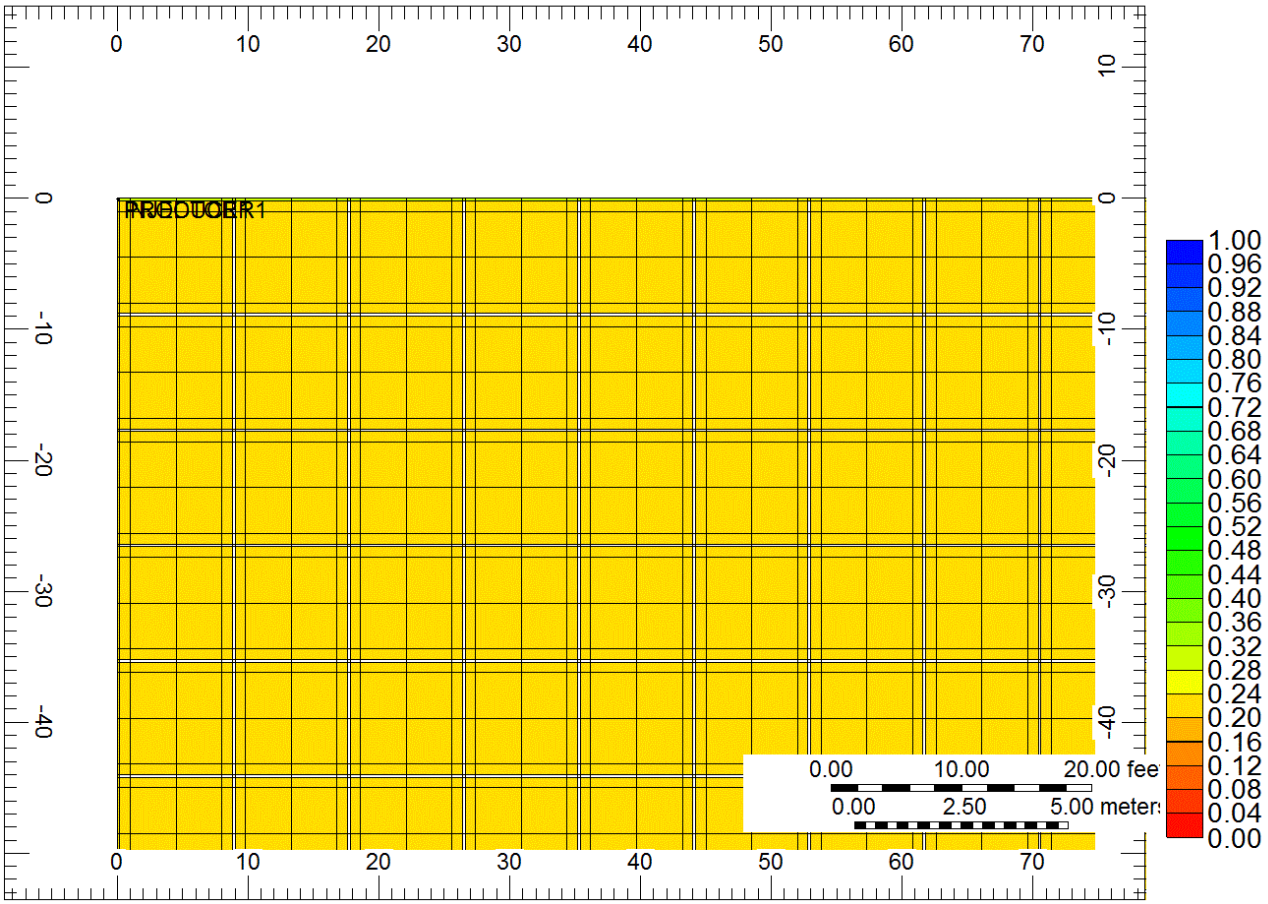

Figure 6-23 Water saturation distribution after a treatment for P_r = 3720 psi, FBHP = 3348 psi, $k_{n.f.}$ = 0.4396 md after 10 years (HF1 ideal case).

Figure 6-24 shows the water distribution at the end of the production, which is 20 years. Same condition applies. We can see water saturation within hydraulic fracture is the same with that in the formation. No matter hydraulic fractures or formations, reducible water is completely depleted from the reservoir.

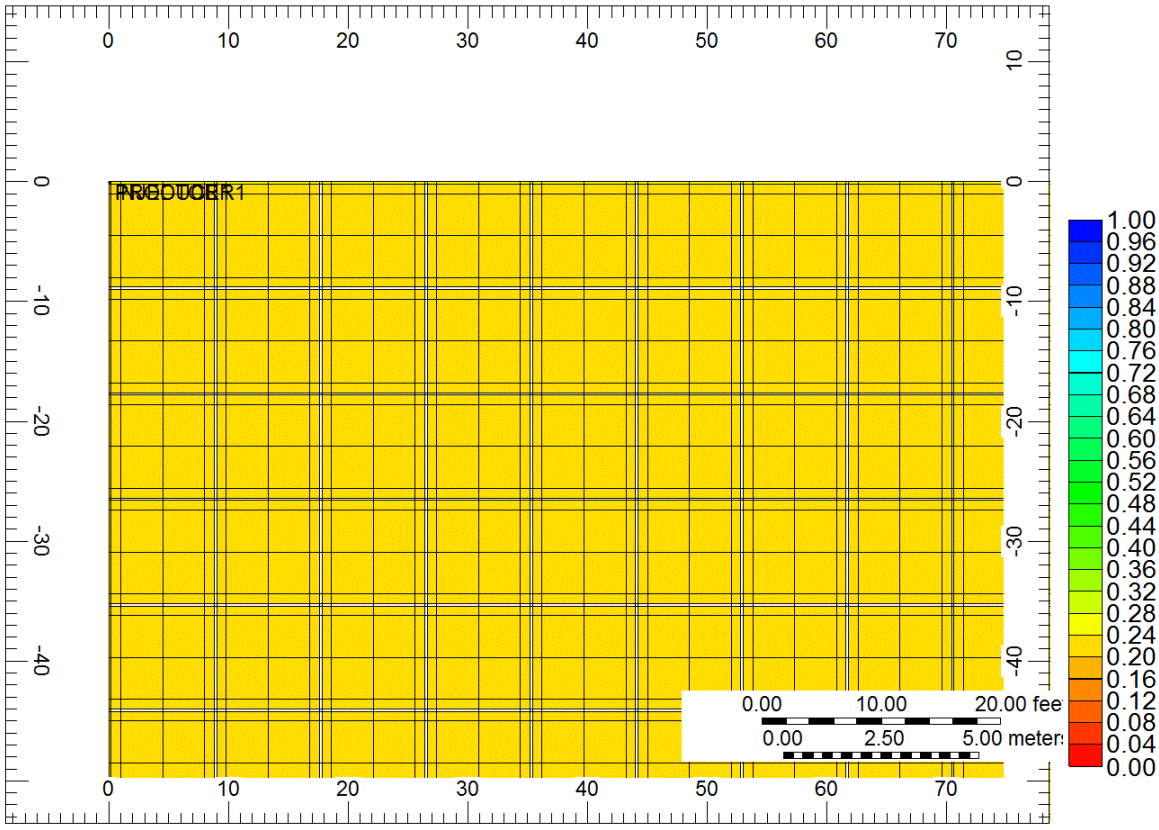

Figure 6-24 Water saturation distribution after a treatment for P_r = 3720 psi, FBHP = 3348 psi, $k_{n.f.}$ = 0.4396 md after 20 years (HF1 ideal case).

In sum, interaction between formation rock and fluid could results in severe damage. An adequate initial concentration of KCl and clay stabilizer can alleviate the damage to some extent.

6.2.2 Simulation results for H.F.2

As mentioned before, H.F.2 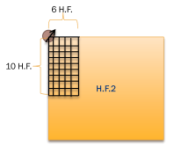

has a hydraulic fracture network around wellbore. Simulation results of gas recovery and gas rate are shown in the following figures.

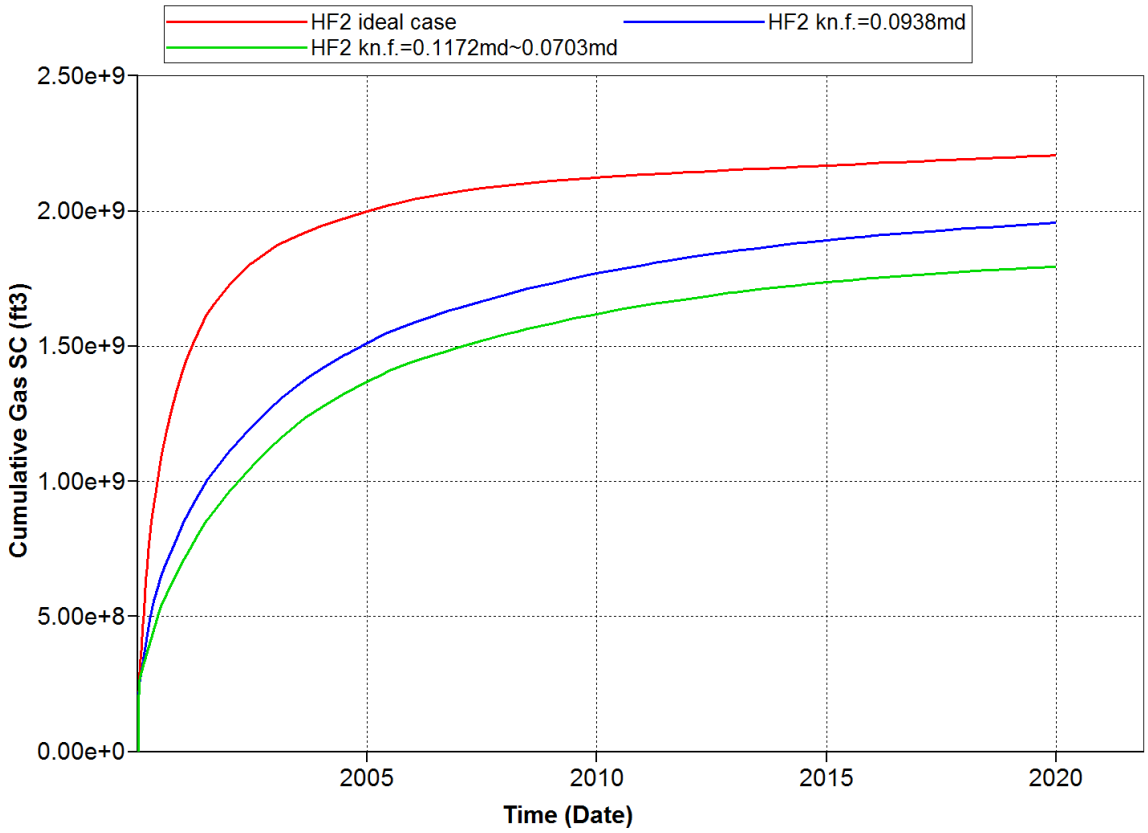

Figure 6-25 Interaction of Marcellus shale and fluid decease cumulative gas production for 20-40Ceramics proppant over 20 years with Pr = 3720 psi, FBHP = 3348 psi, for HF2

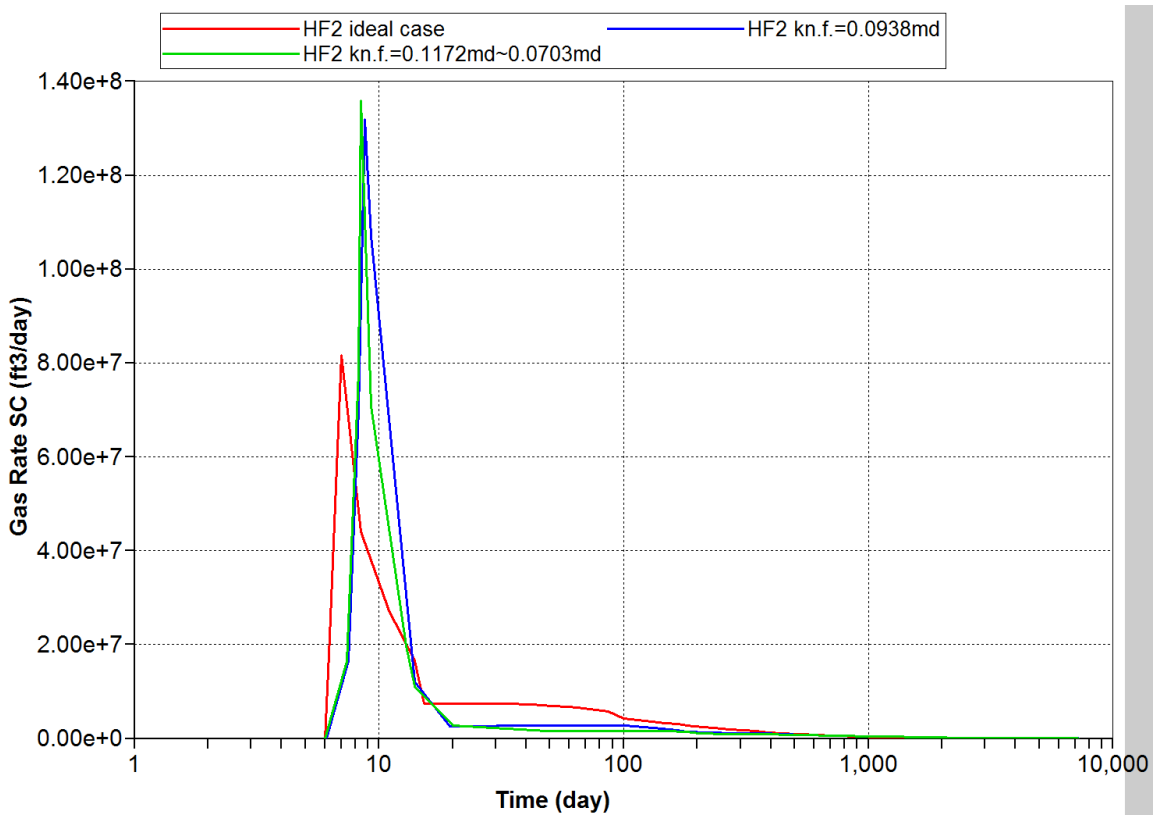

Figure 6-26 Interaction of Marcellus shale and fluid decease gas rate for 20-40Ceramics over 20 years with P_r = 3720 psi, FBHP = 3348 psi, for HF2.

"HF2 ideal case" represents the case without damage, $k_{n.f.}$ for which is 0.4396 md. "HF2 $k_{n.f.}$=0.0938md" represents the case with damaged and constant permeability, $k_{n.f.}$ for which equals to 0.0938md. "HF2 $k_{n.f.}$=0.1172md~0.0703md" represents the case with gradually decreasing permeability, $k_{n.f.}$ for which starts from 0.1172md and gradually decrease to 0.0703md along with time.

Gas recovery curve and gas rate curve for these three models are shown in Figure 6-25 and Figure 6-26. We can see that permeability decrease caused by interaction between fluid and formation rock has decreased gas recovery from 2.2 $\times 10^9$ ft^3 (HF2 ideal case) to 1.95 $\times 10^9$ ft^3 (HF2 $k_{n.f.}$=0.0938md), which is approximately 11.4%. It is much better than the situation in H.F.1. It actually becomes worse if initial high permeability value (ensured by high concentration of KCl

and clay stabilizer) gradually decrease to a low value (KCl and clay stabilizer diluted and replaced by formation water), since it has a gas production of 1.79×10^9 ft^3 (HF2 $k_{n.f.}$=0.1172md~0.0703md). This is also different with the situation in H.F.1.

Gas rate plot shows similar trend with cumulative gas production plot. Gas rate curves for these three models appear different from day 1 to day 15. The different initial gas productions are caused by different initial conditions. HF2 ideal case has high natural fracture permeability, while the other two models have low permeability values.

In sum, interaction between formation rock and fluid may not be a severe damage for a reservoir with a network of hydraulic fracture. In other words, a network of hydraulic fracture could help prevent the damage from happening. Also, high initial concentration of KCl and clay stabilizer may not be helpful in alleviating the damage.

The evolvement of pressure distribution is shown from Figure 6-27 to Figure 6-30.

Figure 6-27 is the initial pressure distribution after a treatment with P_r = 3720 psi, FBHP = 3348 psi, $k_{n.f.}$ = 0.4793 md HF2 ideal case after 7 days of treatment. The area with intense hydraulic fracture network shows signs of high pressure. In other areas, pressure is uniformly distributed in the drainage area.

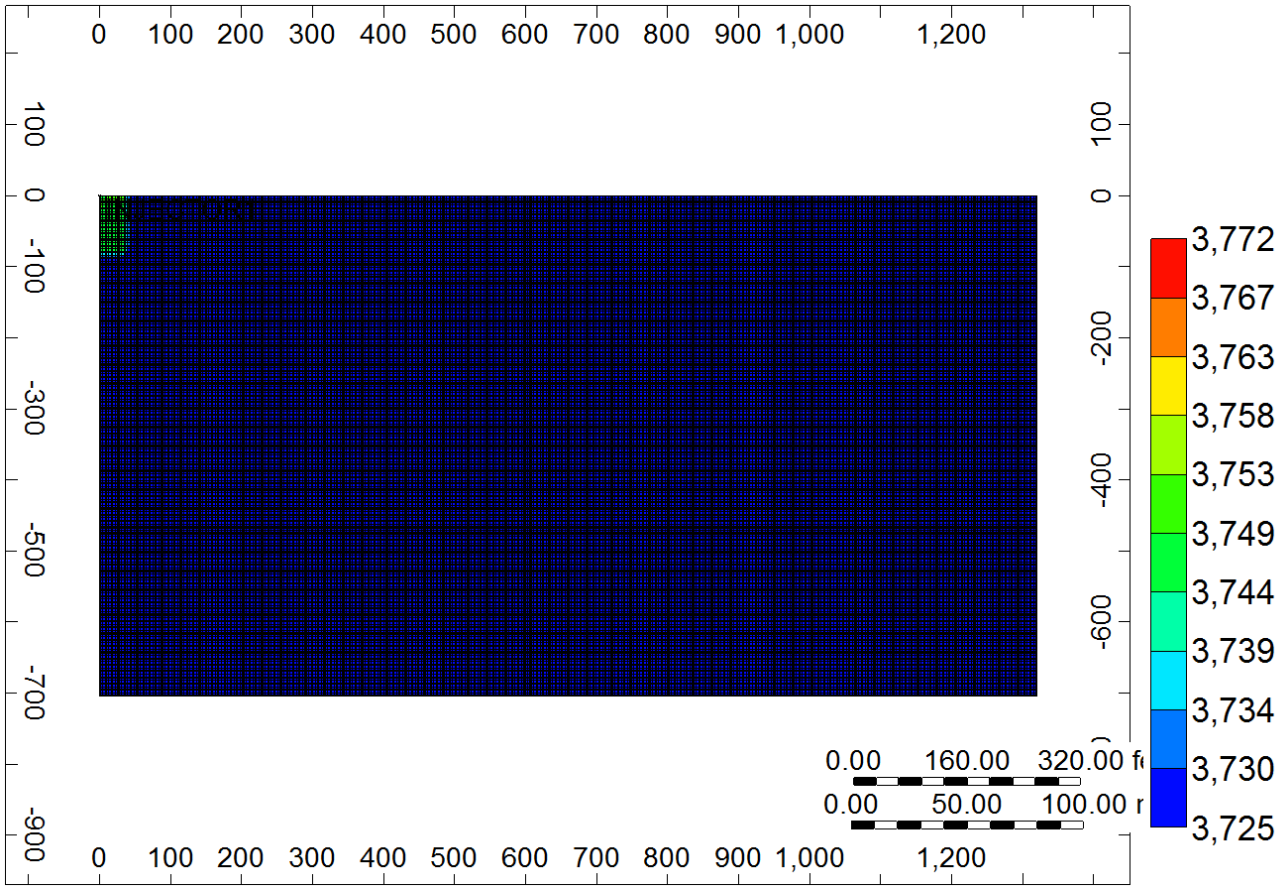

Figure 6-27 Pressure map after a treatment data5 with P_r = 3720 psi, FBHP = 3348 psi, H.F.2.. $k_{n.f.}$ = 0.4793 md after 7 days of treatment (HF2 ideal case)

Figure 6-28 shows a zoomed view of hydraulic fracture network for HF2. We can see that blocks represent hydraulic fractures have extremely high pressure value which is 3772 psi. The blocks adjacent with them also show high values of pressure, which is near 3767 psi. Formation blocks within the surroundings of hydraulic fractures have pressure value of 3750 psi. Once stepped out of the hydraulic facture area, reservoir pressure decreased to 3725 psi, which equals with initial reservoir pressure 3725 psi.

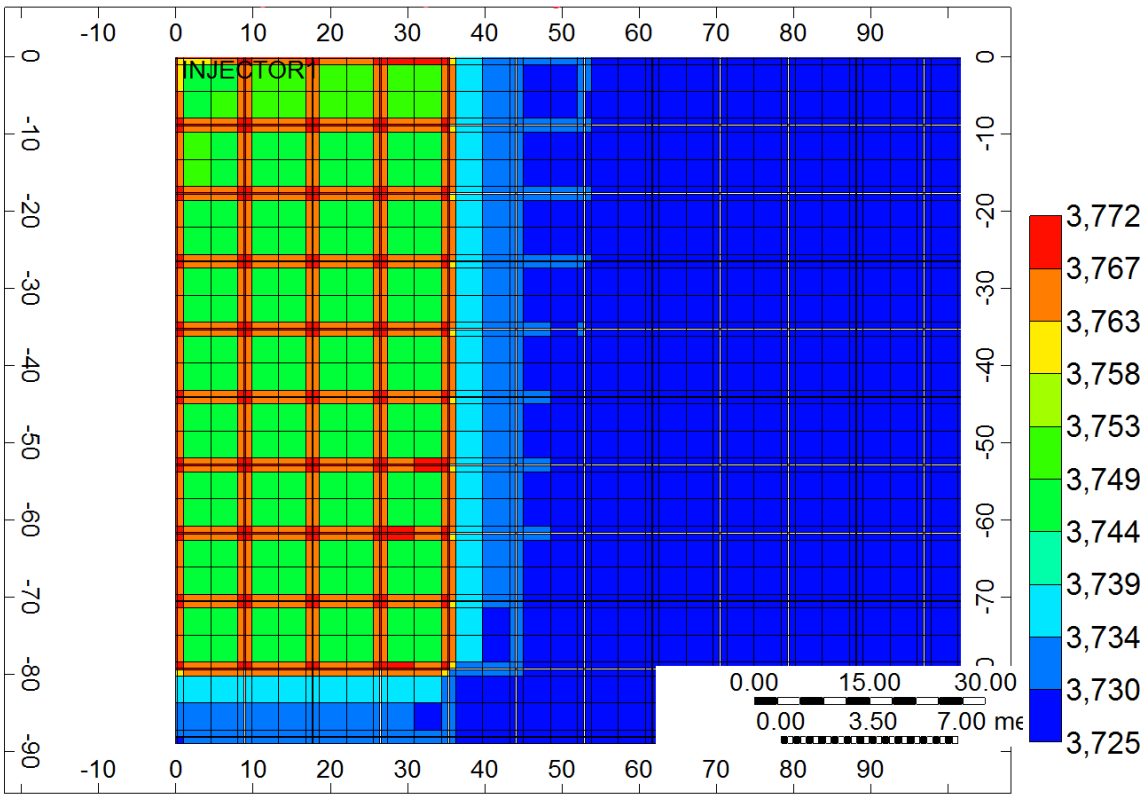

Figure 6-28 Pressure map (zoomed view around fracture network) after a treatment data5 with P_r = 3720 psi, FBHP = 3348 psi, $k_{n.f.}$ = 0.4793 md after 7 days of treatment (HF2 ideal case)

Figure 6-29 represents pressure distribution after 10 years of production. We can see almost 1/3 of the drainage area shows signs of stimulation. Also, the “blue area”, which represents low pressure value area, is occupied by hydraulic fracture network. This is an indication that the network of hydraulic fracture intensely stimulates this area.

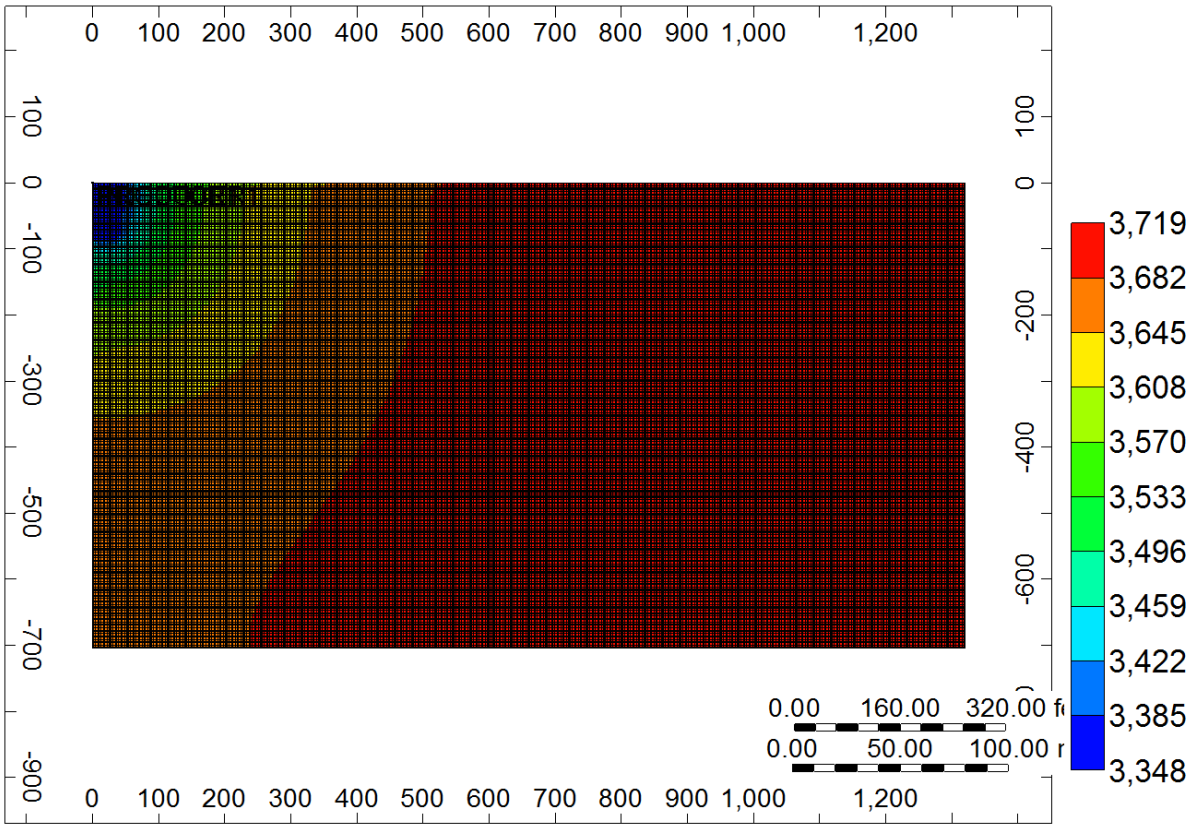

Figure 6-29 Pressure map after a treatment with P_r = 3720 psi, FBHP = 3348 psi, $k_{n.f.}$ = 0.4793 md (HF2 ideal case) after 10 years

Figure 6-30 shows pressure distribution after 20 years production. We can see in the picture that the entire drainage area has been largely stimulated, which is better than the condition in HF1. Still, the “blue area”, which represents intensely stimulated area, is occupied by hydraulic fracture network. Although the stimulation degree of HF2 first 10 years of production is less than satisfactory when compared with that of HF1, the stimulated area in the last 10 years of production is much more promising than that of HF1.

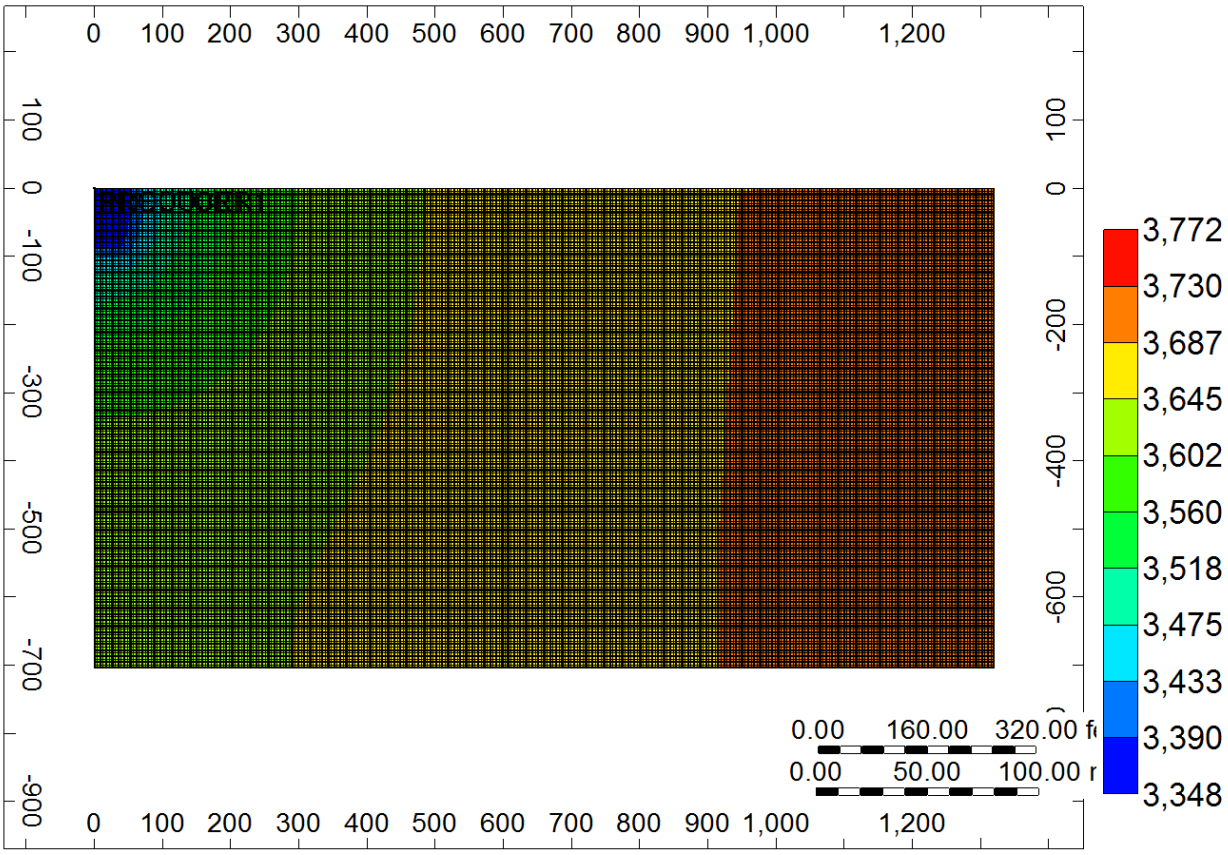

Figure 6-30 Pressure map after a treatment with P_r = 3720 psi, FBHP = 3348 psi, $k_{n.f.}$ = 0.4793 md (HF2 ideal case) after 20 year

The evolvement of water distribution is shown from Figure 6-31 to Figure 6-36. Figure 6-31 represents the initial water distribution of a treatment with P_r = 3720 psi, FBHP = 3348 psi, $L_{h.f.}$ = 836 ft. $k_{n.f.}$ = 0.4793 md (HF2 ideal case).

Figure 6-31 represents water saturation distribution after 7 days of treatment. We can see that hydraulic fracture is filled with water. The blocks near hydraulic fractures also show high values of water saturation. Other formation blocks remain the same water saturation value which is 0.2.

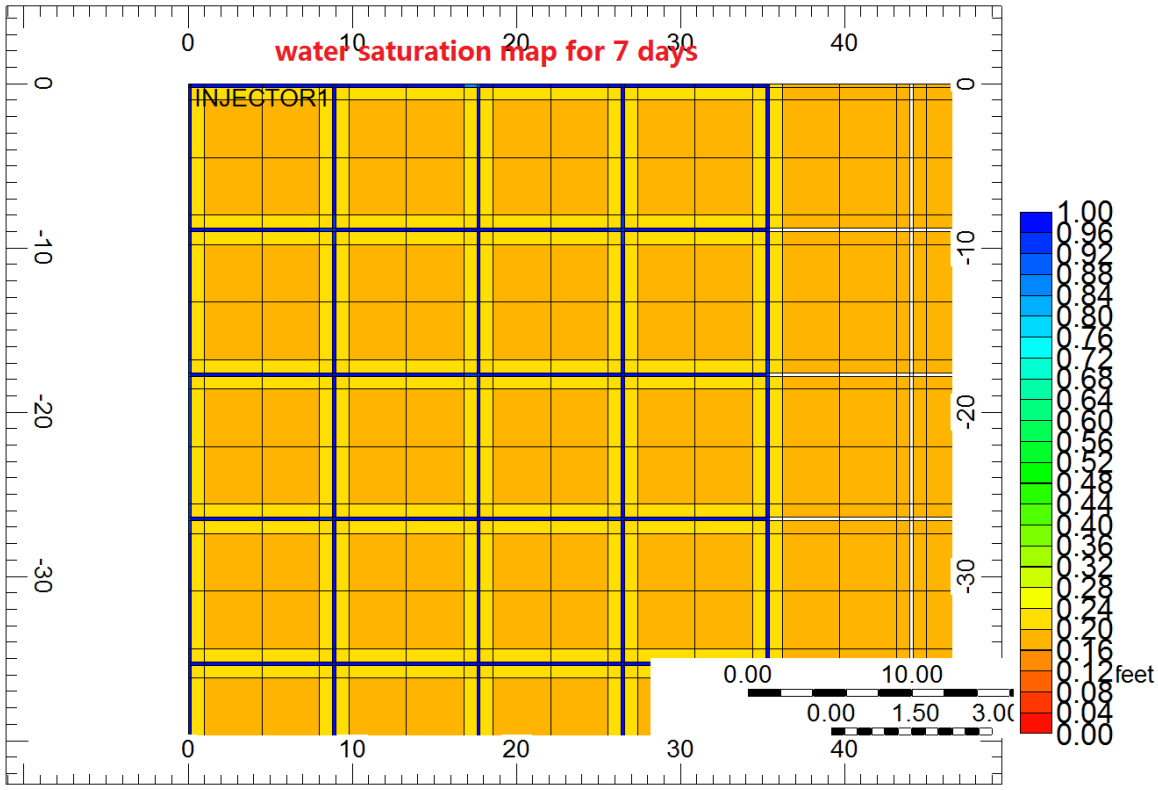

Figure 6-31 Water distribution after a treatment with P_r = 3720 psi, FBHP = 3348 psi, $k_{n.f.}$ = 0.4793 md (HF2 ideal case) after 7 days.

Figure 6-32 represents water saturation distribution after 2 weeks of production. We can see a higher water saturation value in the hydraulic fracture network. Water saturation value decreases to from 1 to 0.6 after 2 weeks of production. Besides hydraulic fracture, other formation blocks do not show obvious sign of water saturation value higher than 0.2, which represents reducible fracture fluid is nearly depleted after 2 weeks of production.

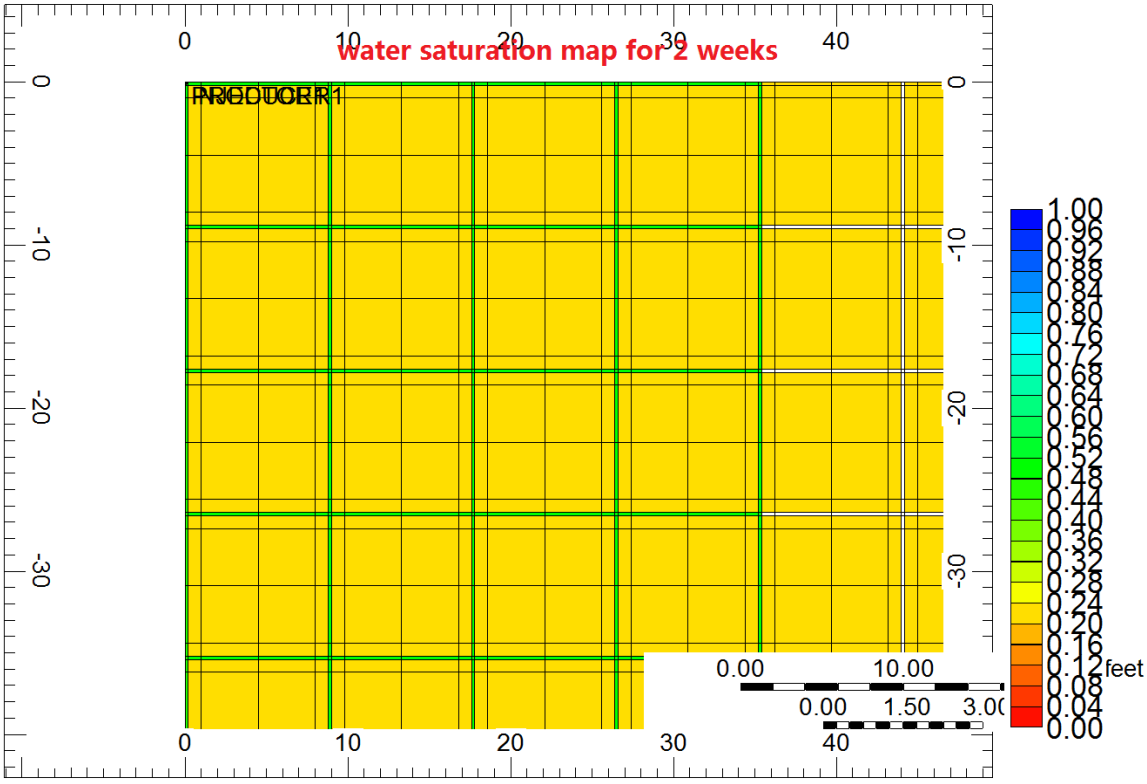

Figure 6-32 Water distribution after a treatment with P_r = 3720 psi, FBHP = 3348 psi, $k_{n.f.}$ = 0.4793 md (HF2 ideal case) after 2 weeks

Figure 6-33 represents water saturation distribution after 6 months. We can see a higher water saturation value in the hydraulic fracture network. Water saturation value decreases to almost 0.4 after 6 months of production. Besides hydraulic fracture, other formation blocks are evenly distributed with water saturation value of 0.2, which represents reducible fracture fluid is almost depleted.

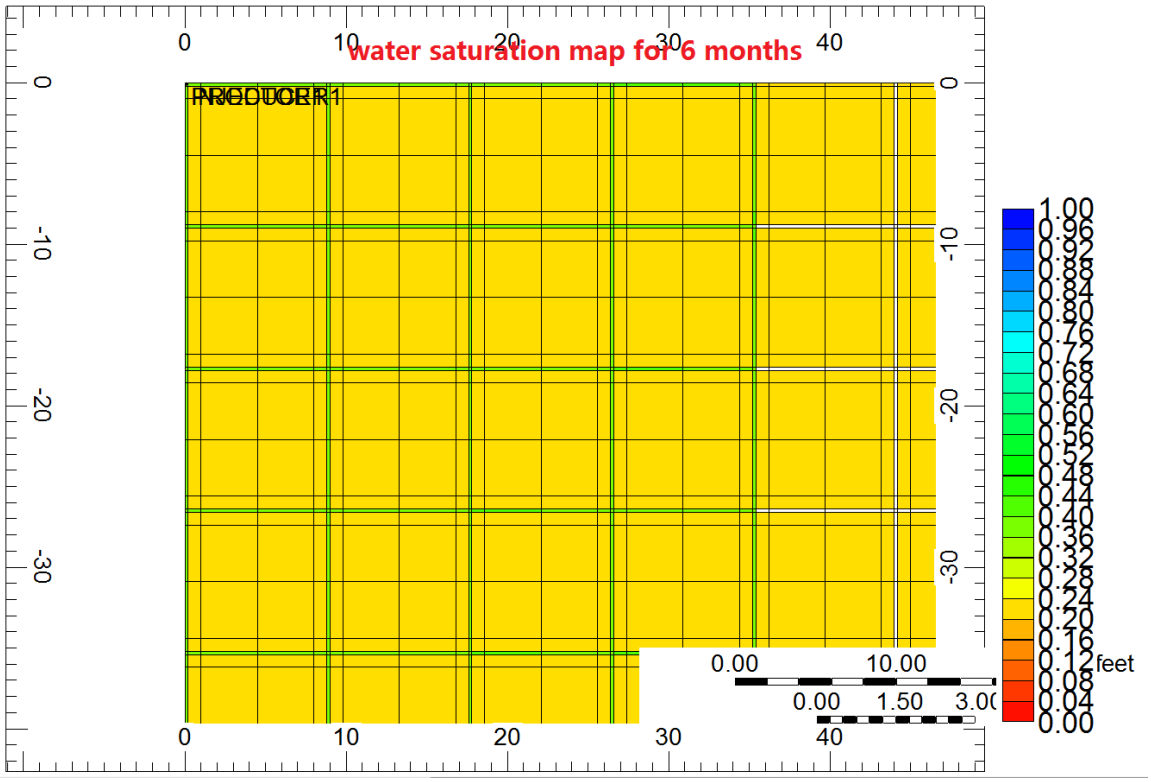

Figure 6-33 Water distribution after a treatment with P_r = 3720 psi, FBHP = 3348 psi, $k_{n.f.}$ = 0.4793 md (HF2 ideal case) after 6 months

Figure 6-34 represents water saturation distribution after 3 years of production. Water saturation within hydraulic fracture network is decreased to 0.32. Also, the blocks near wellbore has higher water saturation value than the blocks distant to wellbore. Water saturation distribution doesn't change much from year3 to year20, which represent the irreducible water saturation.

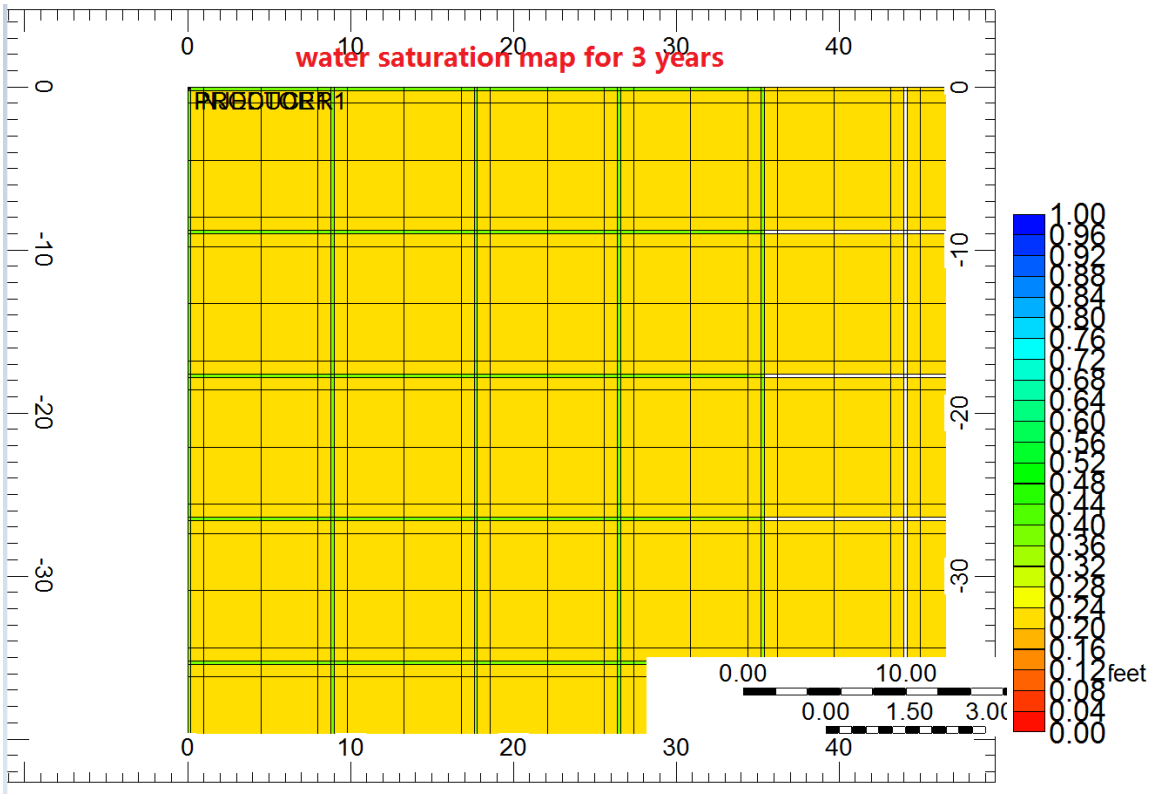

Figure 6-34 Water distribution after a treatment with P_r = 3720 psi, FBHP = 3348 psi, $k_{n.f.}$ = 0.4793 md (HF2 ideal case) after 6 months

Figure 6-35 and Figure 6-36 represent water saturation distribution after 10 years of production and 20 years of production respectively. Water saturation value doesn't show obvious signs of change, which represents the irreducible water saturation.

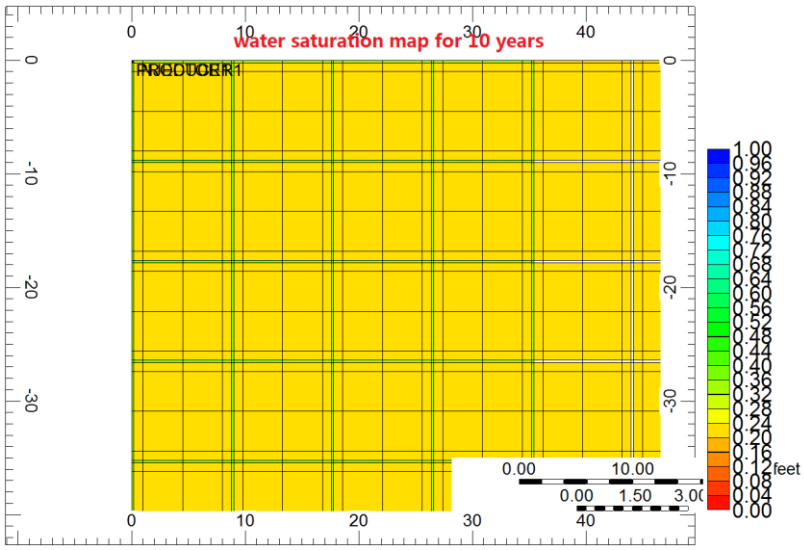

Figure 6-35 Water distribution after a treatment with P_r = 3720 psi, FBHP = 3348 psi, $k_{n.f.}$ = 0.4793 md (HF2 ideal case) after 3 years

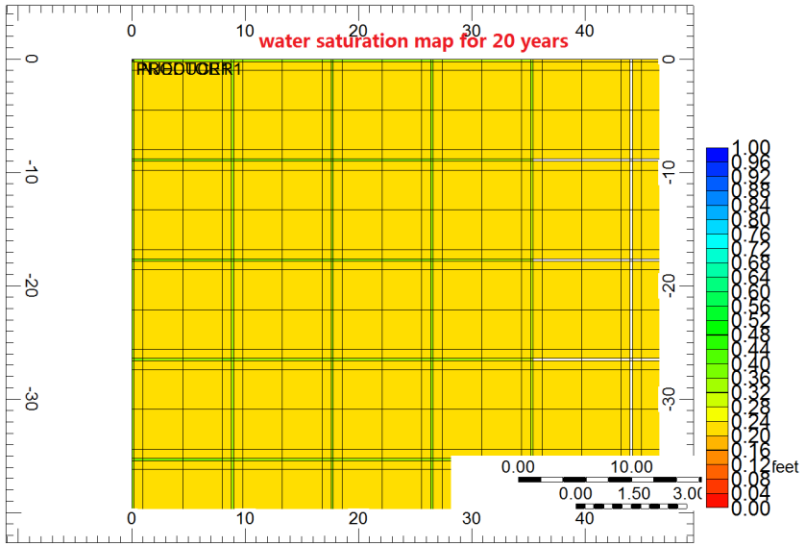

Figure 6-36 Water distribution after a treatment with P_r = 3720 psi, FBHP = 3348 psi, $k_{n.f.}$ = 0.4793 md (HF2 ideal case) after 10 years

6.2.3 Simulation results for H.F.3

As mentioned before, H.F.3 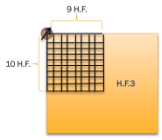

has a broader hydraulic fracture network around wellbore. Simulation results of gas recovery and gas rate are shown in the following figures.

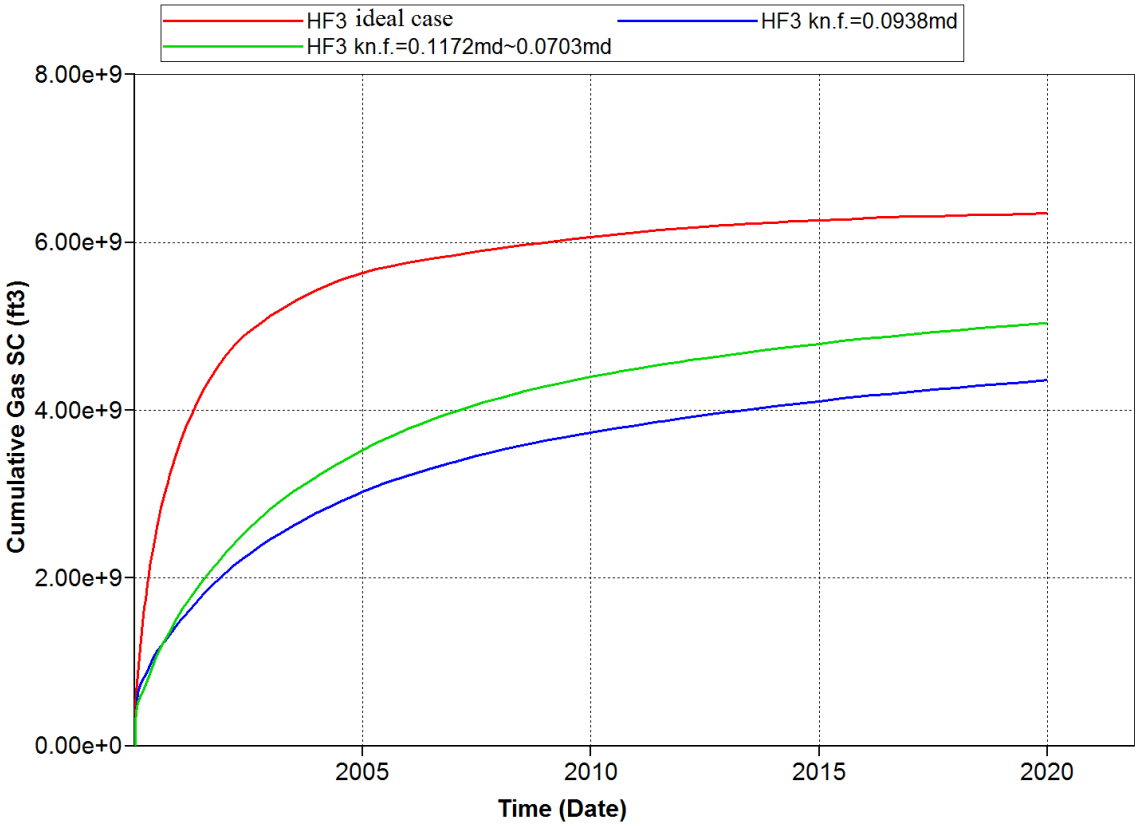

Figure 6-37 Interaction of Marcellus shale and fluid decease cumulative gas production for 20-40Ceramics proppant over 20 years with P_r = 3720 psi, FBHP = 3348 psi, for HF3

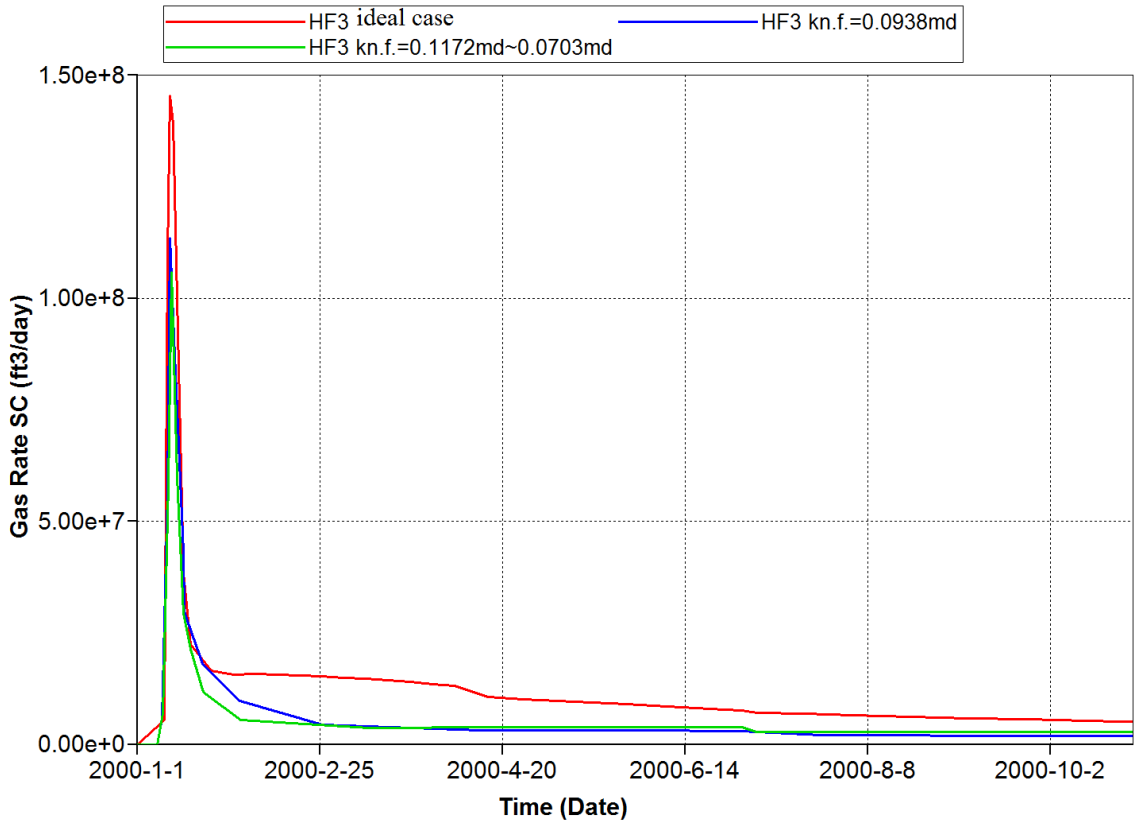

Figure 6-38 Interaction of Marcelluse shale and fluid decease gas rate for 20-40Ceramics proppant over 20 years with P_r = 3720 psi, FBHP = 3348 psi, for HF3.

"HF3 ideal case" represents the case without damage, $k_{n.f.}$ is 0.4395md. "HF3 $k_{n.f.}$=0.0938md"represents the case with damaged and constant natural permeability, $k_{n.f.}$=0.0938md. "HF3 $k_{n.f.}$=0.1172md~0.0703md" represents the case with gradually decreasing permeability, $k_{n.f.}$ starts from 0.1172md and gradually reduce to 0.0703md.

Gas recovery curve and gas rate curve for data4, data5, and data6 are shown in Figure 6-37 and Figure 6-38**.** We can see that permeability decrease caused by interaction between fluid and formation rock has decreased gas recovery from 6.3×10^9 ft^3 (HF3 ideal case) to 4.34×10^9 ft^3 (HF3 $k_{n.f.}$=0.0938md), 5.0×10^9 ft^3 (HF3 $k_{n.f.}$=0.1172md~0.0703md), which is approximately 31% and 20% respectively. The results are similar with H.F.2, and slightly better. Gas rate plot shows similar trend with cumulative gas production plot.

We can get a similar conclusion with H.F.2.

The evolvement of pressure distribution after a treatment with P_r = 3720 psi, FBHP = 3348 psi, $k_{n.f.}$ = 0.4793 md (HF3 ideal case) is shown from Figure 6-39 to Figure 6-42.

Figure 6-39 represents the pressure distribution on day7. We can see signs of high pressure value around fracture network. The highest pressure value is 3,731 psi. Except for the fracture network, pressure is uniformly distributed over the entire drainage area with initial reservoir pressure 3,725 psi.

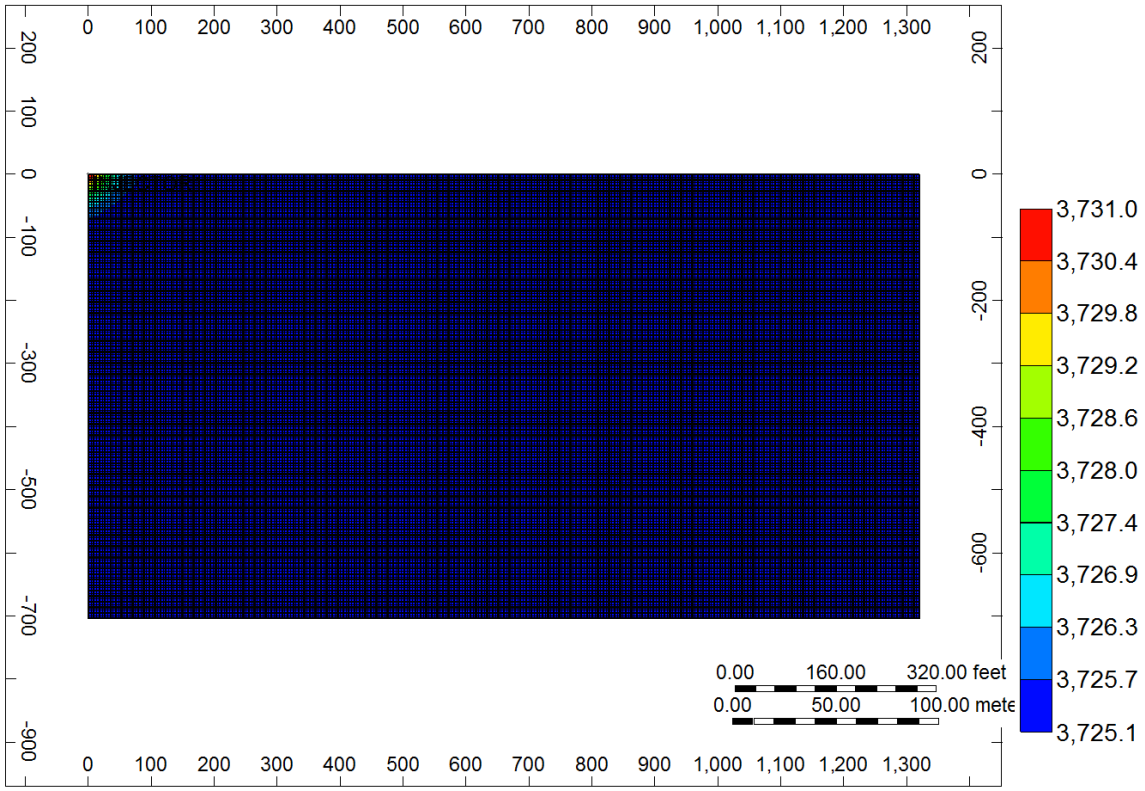

Figure 6-39 Pressure map after a treatment with P_r = 3720 psi, FBHP = 3348 psi, H.F.3. $k_{n.f.}$ = 0.4793 md (HF3 ideal case) after 7 days of treatment.

Figure 6-40 shows the zoomed view around hydraulic fracture network after 7 days of production for HF3 ideal case. In this figure, we can observe closely of the pressure distribution within the hydraulic fracture network. We can see that, blocks near well bore show higher pressure value, while blocks far from wellbore show low permeability value.

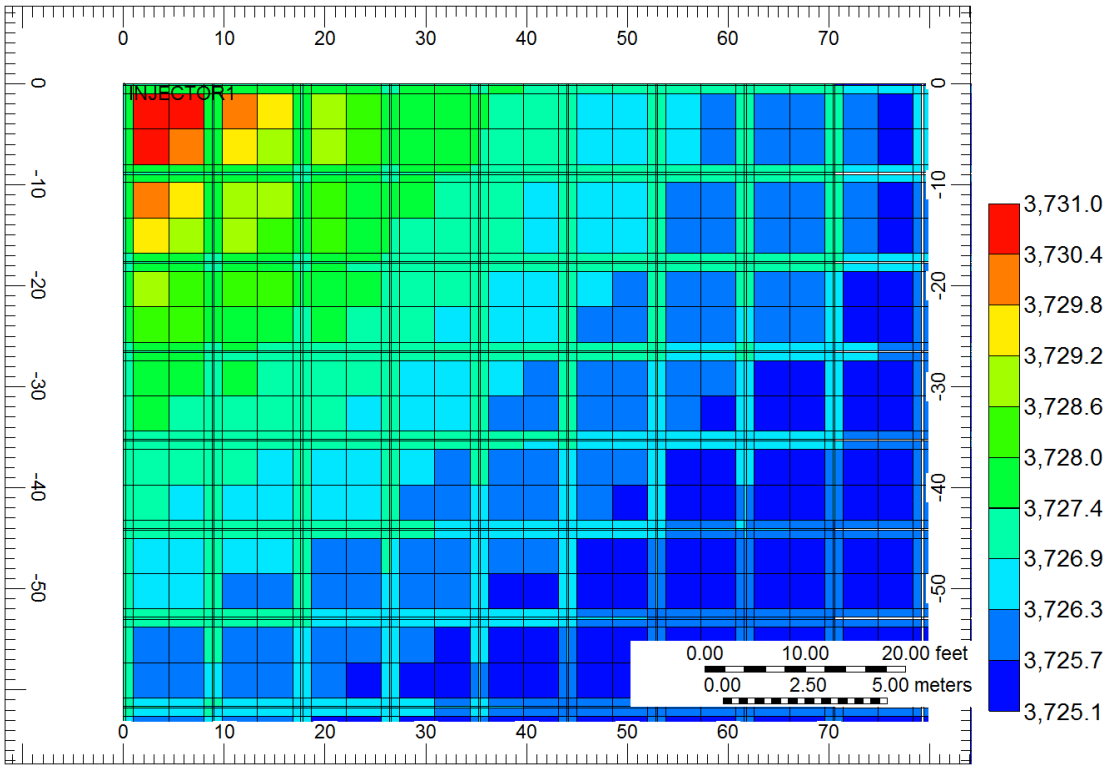

Figure 6-40 Pressure map (zoomed view around hydraulic fracture network) after a treatment with P_r = 3720 psi, FBHP = 3348 psi, $k_{n.f.}$ = 0.4793 md (HF3 ideal case) after 7 days of treatment.

Figure 6-41 and Figure 6-42 represent pressure map over 10 years and 20 years respectively. Similar with those of H.F.2, Figure 6-41 represents pressure distribution after 10 years of production. We can see almost 1/2 of the drainage area shows signs of stimulation. Also, the “blue area”, which represents low pressure value area, is occupied by hydraulic fracture network. This is an indication that the network of hydraulic fracture intensely stimulates this area.

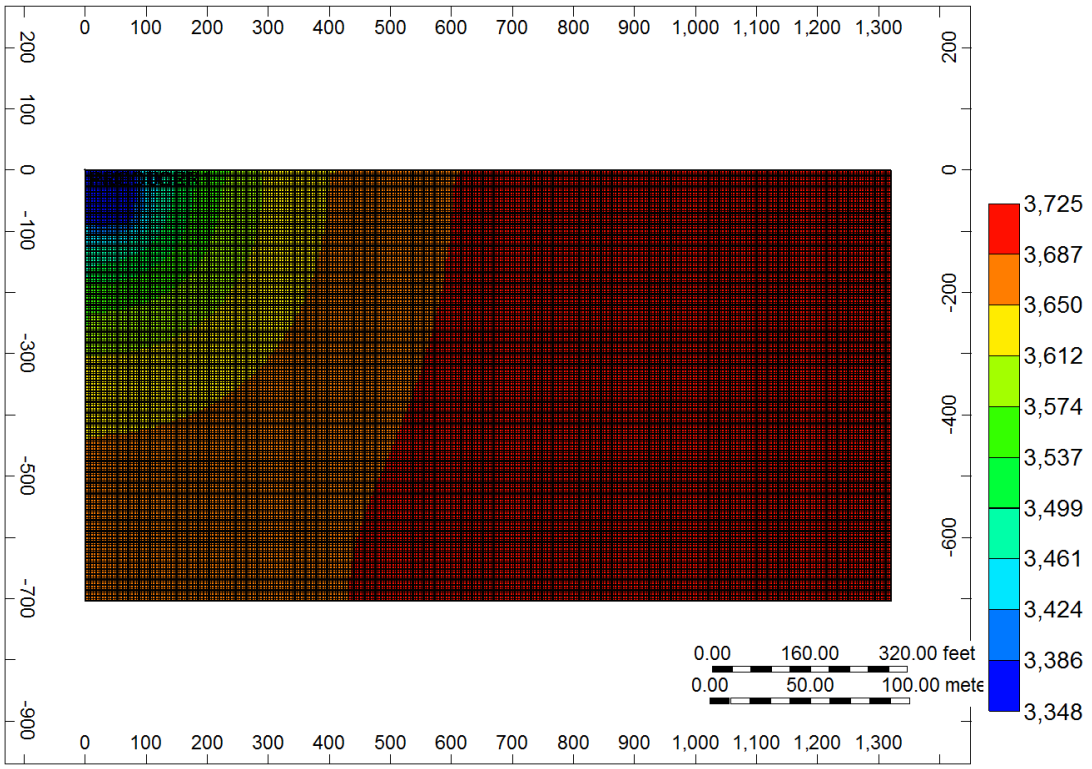

Figure 6-41 Pressure map after a treatment with P_r = 3720 psi, FBHP = 3348 psi, H.F.3. $k_{n.f.}$ = 0.4793 md (HF3 ideal case) after 10 years of production.

Figure 6-42 shows pressure distribution after 20 years production. We can see in the picture that the entire drainage area has been largely stimulated. Still, the “blue area”, which represents intensely stimulated area, is occupied by hydraulic fracture network.

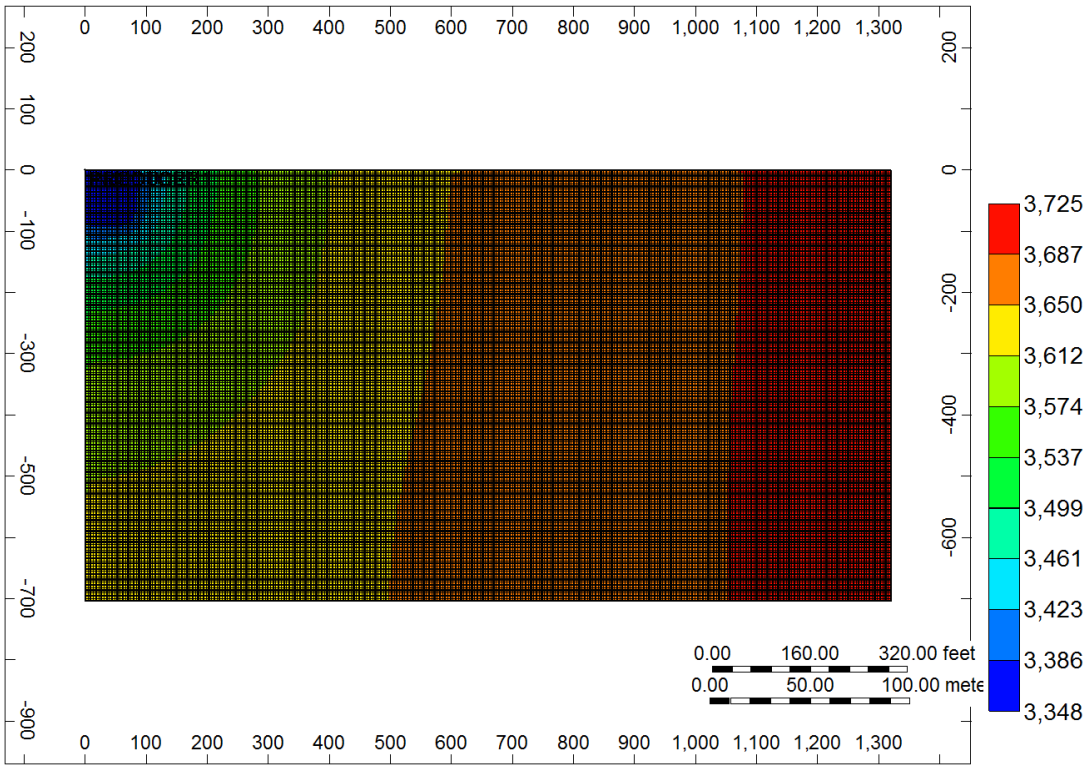

Figure 6-42 Pressure map after a treatment with P_r = 3720 psi, FBHP = 3348 psi, H.F.3. $k_{n.f.}$ = 0.4793 md (HF3 ideal case) after 20 years of production.

Figure 6-43 through Figure 6-48 represents the evolvement of water saturation distribution after the same treatment. The evolvement is based on a treatment with P_r = 3720 psi, FBHP = 3348 psi, $k_{n.f.}$ = 0.4793 md (HF3 ideal case)

Figure 6-43 represents water saturation distribution after 7 days of treatment. We can see that hydraulic fracture is filled with water. The blocks near hydraulic fractures also show high values of water saturation. Other formation blocks remain the same water saturation value which is 0.2.

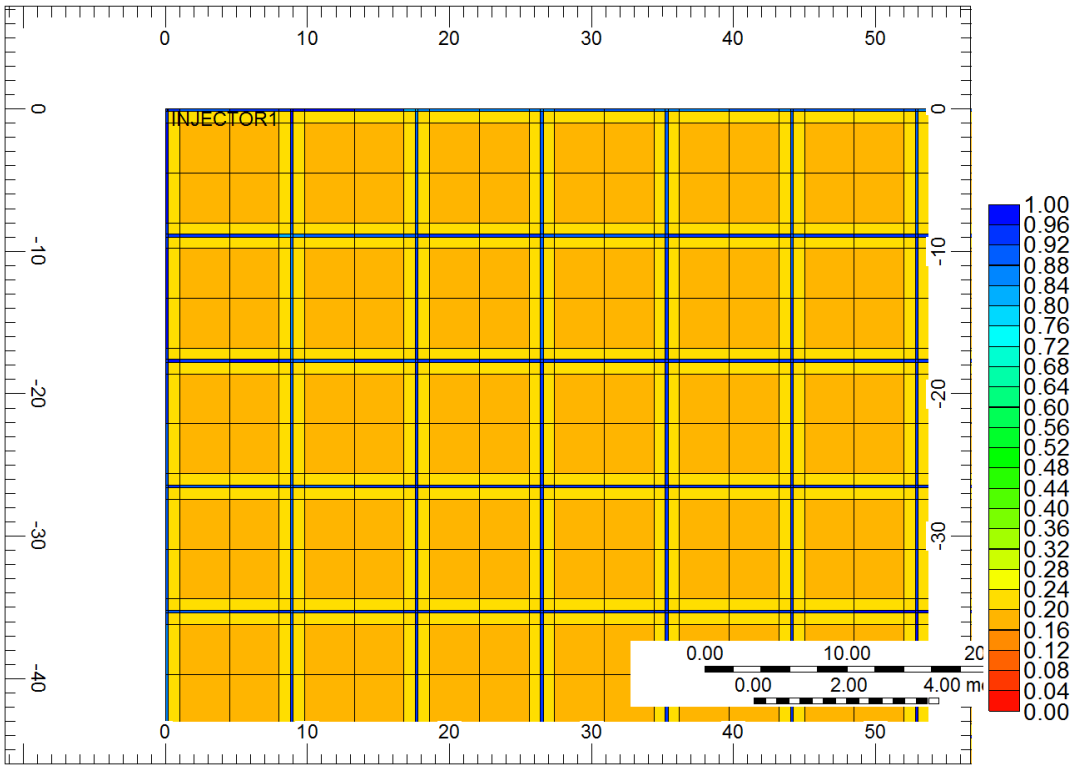

Figure 6-43 Water saturation distribution with a treatment with P_r = 3720 psi, FBHP = 3348 psi, H.F.3. $k_{n.f.}$ = 0.4793 md (HF3 ideal case) after 7 days of treatment.

Figure 6-44 represents water saturation distribution after 2 weeks of production. We can see a higher water saturation value in the hydraulic fracture network. Water saturation value decreases to from 1 to 0.6 after 2 weeks of production. Besides hydraulic fracture, other formation blocks do not show obvious sign of water saturation value higher than 0.2, which represents reducible fracture fluid, is nearly depleted after 2 weeks of production.

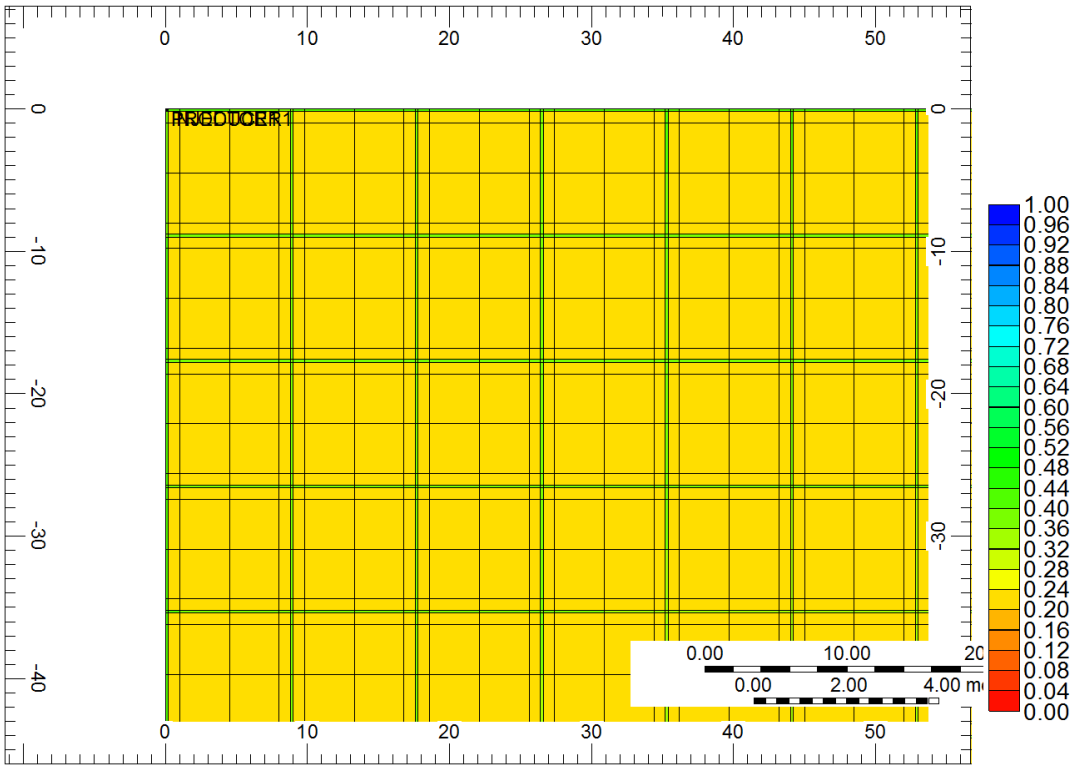

Figure 6-44 Water saturation distribution with a treatment with P_r = 3720 psi, FBHP = 3348 psi, H.F.3. $k_{n.f.}$ = 0.4793 md (HF3 ideal case) after 2 weeks

Figure 6-45 represents water saturation distribution after 6 months. We can see a higher water saturation value in the hydraulic fracture network. Water saturation value decreases to almost 0.4 after 6 months of production. Besides hydraulic fracture, other formation blocks are evenly distributed with water saturation value of 0.2, which represents reducible fracture fluid is almost depleted.

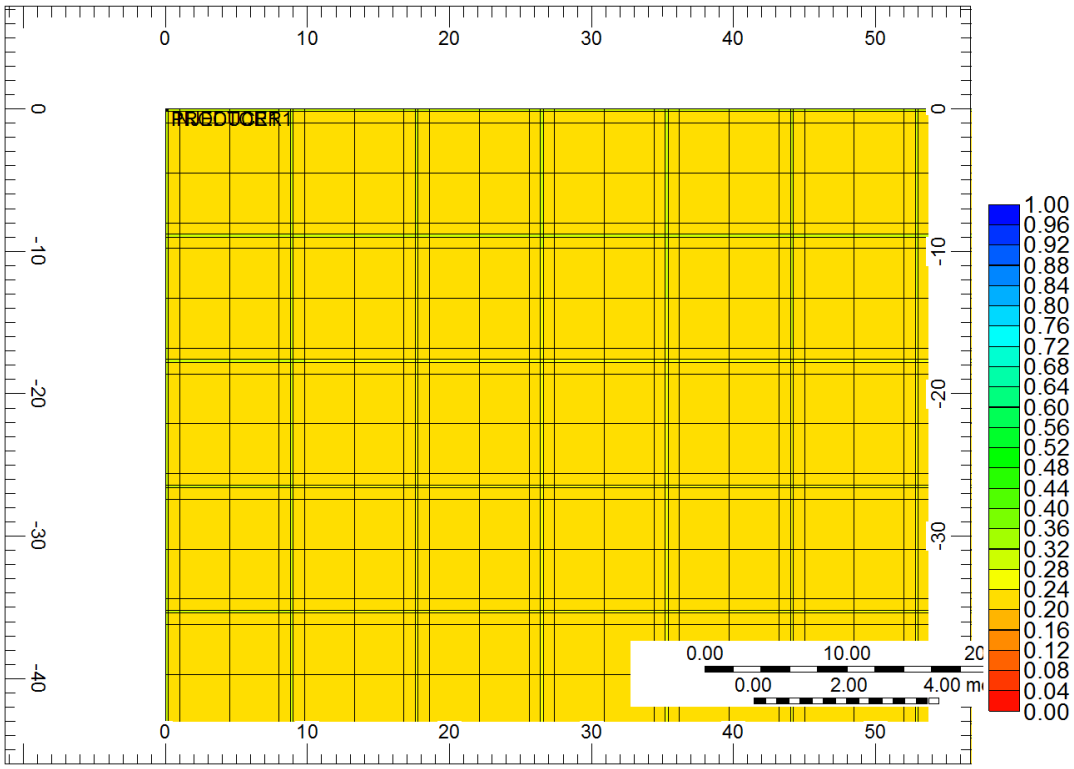

Figure 6-45 Water saturation distribution after a treatment with P_r = 3720 psi, FBHP = 3348 psi, H.F.3. $k_{n.f.}$ = 0.4793 md (HF3 ideal case) after 6 months.

Figure 6-46, Figure 6-47, and Figure 6-48 represent water saturation distribution after 3 years, 10 years, and 20 years of production respective. There is no obvious difference among them. Water saturation within hydraulic fractures almost equals to 0.32~0.36. These values represent the irreducible water. Water saturation within formation blocks are 0.2 as we can see from these figures.

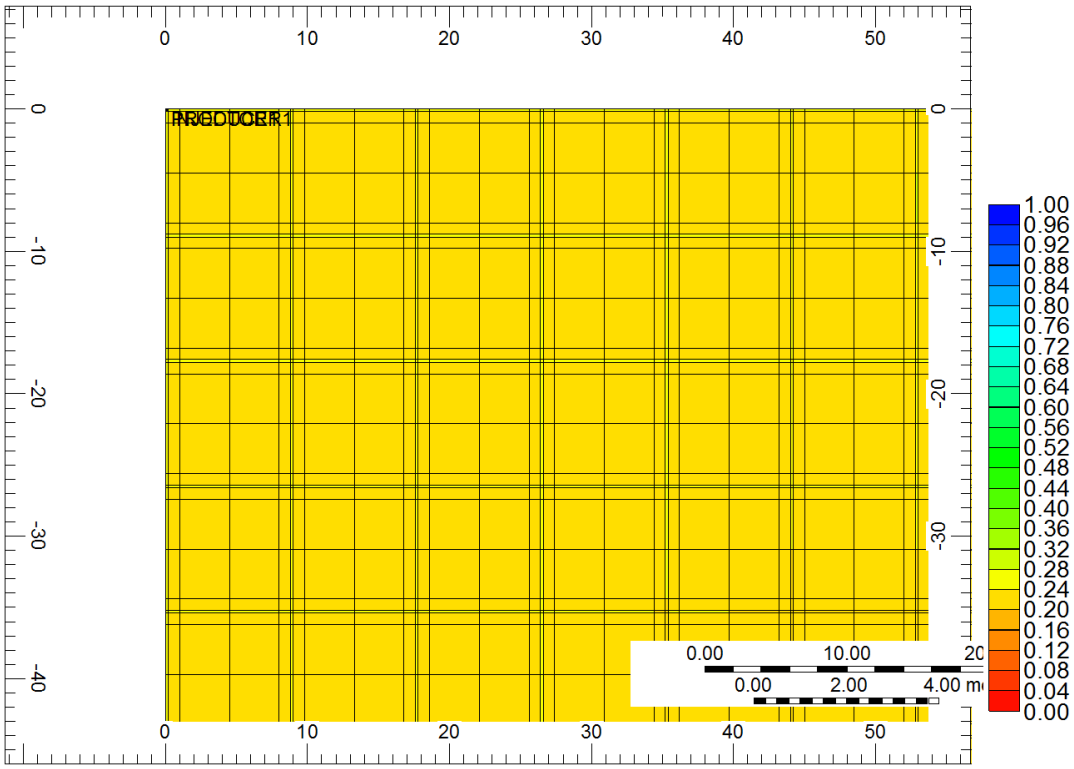

Figure 6-46 Water saturation distribution after a treatment with P_r = 3720 psi, FBHP = 3348 psi, H.F.3. $k_{n.f.}$ = 0.4793 md (HF3 ideal case) after 3 years.

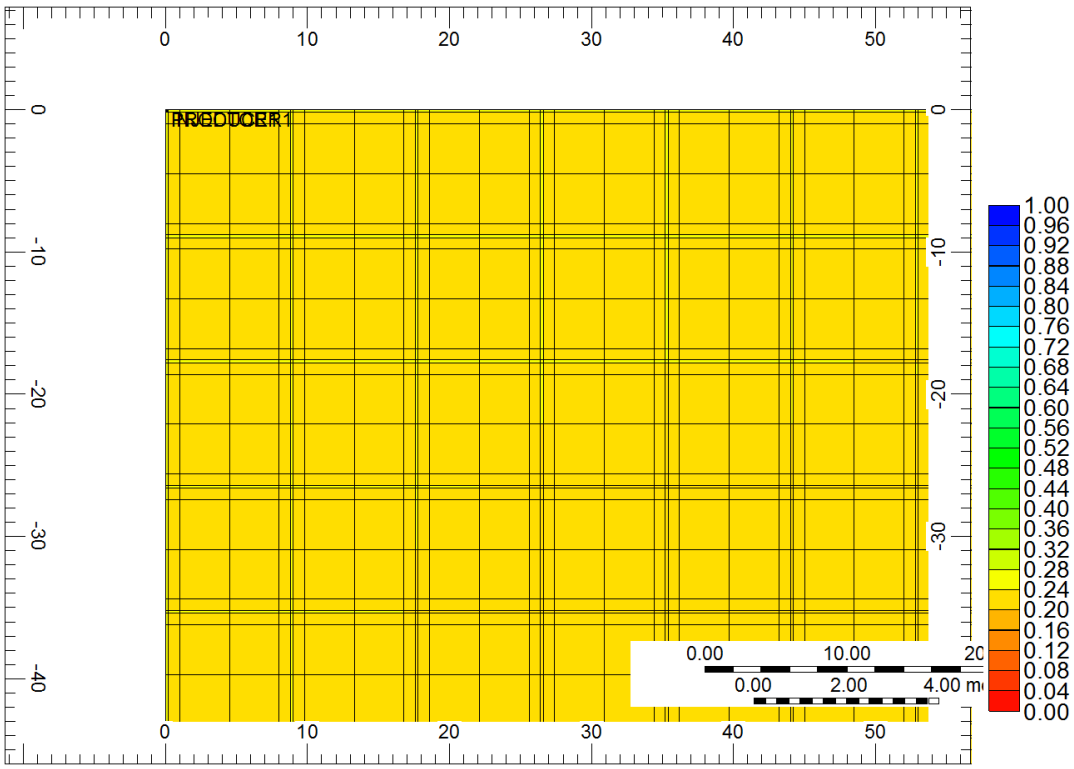

Figure 6-47 Water saturation distribution after a treatment with P_r = 3720 psi, FBHP = 3348 psi, H.F.3. $k_{n.f.}$ = 0.4793 md (HF3 ideal case) after 10 years

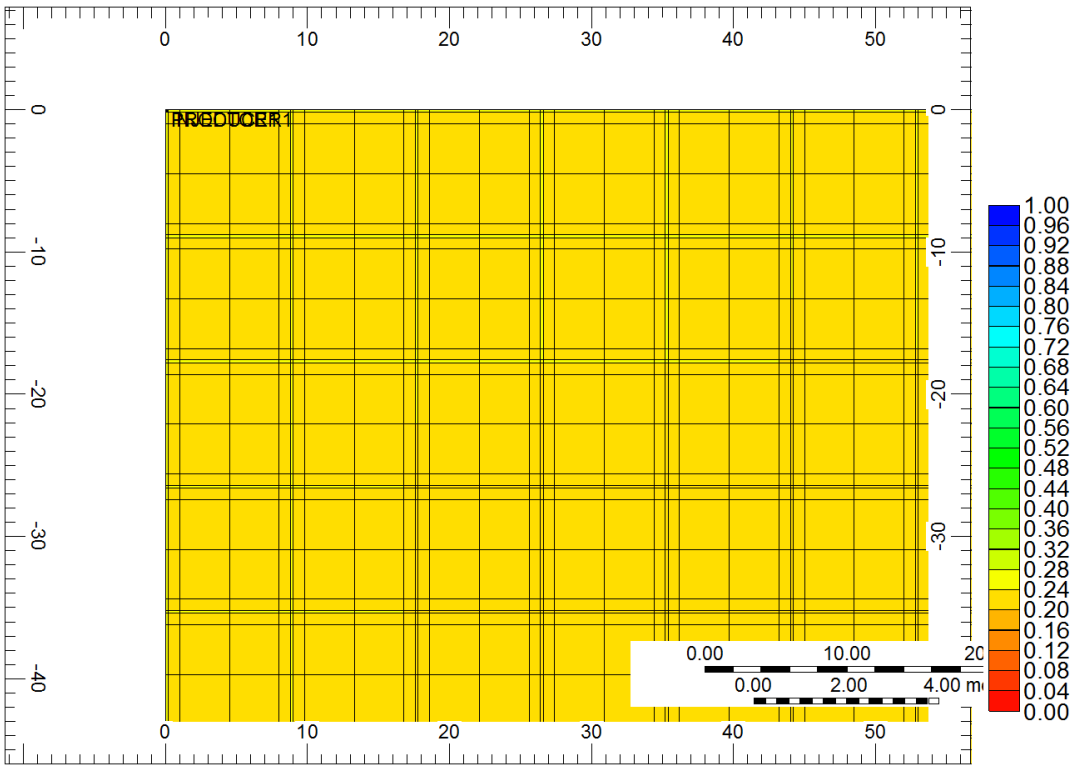

Figure 6-48 Water saturation distribution after a treatment with P_r = 3720 psi, FBHP = 3348 psi, H.F.3. $k_{n.f.}$ = 0.4793 md (HF3 ideal case) after 20 years

6.3 The effect of proppant scaling

As described earlier, chemical scaling in proppant pack is known to be generated by blending of fracture fluid and formation fluid, or simply during the drop of pressure. These scalings plug pores and flow channels, and result in a declined conductivity and productivity. To get an understanding of the magnitude of this kind of damage, we adopted the laboratory data from Weaver 2010's work(Weaver and Nguyen 2010).

Several files were selected to represent the damage effect of proppant scaling. Selected run numbers and their parameters are shown in Table 6-6.

Table 6-6 Run number and parameters selected to represent the damage effect of proppant scale

Run#	File name	scenario of H.F.	Pr(psi)	FBHP(psi)	H.F.(ft)	N.F. k(md)	H.F. k(md)	Δk(md)
HF1 ideal case*	data1	1	3720	3348	500	0.4793	65,500	0
HF1 proppant scaling	data17		3720	3348	500	0.4793	65,500	5080
HF2 ideal case*	data4	2	3720	3348	836	0.4793	39,174	0
HF2 proppant scaling	data20		3720	3348	836	0.4793	39,174	5080
HF3 ideal case*	data7	3	3720	3348	1152.8	0.4793	23,115	0
HF3 proppant scaling	data23		3720	3348	1152.8	0.4793	23,115	5080

* ideal case include effect of multiphase flow and proppant crushing .

6.3.1 Simulation results for H.F.1

As mentioned before, H.F.1 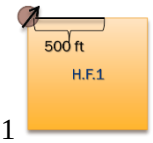

has a primary planar hydraulic fracture. Simulations results of gas recovery and gas rate are shown in the following figures.

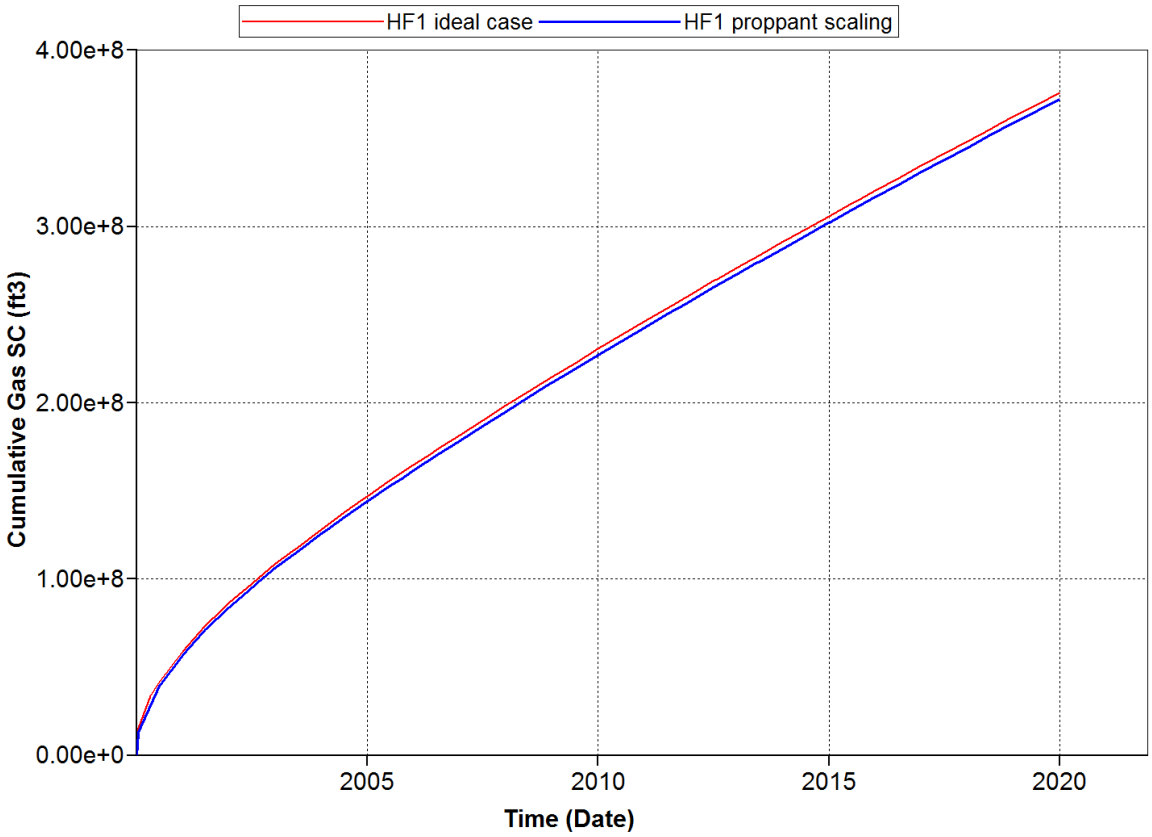

Figure 6-49 Proppant scale decrease cumulative gas production over 20 years with P_r = 3720 psi, FBHP = 3348 psi, and $k_{n.f.}$ = 0.4396 md, for HF1.

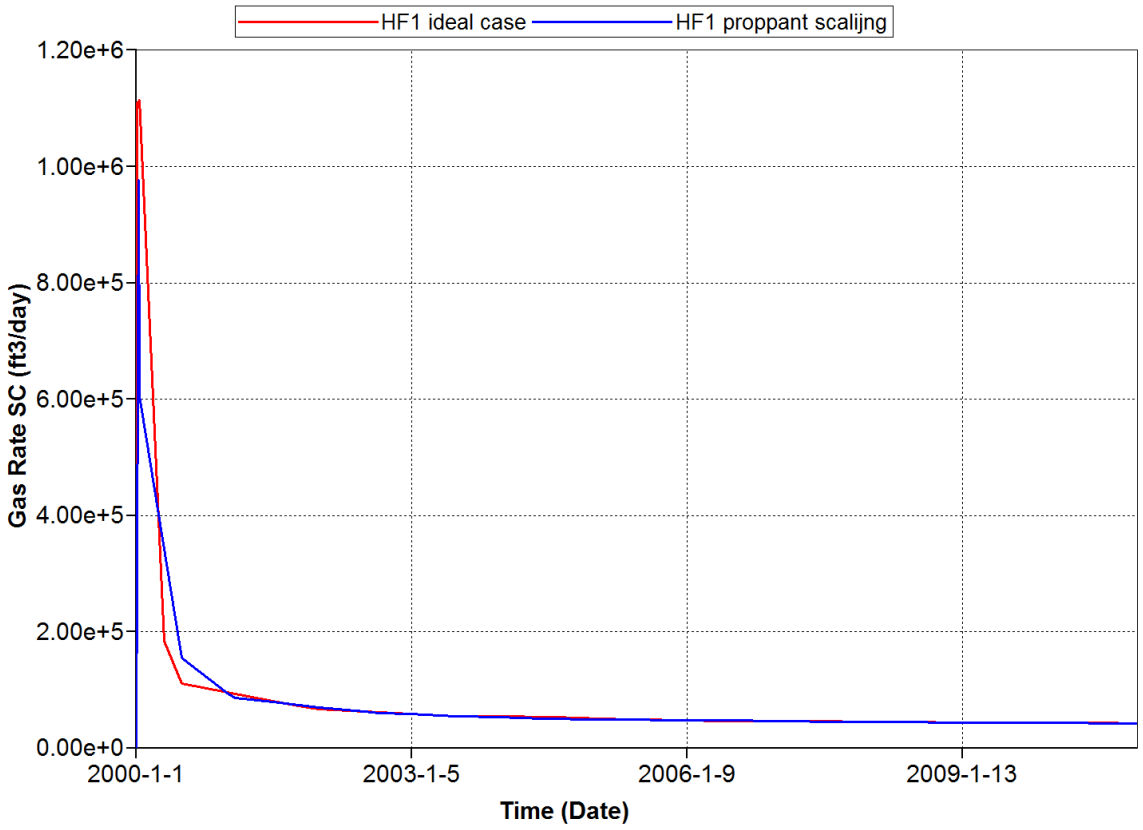

Figure 6-50 Proppant scale decrease gas rate over 20 years with P_r = 3720 psi, FBHP = 3348 psi, and $k_{n.f.}$ = 0.4396 md, for HF1.

"HF1 ideal case" represents the case without damage, in which $k_{h.f.}$ is 65,500md. "HF1 proppant scaling" represents the case with damage caused by chemical scaling, in which $k_{h.f.}$ is 60,420md.

From Figure 6-49 and Figure 6-50, we can see that there is no obvious decrease in cumulative production between these two scenarios. data1's cumulative gas production is 3.76×10^8 ft^3, while data55 is 3.72×10^8 ft^3. Gas rate plots are almost identical. Although there is permeability decrease in the fracture permeability (5,080 md), due to the big base number of the permeability value of hydraulic fracture (65,500 md), the reduction in cumulative production seems negligible. For gas rate, there is slight difference between these two cases in the first year

of production, which is the major cause for cumulative gas production difference. Gas rates for these two cases are identical from the second year of production to the end of production.

We can come to the understanding that chemical scaling will not cause damage to a planar hydraulic fracture.

6.3.2 Simulation results for H.F.2

As mentioned before, H.F.2 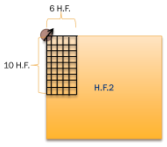

has a hydraulic fracture network around wellbore. Simulation results of gas recovery and gas rate are shown in the following figures.

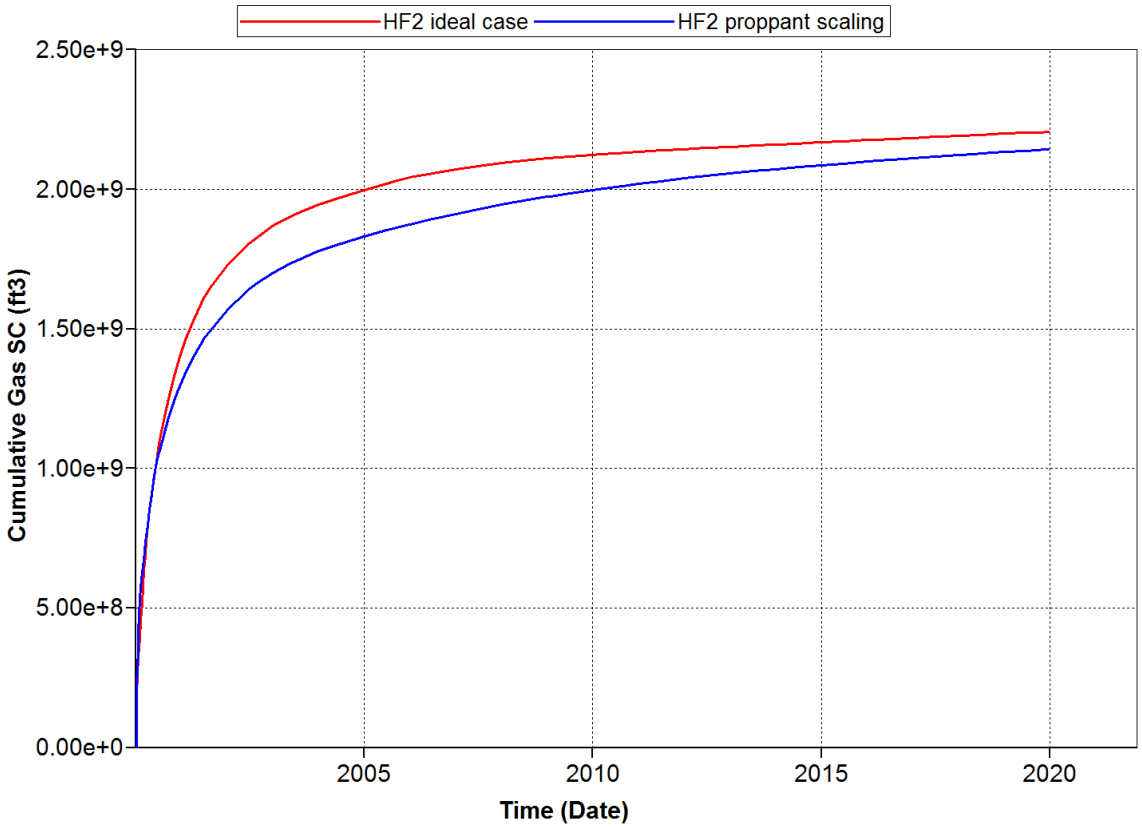

Figure 6-51 Proppant scale decrease cumulative gas production over 20 years with P_r = 3720 psi, FBHP = 3348 psi, and $k_{n.f.}$ = 0.4396 md, for HF2.

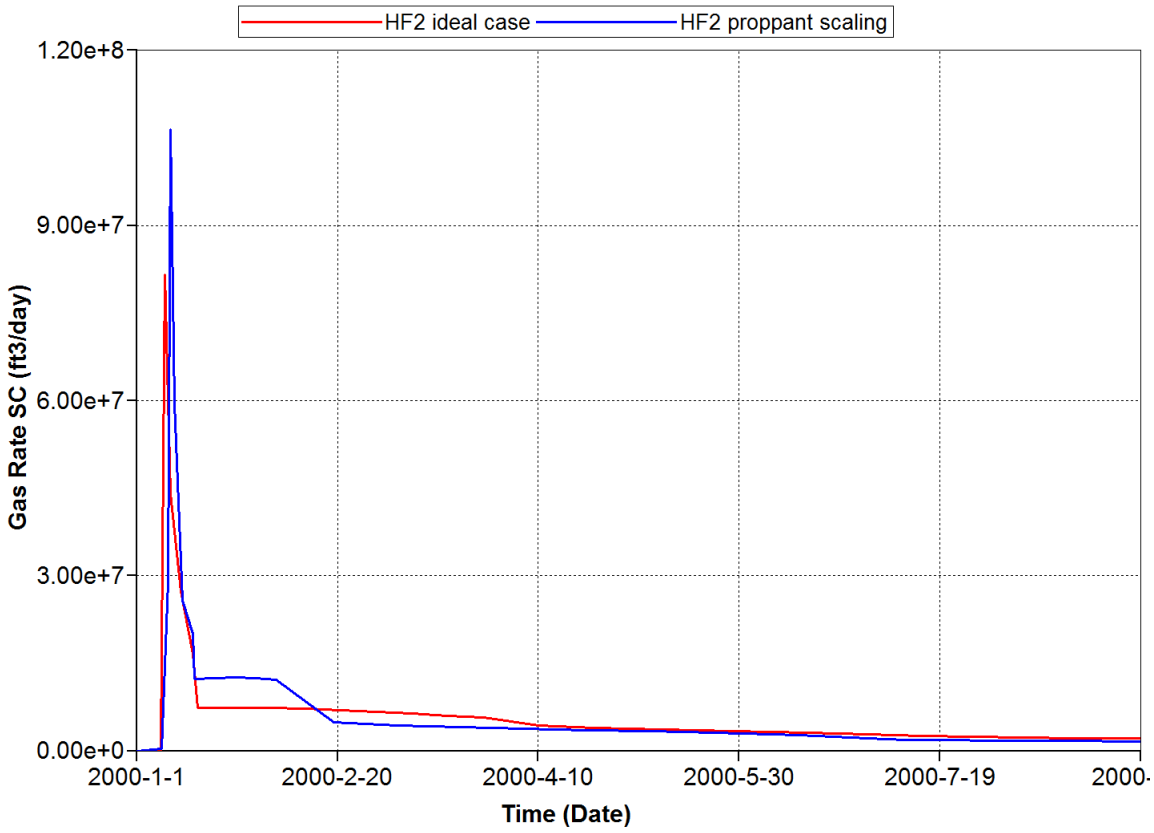

Figure 6-52 Proppant scale decrease gas rate over 20 years with P_r = 3720 psi, FBHP = 3348 psi, and $k_{n.f.}$ = 0.4396 md, for HF2.

"HF2 ideal case" represents the case without any damage, $k_{h.f.}$ is 39,174 md. "HF2 proppant scaling" represents the case with damage caused by chemical scaling, and $k_{h.f.}$ is 34,094 md.

From Figure 6-51 and Figure 6-52, we can see that ideal case for HF2 has a cumulative gas production of almost 2.2×10^9 ft^3 after 20 years of production, while the case with chemical scaling gives a cumulative production of 2.14×10^9 ft^3. Chemical scaling decreases gas production by 6×10^6 ft^3, which is 4.4%. Although the damage caused by chemical scaling is not prominent in HF1, it gradually shows its power in hydraulic fracture networks. From the gas rate

plot, which is Figure 6-52, we can see that the major difference of gas rate is also generated from the first year of production.

We can come to the conclusion that chemical scaling will cause some decrease in gas cumulative production in hydraulic fracture network.

6.3.3 Simulation results for H.F.3

As mentioned before, H.F.3 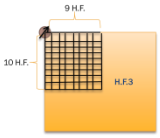

has a broader hydraulic fracture network around wellbore. Simulation results of gas recovery and gas rate are shown in the following figures.

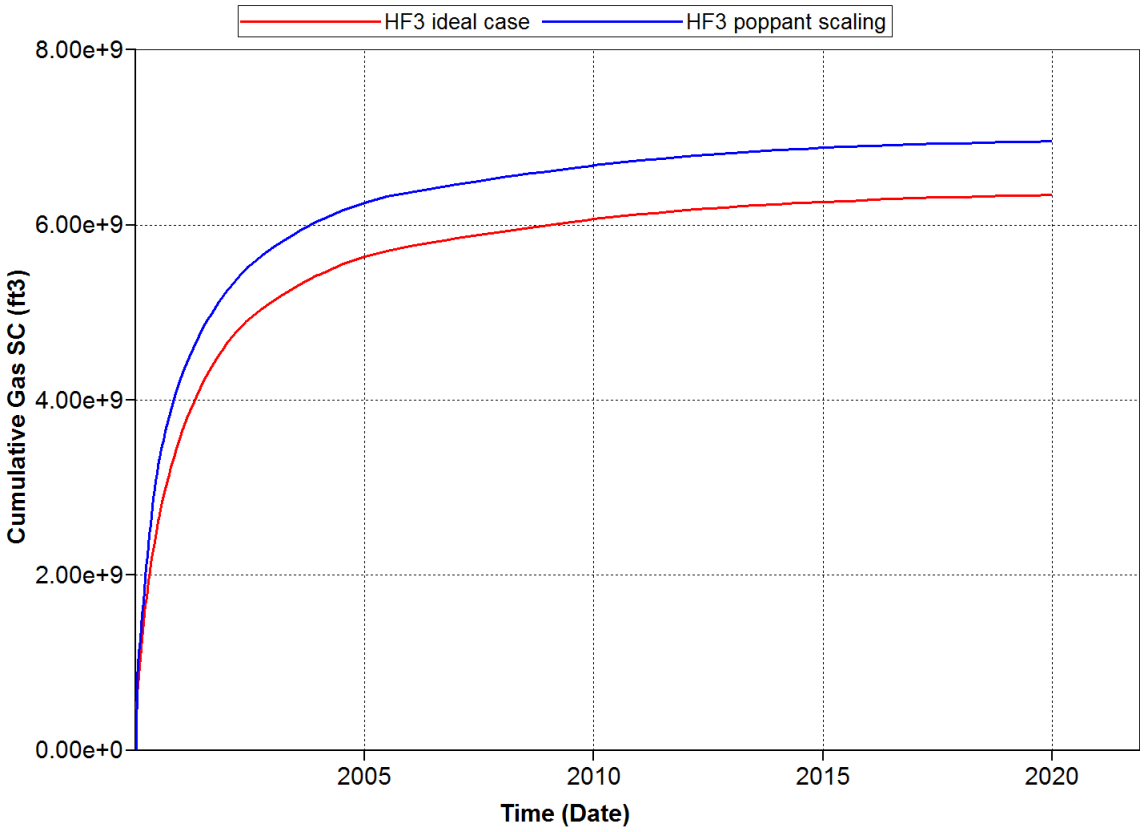

Figure 6-53 Proppant scale decrease cumulative gas production over 20 years with P_r = 3720 psi, FBHP = 3348 psi, and $k_{n.f.}$ = 0.4396 md, for HF3.

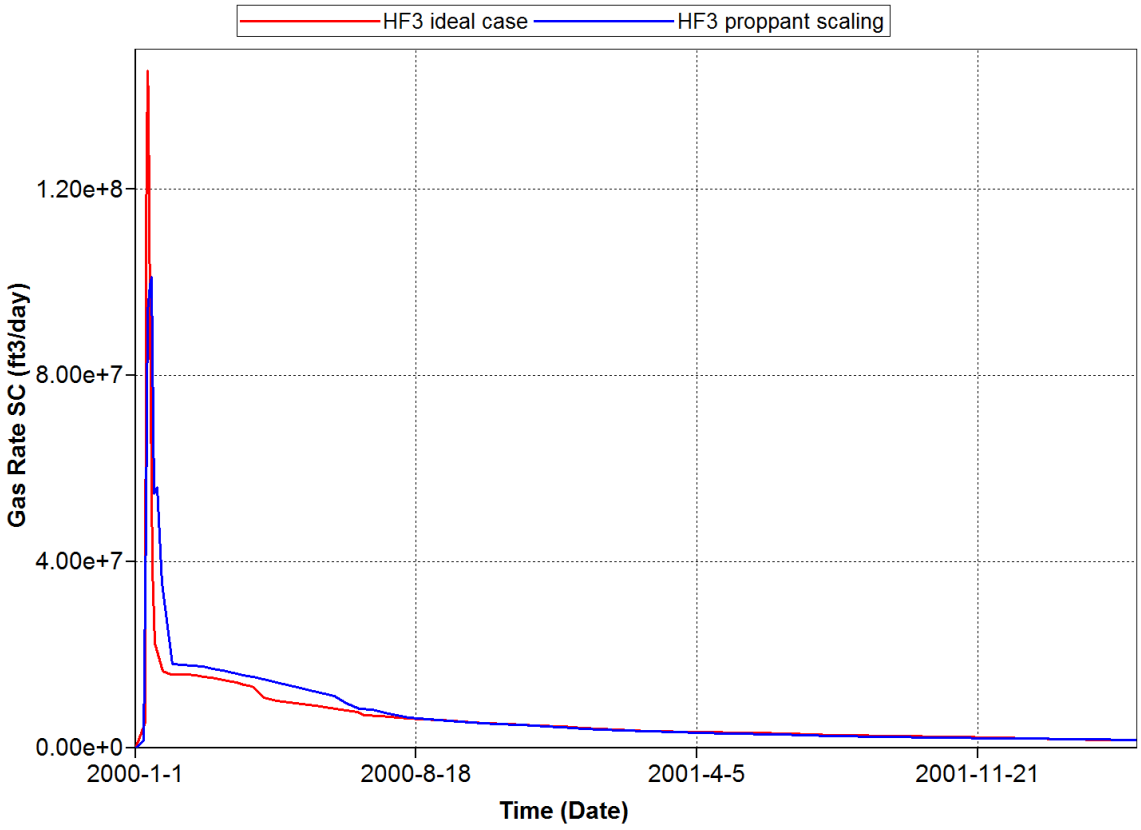

Figure 6-54 Proppant scale decrease gas rate over 20 years with P_r = 3720 psi, FBHP = 3348 psi, and $k_{n.f.}$ = 0.4396 md for HF3.

"HF3 ideal case" represents the case without damage, $k_{h.f.}$ = 23,115 md. "HF proppant scaling" represents the case with damage caused by chemical scaling, $k_{h.f.}$ = 18,035 md.

From Figure 6-53 and Figure 6-54, we can see that ideal case for HF3 has a cumulative gas production of 6.95 $\times 10^9$ ft^3, while the case with proppant scaling has a gas production of 6.35 $\times 10^9$ ft^3. The decrease is 6 $\times 10^9$ ft^3, which renders a deduction percentage of 8.6%. The decrease keeps on escalating as hydraulic fracture network expands. From the gas rate plot, we can see that the difference is mainly caused from the first year of production.

According to the above simulations from HF1, HF2, and HF3, we can come to the conclusion that proppant scaling shouldn't be considered a serious damaging effect in planar

hydraulic fracture. However, it will cause some decrease in gas cumulative production in hydraulic fracture network, and this decrease will escalate with the expansion of hydraulic fracture network.

6.4 The effect of proppant diagenesis

As is discussed earlier, a lot of recent studies provided insights that geochemical reactions likely occur during production from hydraulically generated fractures and gave evidence of possible long-term proppant instability. We hope this will give new insights about diagenesis and its influence.

Three scenarios are discussed about proppant diagenesis. In the first scenario, hydraulic fracture does not endure any damage. Permeability remains constant and retains 100% through production.

In the second scenario, only one high-strength aluminum-based proppant exits in hydraulic fractures. Diagenesis assumed to occur, and caused a decrease in retained permeability. The retained percentage is shown in Table 6-7, which is adopted from (Raysoni and Weaver 2012; Raysoni and Weaver 2012).

In the third scenario, both one high-strength aluminum-based proppant and a formation grains exit in hydraulic fractures. Diagenesis assumed to occur, and caused a decrease in retained permeability. The retained percentage is shown in Table 6-7, which is adopted from (Raysoni and Weaver 2012; Raysoni and Weaver 2012).

Table 6-7 Permeability data in long-term static-cell proppant evaluation (Weaver 2012)

Time, days				15	45	90	180
Retained permeability, %	Scenario1	No damage		100	100	100	100
	Scenario2	Damaged	20-40 ceramics	55	45.5	20	15
	Scenario3		20/40ceramics + formation grains	76	55	49	25

Detailed description of experiment procedures and assemblies can be found in previous literature review. We incorporated the following retained permeability percentage (Table 6-8) in to our simulations**.** Table 6-8 is summarized from Figure 4-16 in Chapter 4.

Table 6-8 Calibrated permeability for different date

	Proppant and formation grain	Proppant only
Days	Retained permeability, %	Retained permeability, %
15	73.79628749	51.31189495
45	61.63984065	40.36336617
90	47.05459039	28.16056502
150	32.82887375	17.42528994
270	15.97952836	6.672019553
360	9.312042223	3.247620569
510	3.785993838	0.978164518
630	1.842841042	0.374532235
720	1.073912397	0.18230441
870	0.436620198	0.054909033
990	0.212525866	0.021024278

In order to observe the effect of proppant diagenesis, the following data files are selected. Details of these data files are indicated in Table 6-9.

Table 6-9 Run number and parameters selected to represent the damage effect of proppant diagenesis

Run#	File name	scenario #	scenario of H.F.	Pr (psi)	FBHP (psi)	H.F. (ft)	N.F. k(md)	H.F. k (md) at day1	H.F. k (md) day990
HF1 ideal case*	data1	1	1	3720	3348	500	0.4793	65,500	65,500
HF1 diagenesis(proppant only)	data26	2		3720	3348	500	0.4793	65,500	14
HF1 diagenesis(proppant + formation grain)	data35	3		3720	3348	500	0.4793	65,500	139
HF2 ideal case*	data4	1	2	3720	3348	836	0.4793	39,174	39,174
HF2 diagenesis(proppant only)	data29	2		3720	3348	836	0.4793	39,174	8
HF2 diagenesis(proppant + formation grain)	data38	3		3720	3348	836	0.4793	39,174	83
HF3 ideal case*	data7	1	3	3720	3348	1152.8	0.4793	23,115	23115
HF3 diagenesis(proppant only)	data32	2		3720	3348	1152.8	0.4793	23,115	5
HF3 diagenesis(proppant + formation grain)	data41	3		3720	3348	1152.8	0.4793	23,115	49

* ideal case include effect of multiphase flow and proppant crushing .

Scenario1 represents ideal case (no damage). Scenario2 represents damage of proppant diagenesis with proppant in hydraulic fractures. Scenario3 represents damage of proppant diagenesis with both proppant and formation grains in hydraulic fractures.

6.4.1 Simulation results for H.F.1

As mentioned before, H.F.1 

has a primary planar hydraulic fracture. Simulations results of gas recovery and gas rate are shown in the following figures.

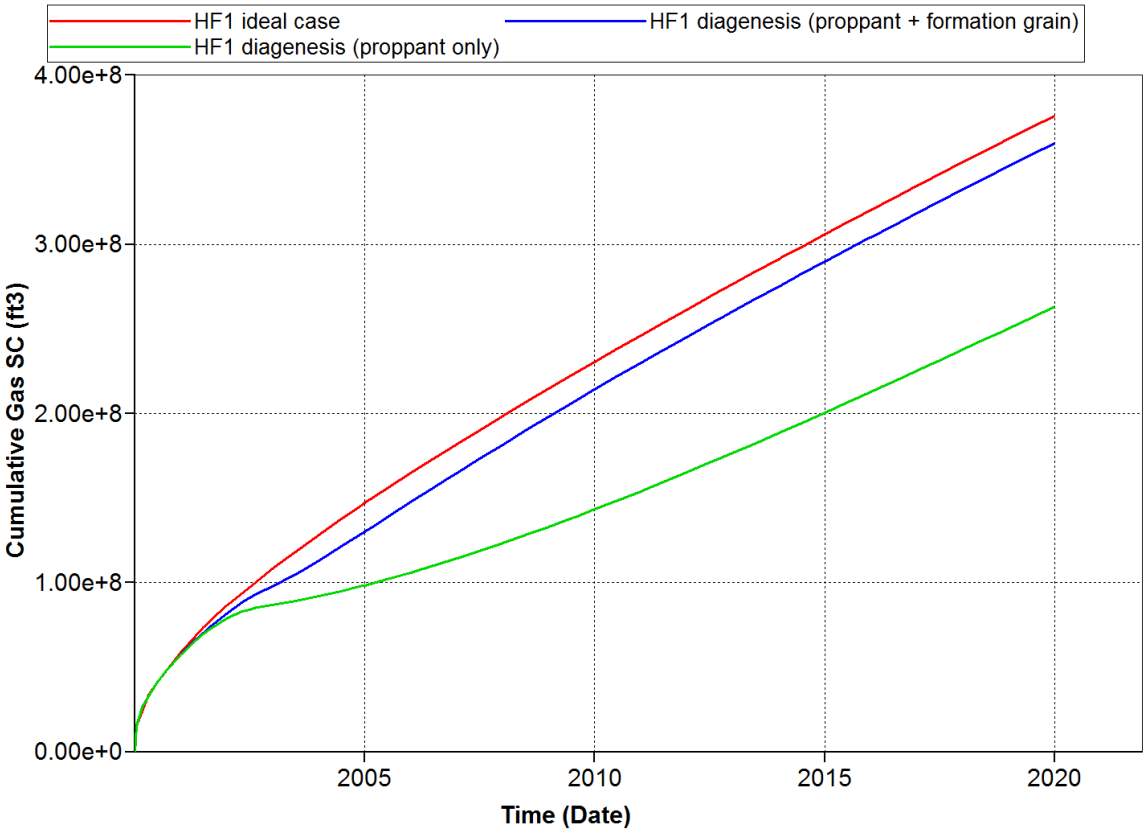

Figure 6-55 Proppant diagenesis decrease cumulative gas production for 20-40Ceramics proppant over 20 years with Pr = 3720 psi, FBHP = 3348 psi, and $k_{n.f.}$ = 0.4793 md for HF1.

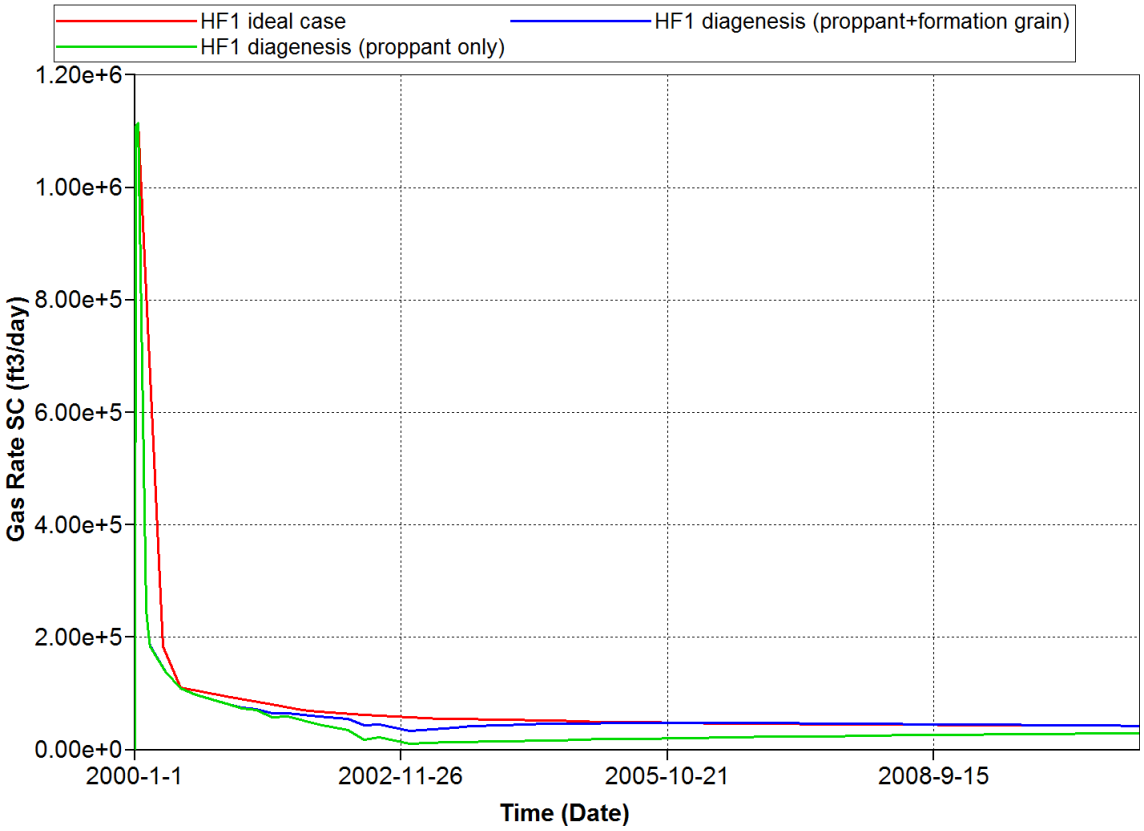

Figure 6-56 Proppant diagenesis decrease gas rate for 20-40Ceramics proppant over 20 years with Pr = 3720 psi, FBHP = 3348 psi, and $k_{n.f.}$ = 0.4793 md for HF1

"HF1 ideal case" represents the case without damage, in which $k_{h.f.}$ is 65,500 md. "HF1 diagenesis (proppant only)" represents the case with damage caused by proppant diagenesis with pure proppant in hydraulic fracture, in which $k_{h.f.}$ starts from 65,500 md and decreases gradually to 14 md with time. "HF1 diagenesis (proppant +formation grain)" represents the case with damage caused by proppant diagenesis with both proppant and formation grain in hydraulic fracture, in which $k_{h.f.}$ starts with 65,500 md and gradually decreases to 139 md with time.

We can observe that "HF1 diagenesis (proppant only)", when compared with "HF1 ideal case", decreases cumulative gas production from 3.76×10^8 ft^3 to 2.63×10^8 ft^3, which is about

30%. Proppant diagenesis could cause severe damage on gas production if proppant is the only particle in hydraulic fractures. While for "HF1 diagenesis (proppant +formation grain)", when compared with the ideal case, reduces cumulative gas production from 3.76×10^8 ft^3 to 3.6×10^8 ft^3, which is about 4.5%. The decrease is much smaller than the decrease from previous condition. The existence of formation grains increases the concentration of dissolved quarts in fracture fluid and thus decreased the available "free" concentration that proppant can occupy, since solubility of quarts in fracture fluid is constant at certain temperature and pressure. Figure 6-57 shows the plot of gas flow rate with the damage of proppant diagenesis. We can draw similar conclusion from this figure.

In conclusion, diagenesis effect, if it does occur under reservoir condition may seriously decrease gas over all recovery for a planar hydraulic fracture, especially in the condition where only proppant exists in hydraulic fracture.

6.4.2 Simulation results for H.F.2

As mentioned before, H.F.2 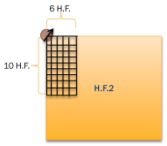

has a hydraulic fracture network around wellbore. Simulation results of gas recovery and gas rate are shown in the following figures.

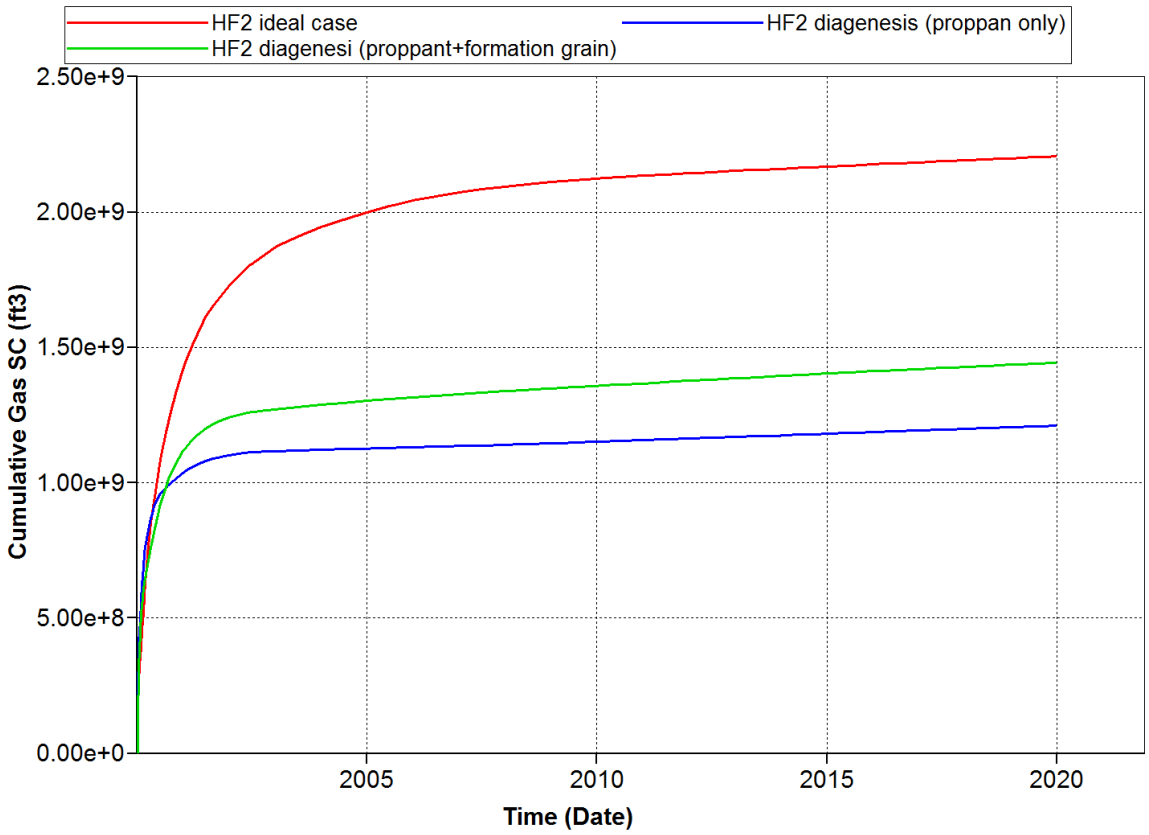

Figure 6-57 Proppant diagenesis decrease cumulative gas production for 20-40Ceramics proppant over 20 years with Pr = 3720 psi, FBHP = 3348 psi, and $k_{n.f.}$ = 0.4793 md, for HF2.

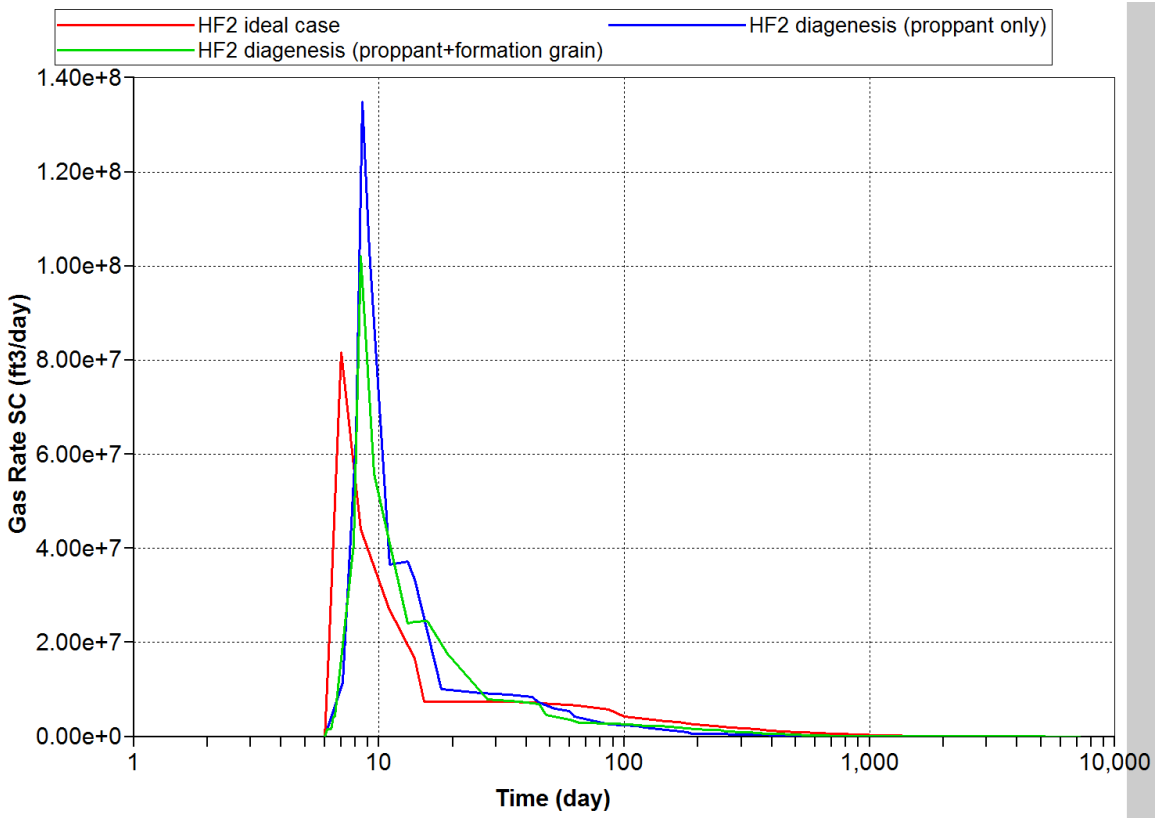

Figure 6-58 Proppant diagenesis decrease gas rate for 20-40Ceramics proppant over 20 years with Pr = 3720 psi, FBHP = 3348 psi, and $k_{n.f.}$ = 0.4793 md, for HF2.

"HF2 ideal case" represents the case without damage, $k_{h.f.}$ is 39,174md. "HF2 diagenesis (proppant only)" represents the case with damage caused by proppant diagenesis with pure proppant in hydraulic fracture, $k_{h.f.}$ starts from 39,174 md and decreases to 8 md along with time. "HF2 diagenesis (proppant + formation grain)" represents the case with damage caused by proppant diagenesis with both proppant and formation grain in hydraulic fracture, $k_{h.f.}$ starts form 39,174 md and decreases to 83 md along with time.

We can observe that "HF2 diagenesis (proppant only)", when compared with "HF2 ideal case", decreases cumulative gas production from 2.2×10^9 ft^3 to 1.2×10^9 ft^3, which is also about 45.5%. While for "HF2 diagenesis (proppant + formation grain)", when compared with ideal case, reduces cumulative gas production from 2.2×10^8 ft^3 to 1.44×10^8 ft^3, which is about 34.5%. The decrease is slightly smaller than the decrease from previous condition, but very close. The

existence of formation grains doesn't help alleviate damage caused by proppant diagenesis as it does in previous condition. Figure 6-57 shows the plot of gas flow rate with the damage of proppant diagenesis. We can draw similar conclusion from this figure.

In conclusion, diagenesis effect, if it does occur under reservoir condition may cause severe damage to hydraulic fracture network.

6.4.3 Simulation results for H.F.3

As mentioned before, H.F.3 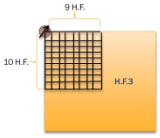

has a broader hydraulic fracture network around wellbore. Simulation results of gas recovery and gas rate are shown in the following figures.

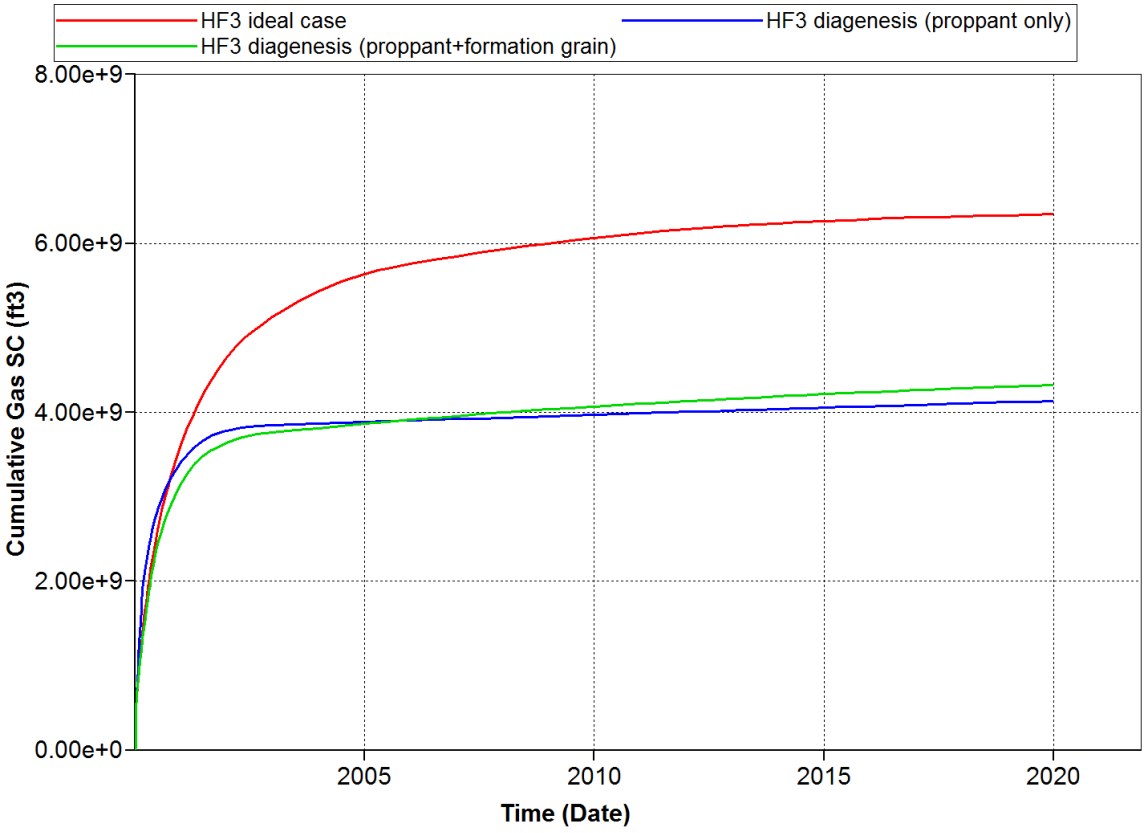

Figure 6-59 Proppant diagenesis decrease cumulative gas production for 20-40Ceramics proppant over 20 years with Pr = 3720 psi, FBHP = 3348 psi, $L_{h.f.}$ = 1152.8 ft, and $k_{n.f.}$ = 0.4793 md.

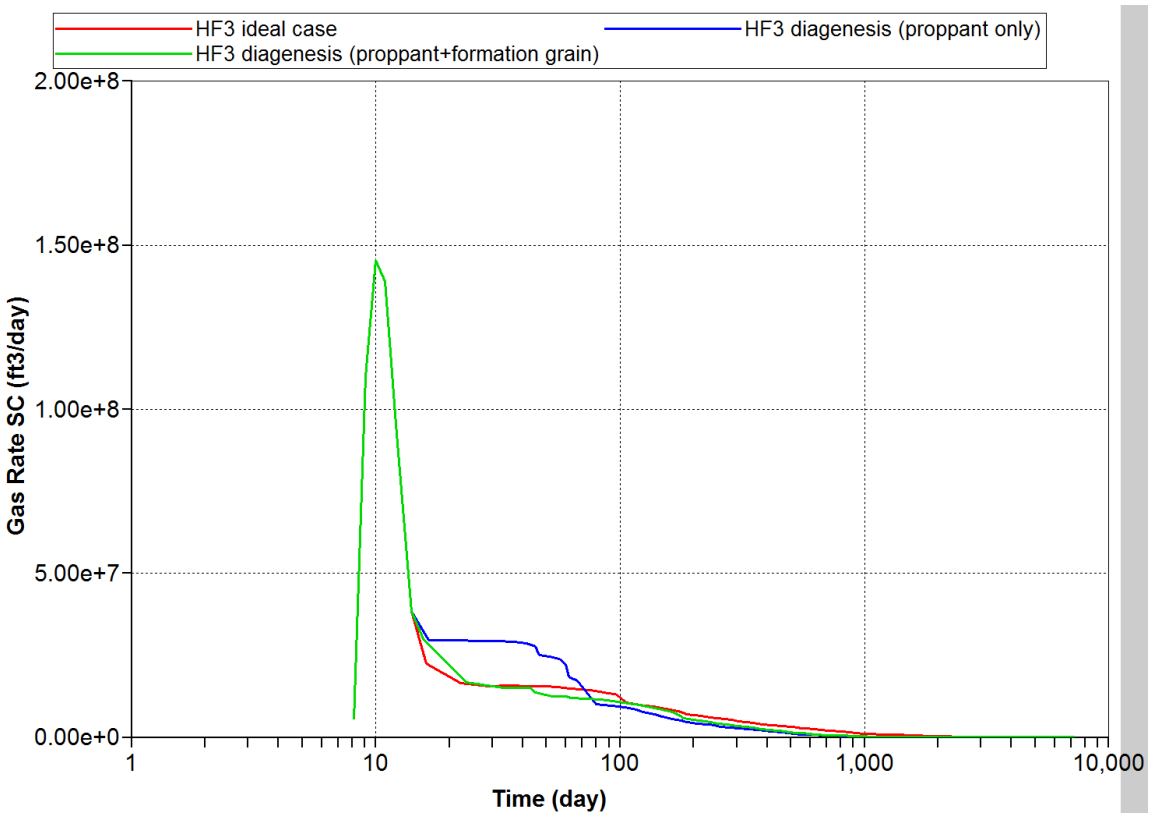

Figure 6-60 Proppant diagenesis decrease gas rate for 20-40Ceramics proppant (data1, data109, and data56) over 20 years with Pr = 3720 psi, FBHP = 3348 psi, $L_{h.f.}$ = 1152.8 ft, and $k_{n.f.}$ = 0.4793 md.

"HF3 ideal case" represents the case without damage, $k_{n.f.}$ is 23,115 md. "HF3 diagenesis (proppant only)" represents the case with damage caused by proppant diagenesis with pure proppant in hydraulic fracture, $k_{n.f.}$ of it starts from 23,115md and gradually decreases to 5 md. "HF3 diagenesis (proppant +formation grain)" represents the case with damage caused by proppant diagenesis with both proppant and formation grain in hydraulic fracture, $k_{n.f.}$ starts from 23,115 md and decreases to 49 md along with time.

We can observe that "HF3 diagenesis (proppant only)", when compared with ideal case, decreases cumulative gas production from 6.34 $\times 10^9$ ft^3 to 4.13 $\times 10^9$ ft^3, which is about 34.9%. While for "HF3 diagenesis (proppant +formation grain)", when compared with ideal case, reduces cumulative gas production from 6.34 $\times 10^9$ ft^3 to 4.3 $\times 10^9$ ft^3, which is about 32.2%. The

decrease is slightly smaller than the decrease from previous condition. Damage caused by proppant diagenesis is alleviated by the expansion of hydraulic fracture network, since more fluid pass ways are involved in gas production, it counteract with the damaged permeability value. The existence of formation grains helps alleviate damage caused by proppant diagenesis, but as fracture expands, its prominence gradually diminishes to invisible. Figure 6-57 shows the plot of gas flow rate with the damage of proppant diagenesis. We can draw similar conclusion from this figure. We can see that the first 10 days of production are identical among these 3 models, and the differences gradually grow and evolve for the following production, which indicates the effect of diagenesis.

In conclusion, diagenesis effect may cause severe damage to hydraulic fracture network. As hydraulic fracture network expands, possible damage will increase.

6.5 Comparison and discussion

Note that the damage effects we addressed in this research are based on 19 base models or conditions. These models are called ideal cases because except for formation depth, operational condition (bottom hole pressure), and hydraulic fracture, there are no damage effects in these models. There are several other results and recommendations we can come up with from these ideal cases.

6.5.1 Single hydraulic fracture VS hydraulic fracture net work

Before we present the results on this topic, explanations of hydraulic fracture length and permeability need to be addressed first. We chose 3 hydraulic fracture layouts in our research. These 3 kinds of hydraulic fracture share the same proppant volume. Since same amount of proppant is injected underground, different gas productions with different fracture layouts may give us some insights about efficient hydraulic fracture plan. HF1 ideal case, HF2 ideal cas, and HF3 ideal case are chosen to represent the influence of hydraulic fracture. Proof can be found in Figure 6-61 and Figure 6-62. Run number and parameters selected to represent the comparison among fracture layouts is listed in Table 6-10.

Table 6-10 Run number and parameters selected to represent the comparison among fracture layouts

Run#	File name	scenario of H.F.	Pr (psi)	FBHP (psi)	H.F. (ft)	N.F. k(md)	H.F. k (md)
HF1 ideal case*	data1	1	3720	3348	500	0.4793	65,500
HF2 ideal case*	data4	2	3720	3348	836	0.4793	39,174
HF3 ideal case*	data7	3	3720	3348	1152.8	0.4793	23,115

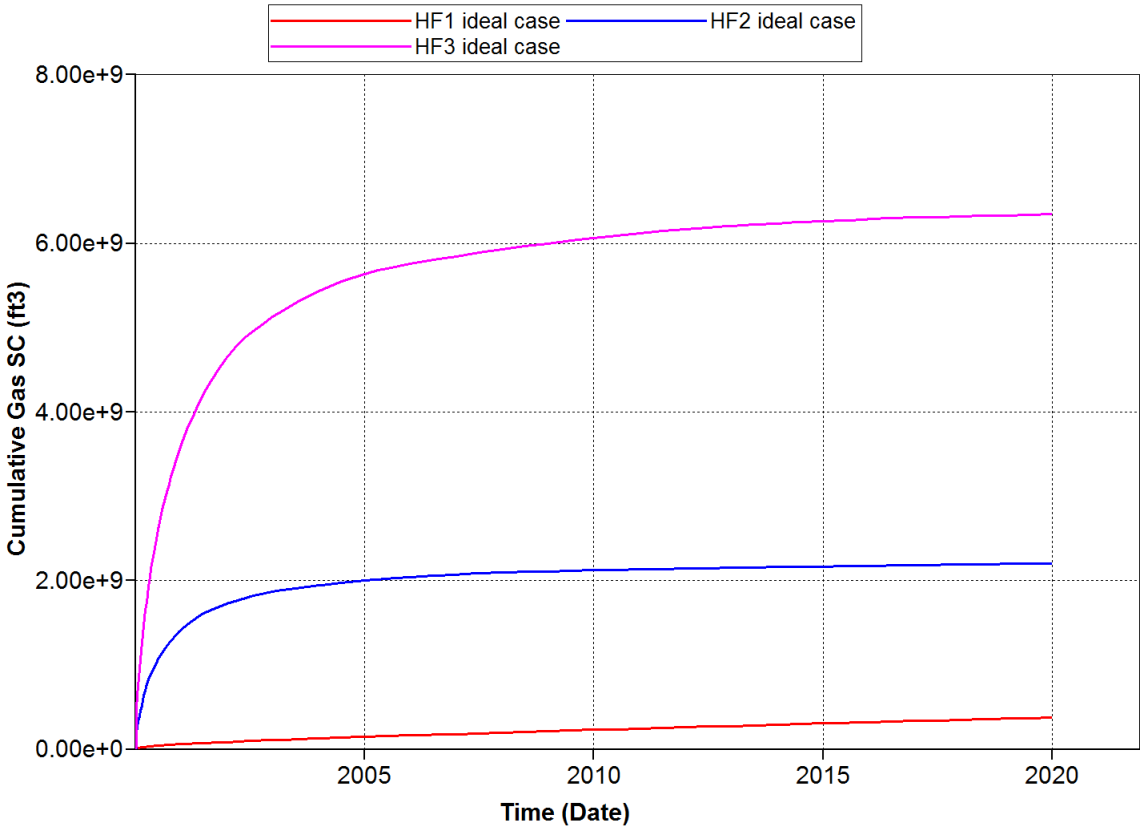

Figure 6-61 Cumulative gas productions from different hydraulic fracture layouts (HF1, HF2, and HF3). P_r=3720 psi, FBHP=3348 psi.

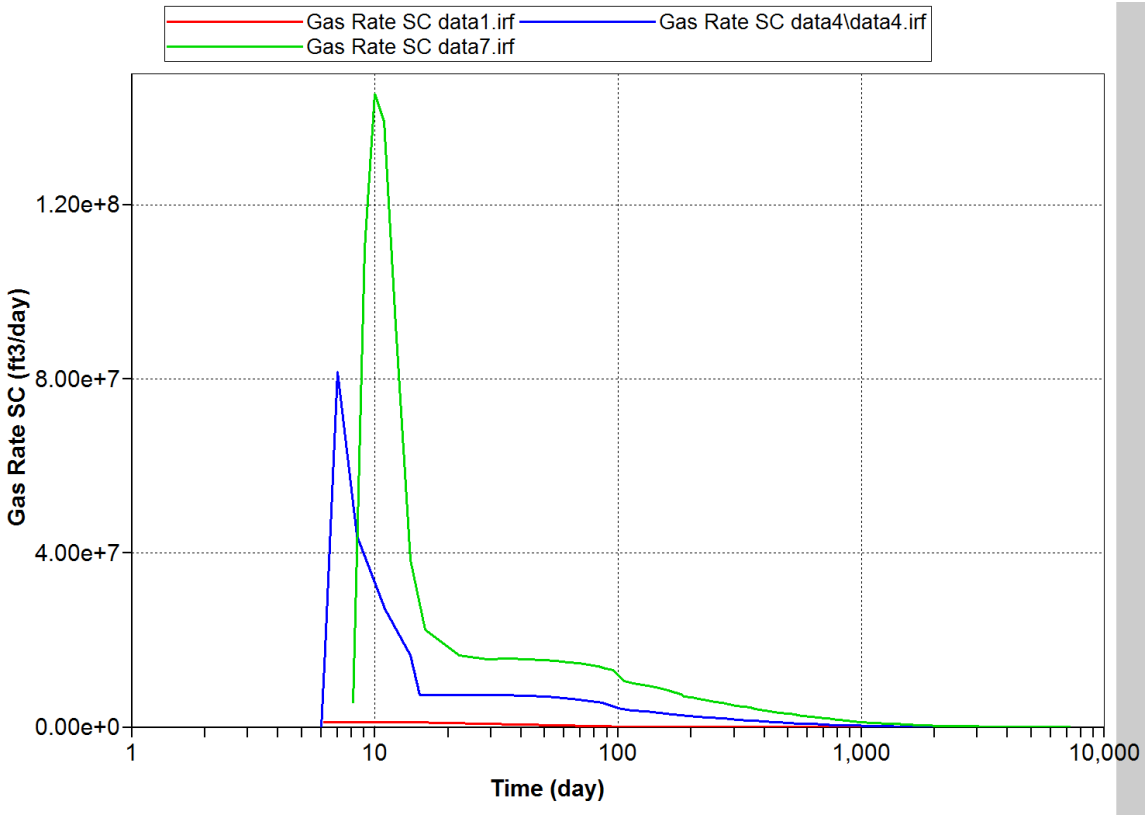

Figure 6-62 Gas rate of different hydraulic fracture layouts (HF1, HF2, and HF3). P_r=3720 psi, FBHP=3348 psi.

HF1 ideal case represents the case of H.F.1 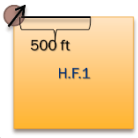

.

HF2 ideal case represents the case of H.F.2 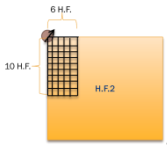

.

HF3 ideal case represents the case of H.F.3 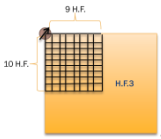

.

According to the figures above, we can come to the understanding that hydraulic fracture is definitely a good stimulation method for gas production. Among different layouts of hydraulic

fracture, it is more rewarding if we can open a fracture network around wellbore area. While a planar hydraulic fracture is efficient if we want to produce as much productions in the shortest possible time, a network of hydraulic fracture is more favorable if long-time profit is anticipated.

6.5.2 High flowing bottom hole pressure VS low flowing bottom hole pressure

Flowing bottom hole pressure (FBHP) is directed related with operational conditions. Here we want to represent how much difference FBHP can cause in gas production.

Since different hydraulic fracture layouts gives similar trend. We will only include simulations with a planar hydraulic fracture as examples.

"HF1 FBHP=3348psi", "HF1 FBHP=1860psi", and "HF1 FBHP=372psi" are chosen to represent this case. While they all have a planar hydraulic fracture, "HF1 FBHP=3348psi" (which is referred as HF1 ideal case in the previous chapters) represents FBHP equals to 90% of reservoir pressure, "HF1 FBHP=1860psi" represents FBHP equals to 50% of reservoir pressure, and "HF1 FBHP=372psi" represents FBHP equals to 20% of reservoir pressure. Simulations are shown in Figure 6-63 and Figure 6-62. The chosen models in these two figures share the same hydraulic fractures, reservoir pressure, and formation depth. Run number and parameters selected to represent the comparison among different bottom hole pressures are listed in Table 6-11.

Table 6-11 Run number and parameters selected to represent the comparison among different bottom hole pressures

Run#	File name	scenario of H.F.	Pr (psi)	FBHP (psi)	N.F. k(md)	H.F. k (md)
HF1 FBHP=3348psi	data1	1	3720	3348	0.4793	65,500
HF1 FBHP=1860psi	data10		3720	3348	0.4793	
HF1 FBHP=372psi	data13		3720	3348	0.4793	

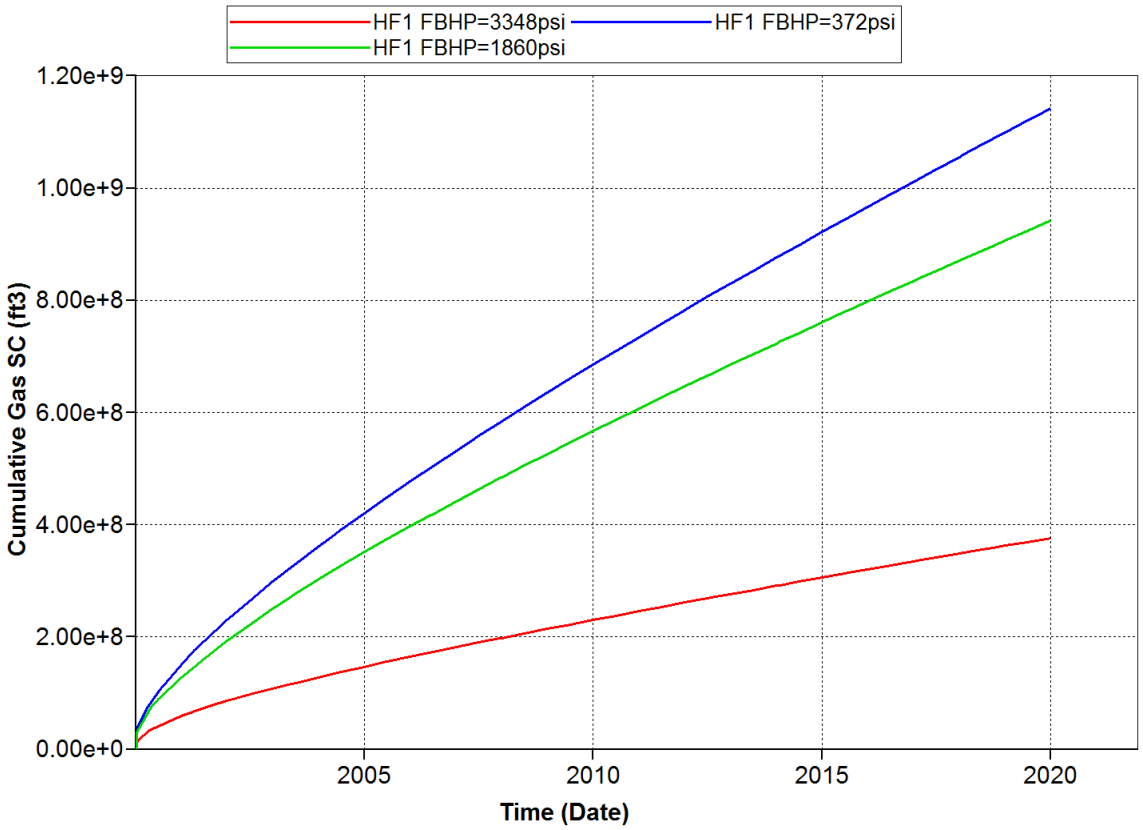

Figure 6-63 FBHP affect cumulative gas productions with P_r=3720 psi, FBHP=3348 psi. FBHP=1860 psi. FBHP=372 psi respectively, for HF1.

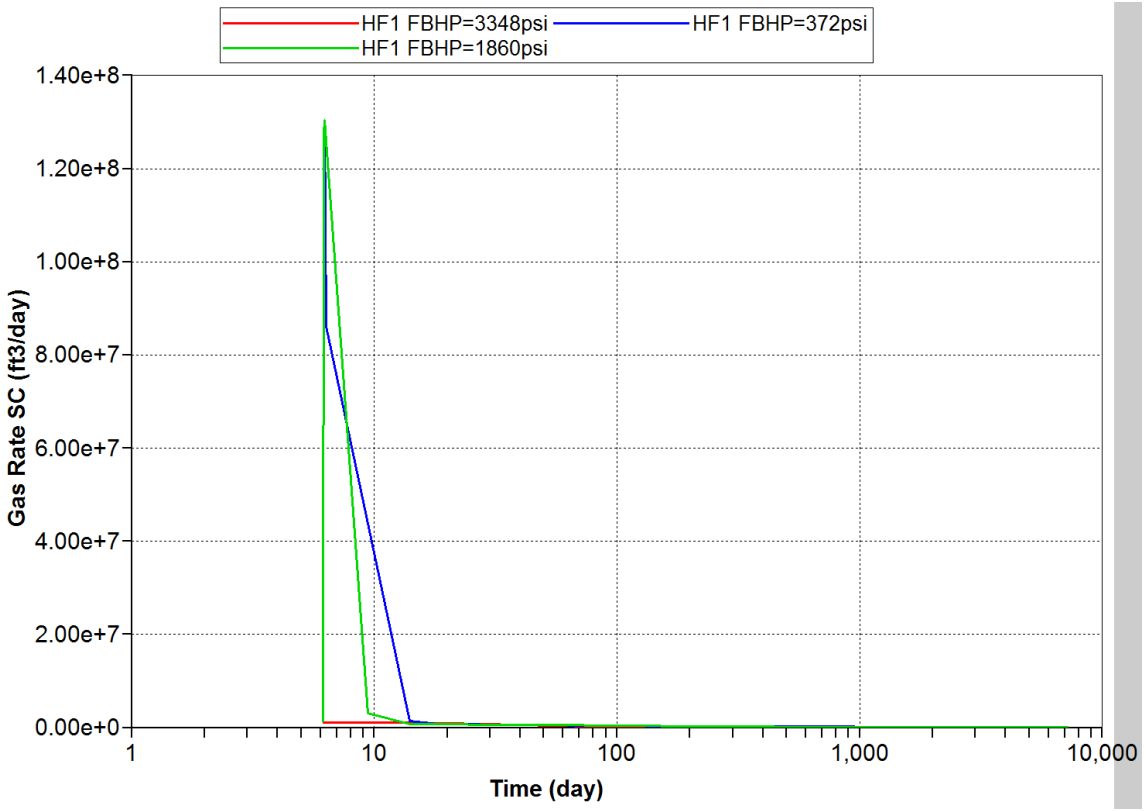

Figure 6-64 FBHP affect gas rate with P_r=3720 psi, FBHP=3348 psi. FBHP=1860 psi. FBHP=372 psi respectively, for HF1.

From the figures above, we can observe that as when FBHP is 3348 psi, cumulative gas production is 3.42443 $\times 10^8$ ft^3. When FBHP is decreased to 1860 psi, cumulative gas production is increased to 8.96137 $\times 10^8$ ft^3, which is an increase of 162%. While FBHP is further decreased to 372 psi, cumulative gas production reaches 1.13289 $\times 10^8$ ft^3, which is an increase of 230%. The plot of gas rate gives similar trend.

In summary, as FBHP approaches low pressure, production increases.

6.5.3 Upper Marcellus VS lower Marcellus

For upper Marcellus, formation depth is set as 5000 ft, and reservoir pressure as 2325 psi, while for lower Marcellus, formation has depth of 8000 ft, and reservoir pressure of 3720 psi.

Comparison and results in this case could give us ideas about production differences between these two drainage depths. Since different hydraulic fracture layouts gives similar trend. We will only include simulations with a planar hydraulic fracture as examples. “HF1 lower Marcellus” represents lower Marcellus, while “HF1 upper Marcellus” represents upper Marcellus. These models are both based on a single planar hydraulic fracture. Production results are shown in Figure 6-65 and Figure 6-66. Run number and parameters selected to represent the comparison among different bottom hole pressures are listed in Table 6-12.

Table 6-12 Run number and parameters selected to represent the comparison between upper Marcellus and Lower Marcellus

Run#	File name	scenario of H.F.	Pr (psi)	FBHP (psi)	N.F. k(md)	H.F. k (md)
HF1 lower Marcellus	data1	1	3720	3348	0.4793	65,500
HF1 upper Marcellus	data16		3720	3348	0.4793	

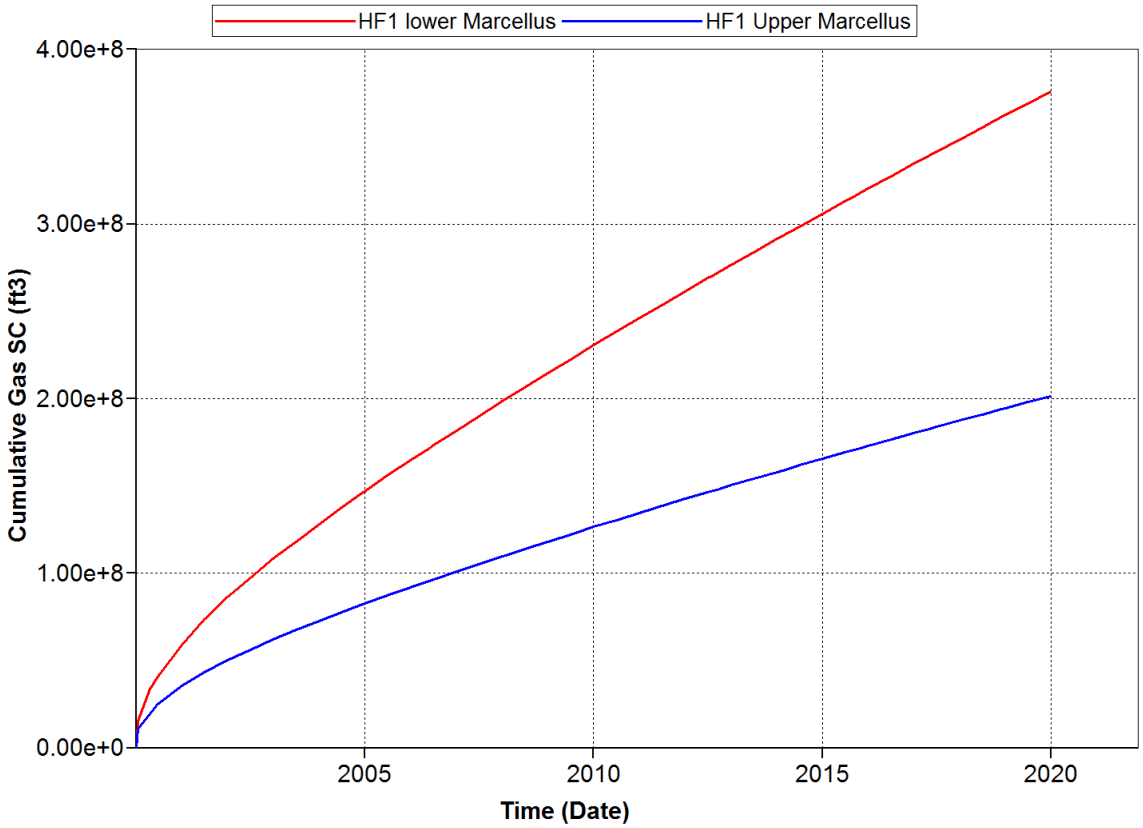

Figure 6-65 Cumulative gas production differs from different formation depth with Pr=3720 psi and 2325 psi respectively, for HF.

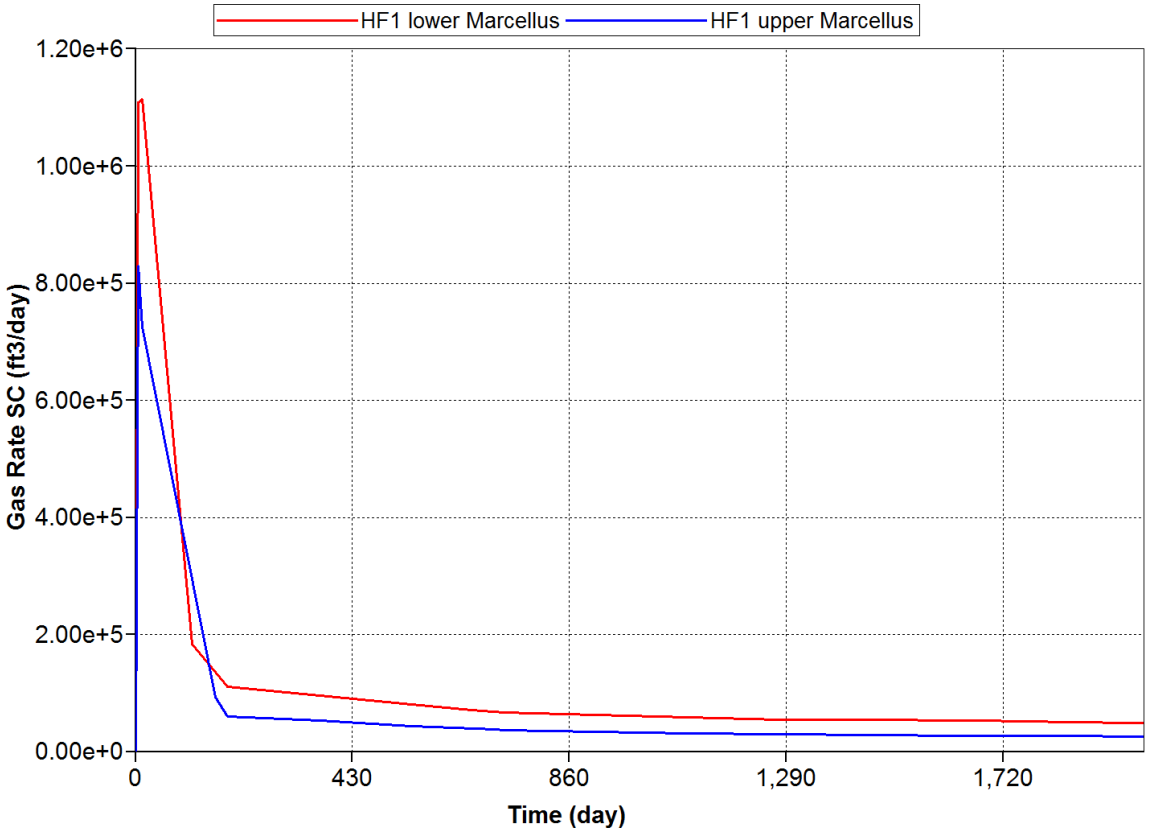

Figure 6-66 Gas rate differs from different formation depth with Pr=3720 psi and 2325 psi respectively, for HF.

From the figures above we can interpret that lower Marcellus has a better production than upper Marcellus.

Chapter 7

Conclusions and recommendations

In this thesis, three damages are investigated through a compute and critical review of published and unpublished laboratory experiments, mathematical models, and field datarelated to the interaction of fluids with existing natural fractures/unpropped hydraulic fractures, proppant scaling, proppant diagenesis.

We then obtained an optimized model after conducting sensitivity studies of gridding and drainage area. Parametric studies were conducted by varying reservoir pressure, hydraulic fracture geometries (HF1, HF2, and HF3), flowing bottom hole pressure (FBHP), and reservoir pressure (upper vs. lower Marcellus), for cases with and without three damages after analyzing these results, we drew the following conclusions:

1. Interaction between formation rock and fluids could be a severe damage if a primary/planar fracture is created. It could reduce 20-year gas recovery by 50%.
2. This damage becomes less sever if a larger facture network is created, but it could still reduce the gas recovery by 30% in 20-year.
3. Proppant scale (chemical precipitations on the surfaces of proppant) does not affect well performance in planar hydraulic fracture. However, it can decrease total gas production in 20 years by 6~8% for complex hydraulic fractures.
4. Proppant diagenesis could be a severe damage. It could reduce 20-year gas recovery by 35~45%. Since unanimity exits in diagenesis effect under downhole condition, both the mechanism and the method of relieving should be further investigated.

References

Bahrami, H., M. R. Rezaee, et al. 2011. Evaluation of Damage Mechanisms and Skin Factor in Tight Gas Reservoirs. Paper SPE 142284 presented at the SPE European Formation Damage Conference, Noordwijk, The Netherlands, 01/01/2011. http://dx.doi.org/10.2118/142284-ms.

Conway, M. W., J. J. J. Venditto, et al. 2011. An Examination of Clay Stabilization and Flow Stability in Various North American Gas Shales. Paper SPE 147266 presented at the SPE Annual Technical Conference and Exhibition, Denver, Colorado, USA, 01/01/2011. http://dx.doi.org/10.2118/147266-ms.

Dewan, J. T.1983. *Essentials of Mordern open-hole log interpretation*. Tulsa. PennWell Corporation.

Duenckel, R. J., M. W. Conway, et al. 2011. Proppant Diagenesis- Integrated Analyses Provide New Insights into Origin, Occurrence, and Implications for Proppant Performance. Paper SPE SPE-139875-MS presented at the SPE Hydraulic Fracturing Technology Conference, The Woodlands, Texas, USA, 01/01/2011. http://dx.doi.org/10.2118/139875-ms.

Economides, M. J. (2010). International State ofHydraulic Fracturing, Halliburton.

Gale, J. F. W., R. M. Reed, et al. 2007. Natural fractures in the Barnett Shale and their importance for hydraulic fracture treatments. *AAPG Bulletin* **91**(4): 603-622. http://dx.doi.org/10.1306/11010606061.

Garzon, F. O., J. R. Solares, et al. 2009. Analysis of Deposition Mechanism of Mineral Scales Precipitating in the Sandface and Production Strings of Gas-Condensate Wells. Paper SPE 120410 presented at the SPE Middle East Oil and Gas Show and Conference, Bahrain, Bahrain, 01/01/2009. http://dx.doi.org/10.2118/120410-ms.

Gijtenbeek, K. A. W. v., A. P. Neyfeld, et al. 2006. One-Molar Salt Solutions Used for Clay Control in Water-Based Frac Fluids in Western Siberia. Paper SPE 101203 presented at the SPE Russian Oil and Gas Technical Conference and Exhibition, Moscow, Russia, 01/01/2006. http://dx.doi.org/10.2118/101203-ms.

Hower, W. F. 1974. Influence of Clays on the Production of Hydrocarbons. Paper SPE 4785 presented at the SPE Symposium on Formation Damage Control, New Orleans, Louisiana, 01/01/1974. http://dx.doi.org/10.2118/4785-ms.

Kaufman, P. B., R. W. Anderson, et al. 2007. Introducing New API/ISO Procedures for Proppant Testing. Paper SPE SPE-110697-MS presented at the SPE Annual Technical Conference and Exhibition, Anaheim, California, U.S.A., 01/01/2007. http://dx.doi.org/10.2118/110697-ms.

Lehman, L. V., M. A. Parker, et al. 1999. Proppant Conductivity â□" What Counts and Why. Paper SPE 52219 presented at the SPE Mid-Continent Operations Symposium, Oklahoma City, Oklahoma, 01/01/1999. http://dx.doi.org/10.2118/52219-ms.

Mackay, E. J. 2010. Comparison of Scale Control Challenges Between Production and PWRI Wells. Paper SPE 129181 presented at the SPE International Symposium and Exhibiton on Formation Damage Control, Lafayette, Louisiana, USA, 01/01/2010. http://dx.doi.org/10.2118/129181-ms.

Nguyen, P. D., J. D. Weaver, et al. 2008. Prevention of Geochemical Scaling in Hydraulically Created Fractures: Laboratory and Field Studies. Paper SPE 118175 presented at the SPE

Eastern Regional/AAPG Eastern Section Joint Meeting, Pittsburgh, Pennsylvania, USA, 01/01/2008. http://dx.doi.org/10.2118/118175-ms.

Osholake, T. A., J. Y. Wang, et al. 2011. Factors Affecting Hydraulically Fractured Well Performances in the Marcellus Shale Gas Reservoirs. Paper SPE SPE-144076-MS presented at the North American Unconventional Gas Conference and Exhibition, The Woodlands, Texas, USA, 01/01/2011. http://dx.doi.org/10.2118/144076-ms.

Raysoni, N. and J. D. Weaver 2012. Long-Term Proppant Performance. Paper SPE SPE-150669-MS presented at the SPE International Symposium and Exhibition on Formation Damage Control, Lafayette, Louisiana, USA, 01/01/2012. http://dx.doi.org/10.2118/150669-ms.

Raysoni, N. and J. D. Weaver 2012. Selection of Proppant for Long-Term Stability. Paper SPE SPE-150668-MS presented at the SPE Hydraulic Fracturing Technology Conference, The Woodlands, Texas, USA, 01/01/2012. http://dx.doi.org/10.2118/150668-ms.

Wang, Holitch, and Mcvay. 2010. Modeling of Fracture Fluid Cleanup in Tight Gas Wells. Paper SPE 119624, SPE Journal, Vol.15, No.3, PP. 783-793.

Weaver, J. D. and P. D. Nguyen 2010. Hydrophobic Filming Reduces Frac Gel and Mineral Scale Damage. Paper SPE 138314 presented at the SPE Eastern Regional Meeting, Morgantown, West Virginia, USA, 01/01/2010. http://dx.doi.org/10.2118/138314-ms.

Appendix A

List of simulation, 20-year gas recovery and fracture fluid flow back

Run NO.	cases	Pr(psi)	FBHP (90%, 50%, 10%)	H.F.	N.F.(md)	5-year gas recovery	20-year gas recover	2-week fracture fluid recovery	6-month fracture fluid recovery	3-year fracture fluid recovery
Grid1	sensitivity analysis on grid	3000	960	H.F.1	0.4793					
Grid 2										
Grid 3										
Grid 4										
Grid 5										
Area1	sensitivity analysis on drainage area	3000	960	H.F.2	0.4793					
Area2										
Area3										
Area4										
data1*	base model* + interaction between formation rock and fluid	3720	3348	H.F.1	0.4793	2.35%	5.96%	11.87%	16.11%	19.22%
data2					0.0938	1.60%	3.22%	5.91%	8.69%	13.88%
data3					0.1172 (0-21days) -0.0703 (after21 days)	1.61%	3.35%	6.19%	9.26%	11.66%
data4*				H.F.2	0.4793	30.71%	33.91%	60.76%	85.06%	96.82%
data5					0.0938	23.24%	30.06%	65.52%	84.86%	100.15%
data6					0.1172 (0-21days) -0.0703 (after 21 days)	21.04%	27.58%	62.38%	76.02%	93.61%
data7*				H.F.3	0.4793	86.62%	97.54%	77.43%	91.55%	96.06%
data8					0.0938	46.05%	66.97%	89.77%	101.13%	101.89%
data9					0.1172 (0-21days) -0.0703 (after 21 days)	54.17%	77.45%	91.47%	101.16%	101.27%
data10*			1860	H.F.1	0.4793	5.33%	14.48%	23.54%	27.40%	29.21%
data11*				H.F.2	0.4793	38.86%	45.93%	93.62%	100.23%	100.93%
data12*				H.F.3	0.4793	65.16%	77.13%	85.78%	93.56%	97.88%
data13*			372	H.F.1	0.4793	6.46%	17.56%	25.41%	27.41%	29.21%
data14*				H.F.2	0.4793	26.25%	32.34%	96.02%	101.08%	101.27%
data15*				H.F.3	0.4793	27.22%	35.31%	87.19%	94.82%	98.26%
data16*		2325	2092.5	H.F.1	0.4793	1.27%	3.10%	7.58%	10.61%	12.54%
data17	base	3720	3348	H.F.1	0.4793	2.21%	5.72%	14.15%	16.61%	18.19%

data18	model + proppant scale				0.0938	1.59%	3.18%	9.06%	11.89%	13.90%
data19					0.1172 (0-21days) -0.0703 (after21 days)	1.68%	3.38%	6.51%	9.29%	10.98%
data20				H.F.2	0.4793	29.76%	31.97%	58.46%	83.14%	95.63%
data21					0.0938	19.74%	26.81%	59.20%	70.12%	81.88%
data22					0.1172 (0-21days) -0.0703 (after 21 days)	20.59%	25.80%	61.28%	79.65%	88.03%
data23				H.F.3	0.4793	96.09%	100.92 %	82.70%	101.09%	101.17%
data24					0.0938	43.25%	65.75%	66.75%	75.00%	79.49%
data25					0.1172 (0-21days) -0.0703 (after 21 days)	53.15%	76.53%	71.79%	83.74%	91.27%
data26	base model + proppant diagenesis	3720	3348	H.F.1	0.4793	1.51%	4.04%	11.88%	16.47%	18.63%
data27					0.0938	1.21%	2.32%	8.70%	11.59%	13.17%
data28					0.1172 (0-21days) -0.0703 (after21 days)	1.17%	2.21%	7.85%	10.67%	12.11%
data29				H.F.2	0.4793	17.31%	18.63%	68.45%	84.95%	87.90%
data30					0.0938	10.47%	11.64%	54.92%	63.47%	68.09%
data31					0.1172 (0-21days) -0.0703 (after 21 days)	10.73%	11.95%	53.24%	62.66%	66.98%
data32				H.F.3	0.4793	59.72%	63.55%	77.43%	92.08%	94.23%
data33					0.0938	20.99%	23.19%	88.45%	100.16%	101.20%
data34					0.1172 (0-21days) -0.0703 (after 21 days)	24.56%	27.21%	69.91%	77.14%	80.40%
data35	base model + diagenesis of proppant and formation grain	3720	3348	H.F.1	0.4793	2.00%	5.53%	11.36%	16.12%	17.39%
data36					0.0938	0.25%	0.25%	8.30%	11.30%	13.34%
data37					0.1172 (0-21days) -0.0703 (after21 days)	1.48%	3.25%	7.85%	10.71%	12.39%
data38				H.F.2	0.4793	20.02%	22.20%	60.51%	78.37%	83.59%
data39					0.0938	10.99%	14.19%	57.72%	65.42%	71.01%
data40					0.1172 (0-21days) -0.0703 (after 21 days)	12.24%	15.25%	53.24%	62.92%	68.42%
data41				H.F.3	0.4793	59.40%	66.45%	77.43%	91.03%	94.13%
data42					0.0938	28.48%	33.75%	94.94%	100.05%	100.25%
data43					0.1172 (0-21days) -0.0703 (after 21 days)	29.44%	35.52%	93.43%	100.74%	100.99%

* base model, (which was called ideal case in the text) include effect of multiphase flow and proppant crushing . data1, data10, data13, and data16 are base models for H.F.1. data4, data11, and data14 are base models for H.F.2. data6, data12, and data15 are base models for H.F.3.

Appendix B

Proposed laboratory evaluation of interaction of fracture fluid with Marcellus shale

Introduction

Formation damage caused by fracture fluid is severe and irreversible. Figure out the actual change in pore structure of Marcellus Shale when interact with different fracture fluid in critical and helpful in lessen formation damage. This project planned to use laboratory experimental method and Nuclear Magnetic Resonance test to simulate interaction and interpret structure change.

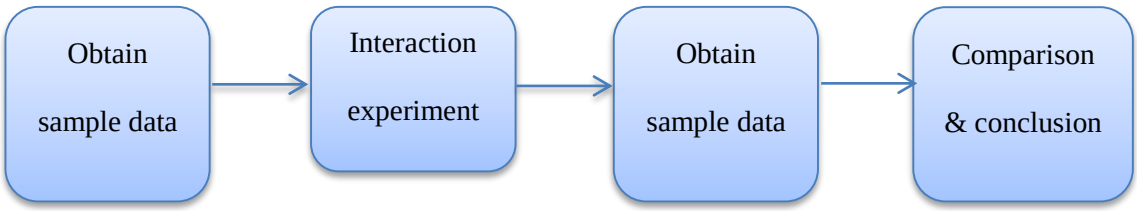

As is shown in the flow chart above, general plan for this project is to firstly select sample to run an initial test. This test is used to gather initial data which can be used as static comparison for later interaction. Data is collected by using Nuclear Magnetic Resonance (NMR) apparatus. Detailed introduction of this instrument and some fundamental principles will be introduced in the following section. After initial data is collected, samples are then divided into different groups. Interactions with different fracture fluid and different time span are then applied. At the end of interaction of each sample, NMR test is applied again to obtain data. The data is compared with the initial data to obtain the actual change of shale samples, conclusions can be made about how Marcellus Shale samples change through interactions with different fracture fluids over different time.

NMR Spectrometers

Location and Belongings

NMR test apparatus locations in Penn State UP campus's chemical department. Dr. Alan Benesi is the Director of the NMR Facility and Lecturer in Chemistry. The laboratory is located in the basement of the Chemistry Building, and is equipped with ten superconducting NMR spectrometers operating in both liquids and solids mode.

Parameters

The spectrometers range from 7 Tesla (300 MHz 1H frequency) to 20 Tesla (850 MHz 1H frequency).

Requirements for Testing Samples

Sample size is restricted into a tube of 0.5cm in diameter and 4.5 in length. In order to get the perfect curve, testing should be in a state of small grain, or small rock. The equipment can do the experiment both with and without spin of the sample tube. But according to suggestions from Dr. Alan, spinning will not make a significant difference on the outcome. Considering the nature of the shale sample we have (which is small rock), experiment without spinning is chose in order to avoid breaking of the tube by the rock inside under high centrifuge force.

Possible Outcome

Unlike NMR apparatus used in the field which can give porosity curve water saturation , gas saturation…at the same time, the NMR Spectrometer used in this experiment can only give out T_2 relaxation curve of a test sample. Adjustment of the apparatus may take 1 hour which is

handled by the assistant in the lab. But after the required state is reached each test require no more than half an hour for a single T_2 relaxation curve.

Equipment and Tools

Equipment and Tools that might be used is listed in the following table. The price and parameters are picked from Fisher Man's handbook.

Table 7-1 Equipment and Tools Used

	Unit	Price /Unit	Item No.	Name & Description
	case$_{(72)}$	$77.66	Mfr. C126-0020	I-Chem 100 Economy Series 20mL vials with closed top with liner
	each	$9.85	Cat. 08-890	Blunt-Pointed/straight serrated, chrome-plained steel forceps
	pack$_{(12)}$	$32.2	Mfr. 70000-250/EMD Cat. 07-250-056	Pyrex*vista*Griffin Beakers/250mL/
	pack$_{(100)}$	$5.81	Cat. 09-795B	Quanlitative Grade Circles & sheets 7cm dia. Grade P8/ filter paper
	each	$22.24	Mfr. 60317 Cat. 12-961A	CoorsTek*Porcelain Mortars O.D. 3'1/2"
	each	$20.94	Mfr. 60317 Cat. 12-961-5A	Porcelain Pestles For Mortar 12-961A
	pack$_{(25)}$	$65.26	Cat. K897193-0000	5 mm O.D. (0.019") Disposable Grade Tubes Wall thickness 0.015"(0.38mm) NMR Tubes 7"(17.7cm)
	each	$17.74	Mfr. 70024-50 Cat. 07-250-068	Pyrex*Vista*Class A Cylinder 50mL Cylinders
	each	$28.73	Mfr. 10024-250 Cat. 07-250-070	Pyrex*Vista*Class A Cylinder 250mL
	pack$_{(6)}$	$27.09	Cat. 03-409-23K	Labeled Wash Bottles For distilled water
	each	$10.38	Cat. 14-375-20	Spoonulet* Lab Spoons L:7'1/4"(18.4cm)
	pack$_{(72)}$	$28.68	Cat. 11-380A	Soft Glass Stirring Rods Dia.1/8" (3mm) L:125mm(5")
	each	$33.75	Cat. 13-374-16	Parafilm M*Laborotory Wrapping Film W×L: 2"×250'
	each	$4.58	Cat. 15-959	Labeling Tape Wid: ¾"(1.9cm)
	each			hammer
	each			ruler

Experiment Procedure

1. Get Marcellus shale sample. If the shale sample is one big rock, use hammer to strike it into small pieces. Discard grains or sands like chippings. Collect all pieces with approximately 0.5cm diameter (can be slightly small than 0.5cm, but cannot exceeds that number) into a tin paper. Make sure the collected pieces are stable, and solid, and won't be crushed in future use. Separate 5 or 6 pieces out into a sealed vile, and mark it as S1-10, as is shown in Fig 1. Divide the rest of the samples into 6 shares, as equal as possible, and mark them as S2, S3, S4, S5, S6, and S7. Make sure each of S2 to S7 is all most 10 times larger than S1.

2. Weigh each sample, and put the number down on a notebook. Be sure to weigh tin paper first, and then weigh sample on the tin paper in order to avoid possible contamination. Samples' weight equals to the subtraction of these two weights.

3. Take out all of the NMR tubes. Mark a black line on every tube, the height of the line should be about 4.5cm from the bottom of the tube.

4. Divide S2 into 10 equal pieces, and put them into 10 sealed vials marked as S2-1, S2-2, S2-3… S2-10. Then do the same job to S3 – S7. As is shown in Fig 1, S2 to S7 are divided into several parts under them.

5. Take out S1. Use forceps to take samples out, and put them on the filter paper. Room-dry them to make sure there is no appearance water. Then put the samples into an NMR tube. Make sure put enough samples into the tube to reach the black line. Run NMR test on it; save the result, and interpret it. Then store the samples into a sealed vial. Put it back to rack. It can be shown in Fig 1 that S1 is not divided into branch shares.

6. Store S2-1, S3-1, S4-1,S5-1,S6-1.S7-1,S8-1,S9-1, and S10-1in sealed vials. They are set as static parameters, and can be used to retrieve initial data whenever they are needed. As is shown in Fig 1, these samples remain the same color with S2-S7, which represents that they are untouched by any fluid.

7. Soak samples S2-2, S2-3, S2-4, S2-5, S2-6, S2-7, S2-8, S2-9 and S2-10 into distilled water. As is shown in Fig 1, the arrow represents distilled water is applied on these samples, and these samples are in color that is in the same serious of the color of the fluid that is used in this group. The color of samples range from light into dark, which represents different time they are soaked in the fluid. The exact time can be found in both follow description and Fig 2.

   Soak samples S3-2, S3-3, S3-4, S3-5, S3-6, S3-7, S3-8, S3-9 and S3-10 into 2% KCl solution.

   Soak samples S4-2, S4-3, S4-4, S4-5, S4-6, S4-7, S4-8, S4-9 and S4-10 into 5% KCl solution.

Soak samples S5-2, S5-3, S5-4, S5-5, S5-6, S5-7, S5-8, S5-9 and S5-10 into 10% KCl solution.

Soak samples S6-2, S6-3, S6-4, S6-5, S6-6, S6-7, S6-8, S6-9 and S6-10 into 20% KCl solution.

Soak samples S7-2, S7-3, S7-4, S7-5, S7-6, S7-7, S7-8, S7- 9 and S7-10 into fracture fluid.

Seal all of the samples, and mark the date as Day1.

8. Day5:

   Take out S1-2, S2-2, S3-2, S4-2, S5-2, S6-2, and S7-2. Use forceps to take samples out, and put them on the filter paper. Room-dry them to make sure there is no appearance water. Then put the samples into 7 separate NMR tubes. Make sure put enough samples into the tube to reach the black line. Run NMR test on them; save the result, and interpret them. Then store the 7 samples into empty sealed vials. The vials can be their original vials, make sure these vials are empty and dry. Put them back to rack.

9. Day10:

   Do the same test on sample groups of SX-3.

10. Day 20

    Do the same test on sample groups of SX-4.

11. Day 35

    Do the same test on sample groups of SX-5.

12. Day 50

    Do the same test on sample groups of SX-6.

13. Day80

    Do the same test on sample groups of SX-7.

14. Day 120

    Do the same test on sample groups of SX-8.

15. Day 180

Do the same test on sample groups of SX-9. Different time span can be found in Fig 2. Severn different colors represent S2 to S7 separately. They follow the same pattern of Fig 1.

16. SX-10s are seal in vials without any test. They are used to possible future test when needed. As is shown in Fig 2, all of the SX-10s are not in solid color fill.
17. Experiment finished

Figure a Graphical representation of sample grouping

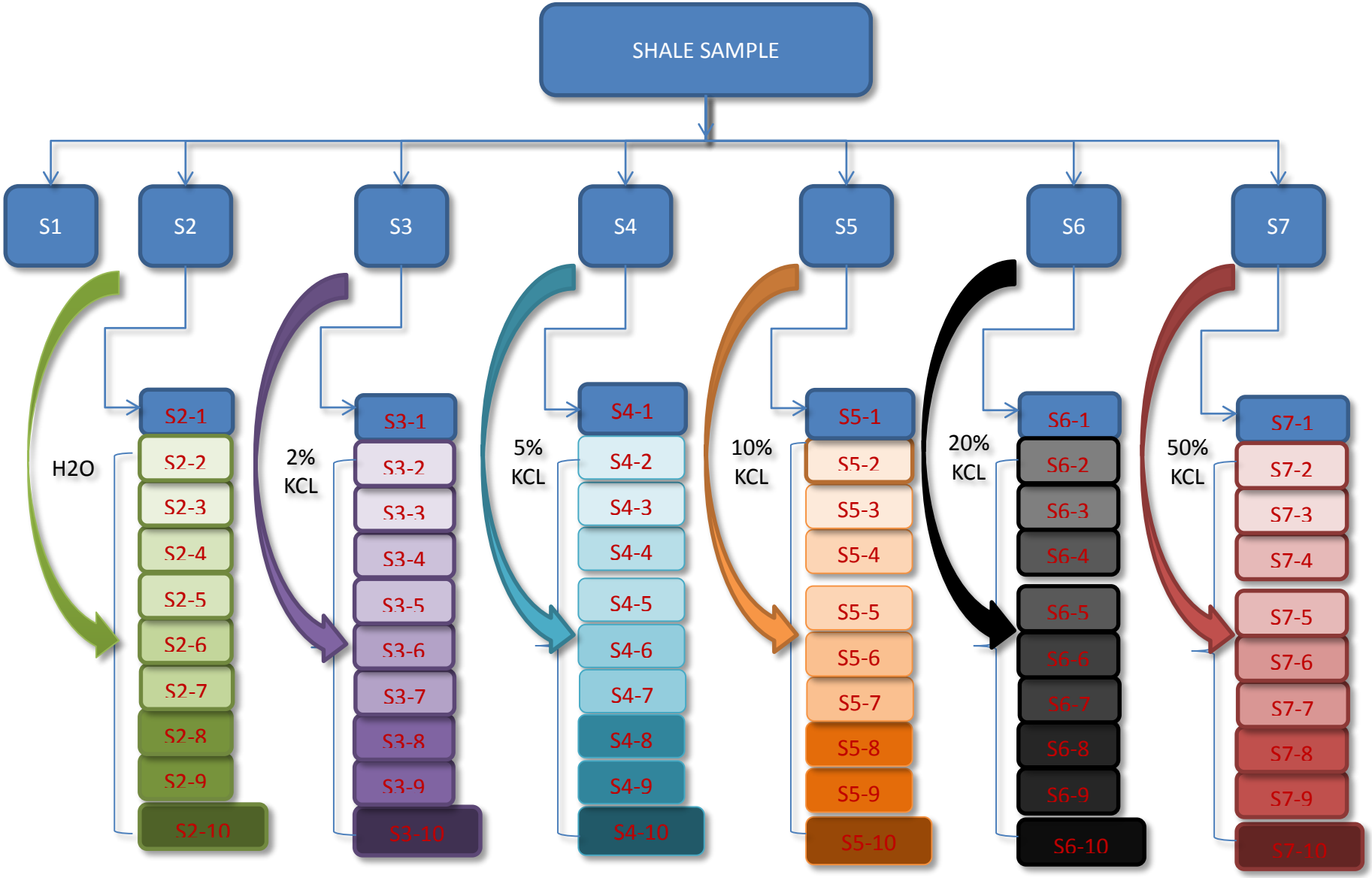

Figure b Representation of Time Span for Each Sample

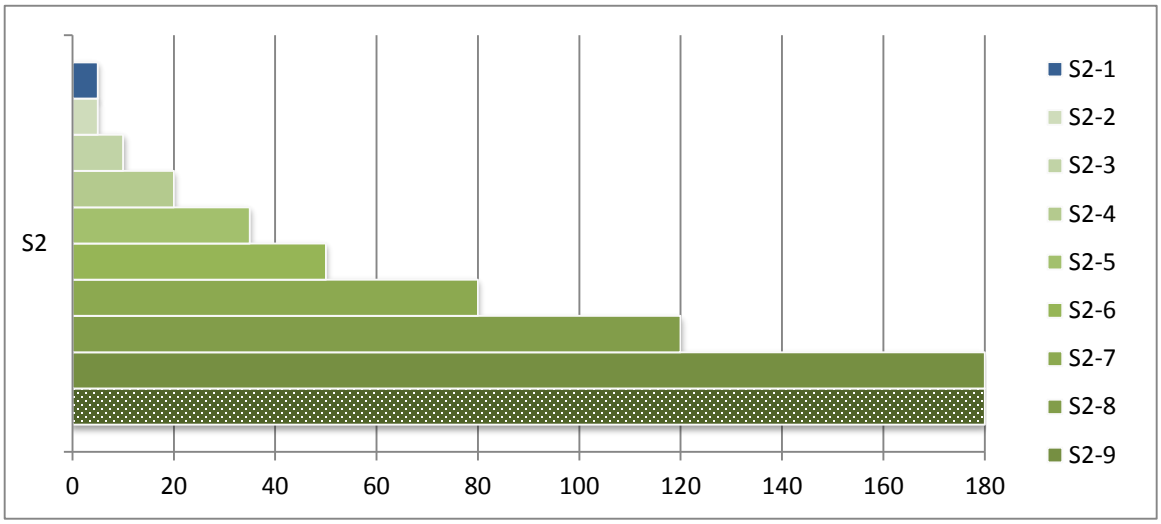

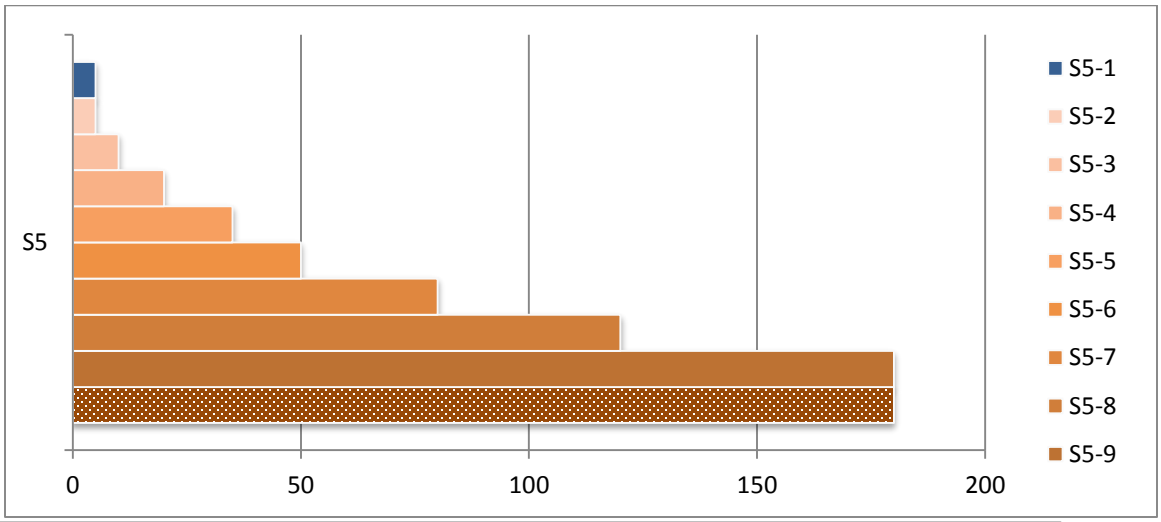

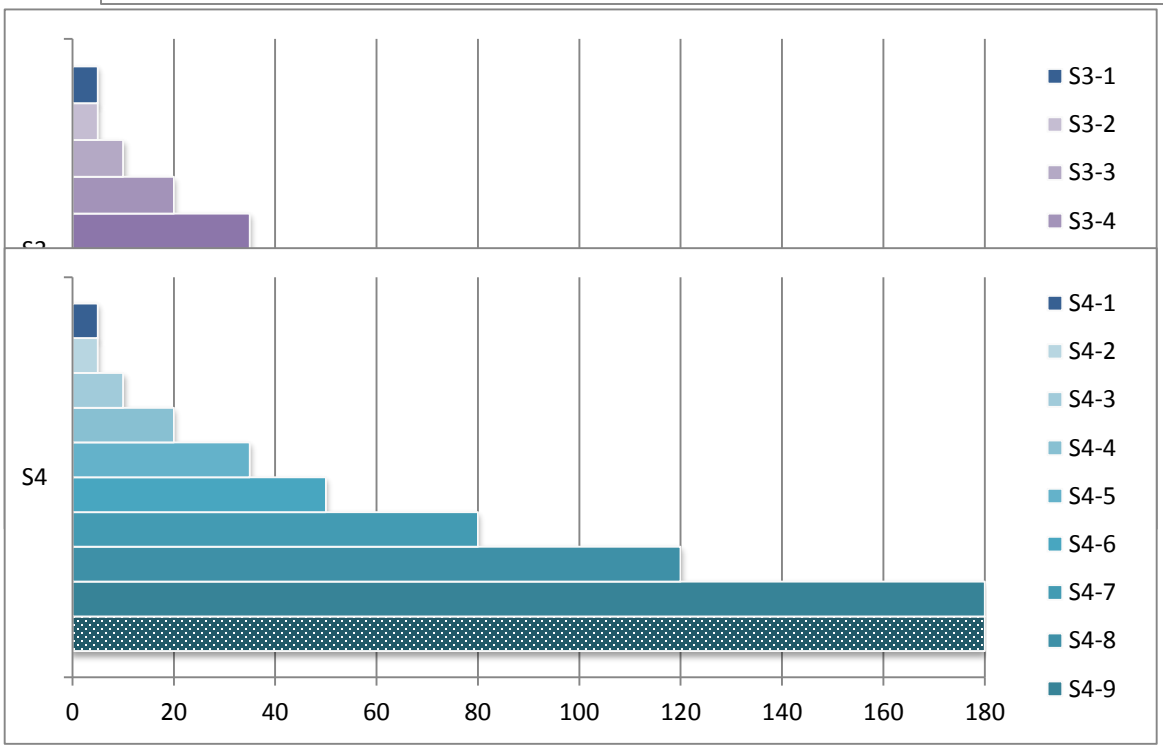

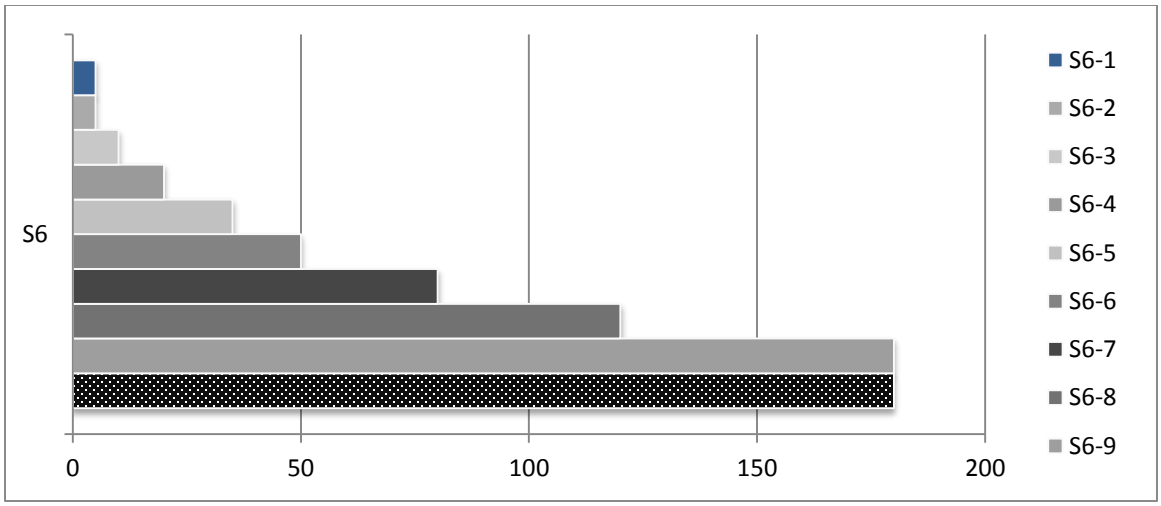
S6
0
50
100
150
200
S6-1
S6-2
S6-3
S6-4
S6-5
S6-6
S6-7
S6-8
S6-9

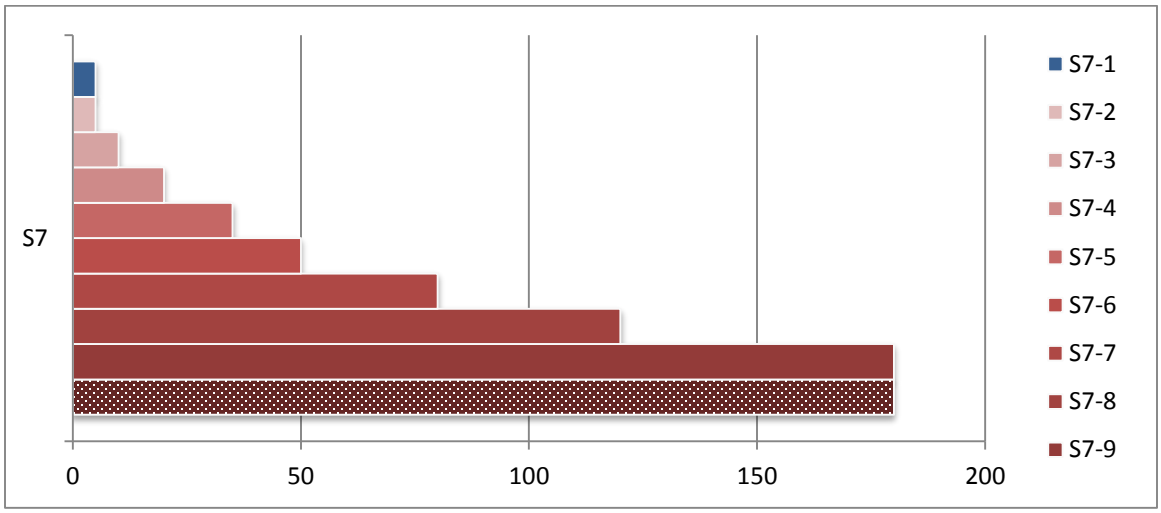
S7
0
50
100
150
200
S7-1
S7-2
S7-3
S7-4
S7-5
S7-6
S7-7
S7-8
S7-9